Chem Soc Rev

REVIEW ARTICLE

View Article Online
View Journal | View Issue

Cite this: *Chem. Soc. Rev.*, 2025, **54**, 11226

Current developments and future perspectives on the formation of luminescent lanthanide supramolecular self-assembly architectures with a focus on nitrogen-based donor ligands

Sandra Fernández-Fariña,[ab] Oxana Kotova,[ac] Shauna R. Donohoe[a] and Thorfinnur Gunnlaugsson *[ac]

Research on luminescent lanthanide (Ln) self-assembly structures has emerged into a discrete field with clear evolution from monometallic to polymetallic systems over the last few decades. The interest in these assemblies stems, on the one hand, from their structural diversity and fascinating complexity, while on the other hand, from the unique luminescence properties of the lanthanide ions, allowing for the expansion of their applications from materials science to mimicking biological systems. This review begins with a description of the recent advances in the design and properties of monometallic Ln^{3+} self-assemblies, with a particular focus on tridentate motifs, such as **dpa**, **pybox**, and **btp**, and other non-tridentate nitrogen donor ligands. Later, polymetallic systems, including helicates and metallocages, are described with their structures, followed by an elaboration on how a careful ligand design allows for the modification of the overall assembly (*i.e.* helical, tetrahedral, cubic and other polyhedra). The influences of counter-anions, concentrations, metal:ligand ratios and solvents are also discussed. The fascinating new developments within mechanically interlocked molecules containing lanthanide ions are highlighted with a focus on their structural complexity and reversible binding properties. Furthermore, this review will focus on the functional properties of lanthanide assemblies including their temperature-dependent luminescence, host–guest interaction and aggregation-induced emission. The use of such ligands in metallo-supramolecular polymers is briefly discussed, including their application in the generation of luminescent hydrogels, supramolecular polymers and other conventional polymers. We conclude this review with the perspective of exploring the biological properties and toxicity of lanthanide complexes, their application in imaging, and the recovery of lanthanides for sustainable use as well as their promising applications in smart materials, sensing and diagnostics.

Received 30th June 2025

DOI: 10.1039/d5cs00750j

rsc.li/chem-soc-rev

1. Introduction

Over the past five decades, supramolecular chemistry[1] has progressed into a highly sophisticated and multidimensional field, leading to diverse functional self-assembled architectures. The developments in this field[1] have been recognised by two Nobel Prizes: in 1987, awarded to Pedersen,[2] Cram[3] and Lehn[1] for their fundamental work on crown ethers, carcerands and cryptands; and later in 2016, to Sauvage,[4] Stoddart[5] and Feringa[6] for their pioneering contributions to the understanding of molecular machines. These advances continue to expand the scope of supramolecular chemistry, driving the development of novel molecular systems with broad real-world applications in nanotechnology, materials science, or biomedicine. Within this field, metallosupramolecular chemistry stands out owing to its distinct advantages over alternative self-assembly strategies based on non-covalent interactions such as hydrogen bonding, hydrophobic effects or van der Waals forces. In contrast, metal-ligand coordination enables the construction of robust and well-defined supramolecular architectures arising from the coordination preferences and geometrical constraints of both d- and f-block metal ions, such as the lanthanides, Ln^{3+}.[7,8] The resulting supramolecular structures not only reflect the geometric arrangement determined by the metal ions but can also incorporate the unique physical properties of the metal ion centre itself.[9] In general, for the formation of self-assembly systems, the careful design of the

[a] School of Chemistry and Trinity Biomedical Sciences Institute (TBSI), Trinity College Dublin, The University of Dublin, Dublin 2, Ireland. E-mail: gunnlaut@tcd.ie
[b] Departamento de Química Inorgánica, Facultade de Química, Campus Vida, Universidade de Santiago de Compostela, 15782 Santiago de Compostela, Spain
[c] Synthesis and Solid-State Pharmaceutical Centre (SSPC), School of Chemistry, Trinity College Dublin, The University of Dublin, Dublin 2, Ireland

ligands is crucial to determine the stability and architecture/structure of the self-assemblies as they must satisfy the coordination requirements of the chosen metal ions.[10] This is also critical for outlining the rationale for the application of the resulting assembly.

Recent progresses within the field of d- and f-metal ions have led to the design and precise control of complex supramolecular architectures including but not limited to helicates,[7,11–13] metallocages,[14,15] metal–organic frameworks (MOFs),[16–19] and mechanically interlocked molecules (MIMs) such as catenanes,[20,21] rotaxanes[21–23] and knots.[24–27] These architectures are inherently dynamic, making them ideal candidates for the development of functional and responsive supramolecular architectures governed by external stimuli such as pH, temperature, or solvent polarity.[28,29] Moreover, self-assembly strategies have enabled the formation of molecular architectures that are difficult to achieve through traditional synthetic approaches, allowing supramolecular chemists the

Sandra Fernández-Fariña

Sandra Fernández Fariña completed her PhD in 2021 at Universidade de Santiago de Compostela under the supervision of Prof. Rosa Pedrido and Prof. Ana M. González Noya, working on metallosupramolecular chemistry. She then joined the molecular spectroscopy service at Universidade da Coruña as a "Programa Investigo" beneficiary (2022-2023). Later, she moved to the School of Pharmacy at Universidad Complutense de Madrid under the supervision of Dr Marco Filice, studying the antibacterial properties of bioactive compounds. In 2024, she became a Postdoctoral Fellow at Universidade do Porto, focusing on porphyrin-derived photosensitisers for photodynamic therapy. Since October 2024, she has been a Xunta de Galicia postdoctoral fellow in the group of Thorri Gunnlaugsson, exploring functional self-assembly architectures for different applications, and she will soon be joining the research group of Prof. David A. Leigh where she will continue her Xunta de Galicia postdoctoral fellowship at the University of Manchester.

Oxana Kotova

Oxana Kotova is a Senior Research Fellow in the group of Prof. T. Gunnlaugsson at the School of Chemistry, Trinity College Dublin, Ireland. Oxana graduated with a Master's degree in Chemistry and Materials Science and completed her PhD in Inorganic Chemistry from Lomonosov Moscow State University (MSU), working on luminescent lanthanide complexes as electroluminescent materials for organic light-emitting diodes under the supervision of Prof. Natalia Kuzmina and Prof. Leonid Lepnev. After completing her PhD Oxana worked on a collaborative project between MSU and Lebedev Physical Institute. She was then supported by the Irish Research Council Grant to continue her research in Ireland. Her current research focuses on lanthanide-based supramolecular assemblies, including chiral systems for imaging and sensing applications. More recently, she worked on the development of MOFs for industrial solvent purification.

Shauna R. Donohoe

Shauna R. Donohoe received her PhD from Trinity College Dublin in 2025. During this time, she studied the self-assembly of novel triazole-pyridine derivatives with lanthanide ions, investigating their luminescence properties. She subsequently began working for Senator Annie Hoey at Houses of the Oireachtas, mainly undertaking policy research related to further & higher education in Ireland. She is currently completing a Postgraduate Diploma in Medical Device Technology & Business at Griffith College Dublin, in collaboration with Innopharma Education.

Thorfinnur Gunnlaugsson

Professor Thorfinnur (Thorri) Gunnlaugsson MRIA holds a Personal Chair in the School of Chemistry at Trinity College Dublin, being appointed in 1998. He has supervised over 60 PhD students and a large number of postdoctoral fellows since then. He is the author of over 300 publications, and in 2022, he co-edited "Supramolecular Chemistry in Biomedical Imaging", Monographs in Supramolecular Chemistry No 33 (published by RSC) with Prof. Stephen Faulkner and Dr Gearóid M. Ó Máille. His work has been recognised with various awards including the Institute of Chemistry (ICI) of Ireland Brown Award in 2023 and the MSMLG Czarnik Award in 2021. He was elected as a Member of the Royal Irish Academy (MRIA) in 2011 and is a fellow of both the ICI and the RSC.

creative freedom to design such beautiful, complex and functional structures. This has further enhanced our understanding of the living systems, especially when chiral ligands are used in self-assembly processes giving us insights into the origin and transfer of chirality within such assemblies.[30] Furthermore, the complexity of self-assemblies can be enhanced through templated synthesis, which is also a powerful approach to achieve MIMs within the metal-directed self-assembly.[31–36]

The potential applications of the aforementioned self-assembled supramolecular architectures are extensive, including fields such as drug delivery,[37,38] optoelectronics,[39–41] imaging,[42–44] and chemical (chemo-) activity based sensing.[45–50] While most of the research in metallosupramolecular chemistry has focused on d-metal ions,[51–53] f-metal ions have emerged as promising candidates due to their many unique properties[54] and coordination behaviour/requirements.[55–57] In particular, the research groups of Horrocks, Bünzli, Piguet and Raymond[58] have pioneered the field of Ln^{3+}-directed self-assemblies, having conducted extensive research in this area over the years.[59–63] Moreover, chiral lanthanide self-assemblies with emission properties have emerged as promising candidates for developing circularly polarised luminescent (CPL) materials.[64] The development of Ln structures with aggregation-induced emission properties (AIE) has also been recently reported, exhibiting aggregation-induced emission along with high g_{lum} and B_{CPL} values. This finding paves the way for the development of dynamic chiral luminescent materials, but the complexes were also used as luminescent inks.[65]

Thus far, many outstanding reviews have been reported covering different aspects of lanthanide chemistry,[64,66–78] highlighting their intricate chemistry, which has been widely used in developing responsive and complex supramolecular structures. We also would like to direct the reader's attention to the outstanding work of Prof. Parker research group on the field of responsive lanthanide complexes based on cyclen ligands. These contributions provide essential insights into the design of new functional complexes.[79–91]

The present review we hope will provide a comprehensive overview of the latest advancements, focusing on the period of 2017 to present, in the field of luminescent lanthanide metallosupramolecular architectures derived from non-macrocyclic, primarily nitrogen-based donor ligands, with a particular focus on the ligand design, their photophysical properties (and that of the assembly), and their applications as functional materials. Within this manuscript we will not be discussing the mechanism of the lanthanide sensitisation, and instead we would like to refer readers to some of the excellent reviews covering such topics.[8,55,92–96]

It has to be noted that research on further understanding of the mechanisms of lanthanide luminescence is ongoing, and includes, but not limited to, studies on the mechanism and pathways of energy transfer processes through the antennae (sensitisation) effect,[97–100] the determination of the lanthanide coordination geometry through a range of luminescence measurements, and theoretical/computational analysis,[101–108] as well as point group assignment,[109] as well as studies on lanthanide luminescence quenching pathways,[110] determination of triplet-state energy behaviours,[111] and creating a method to bypass luminescence quantum yield determination,[112] the effect of chirality, *etc.* The studies of excited-state dynamics and revisiting Horrocks method,[113] as well as development of new theoretical tools to practice Judd–Ofelt theory are also currently under investigations in various laboratories.[114,115]

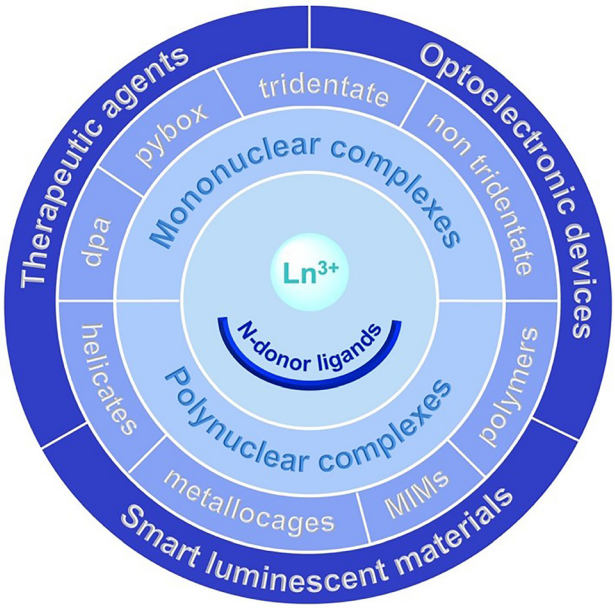

Scheme 1 Main topics discussed in this review.

The outline of our review is depicted in Scheme 1. The first section of our contribution will discuss the recent advances in the formation of monometallic Ln^{3+}-derived self-assemblies, while the following section will discuss new developments in polymetallic Ln^{3+}-derived self-assemblies such as helicates, metallocages and mechanically interlocked molecules (MIMs); an area that has relatively recently emerged within lanthanide chemistry. The role of metallo-supramolecular polymers will also be briefly explored in this context.[76] Given that the extensive work on lanthanide-based coordination polymers and MOF chemistry has been recently reviewed, this topic will not be covered in the present work, and we would like to refer readers to the following references.[17,19,116–118]

2. Recent advances in monometallic Ln^{3+}-derived self-assemblies

A considerable number of mononuclear ligands have been designed for Ln^{3+} assemblies over the years. In particular, the tridentate binding unit is one of the most attractive motifs, as it can readily fulfil the Ln^{3+} coordination requirements by binding in a 1/3 (metal/ligand) ratio to form stable tris complexes. The self-assembly processes involving tridentate ligands have been the subject of extensive research, with a particular focus on pyridine-centred ligands[75,119] such as pyridine-2,6-dicarboxylic acid (**H_2dpa**),[108,120,121] pyridine-bis(oxazoline) (**pybox**),[122] 2,6-bis(1,2,3-triazol-4-yl)pyridine (**btp**),[77,123] 2,6-di(pyrazolyl)pyridine

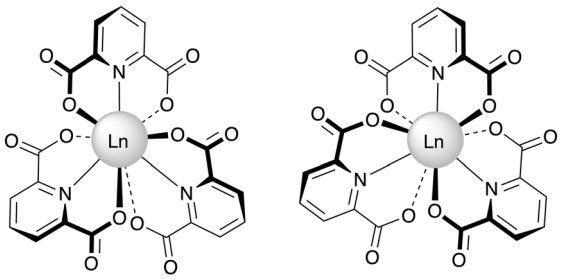

Fig. 1 Structural formulas of Δ-[Ln(**dpa**)$_3$]$^{3-}$ and Λ-[Ln(**dpa**)$_3$]$^{3-}$ enantiomers.[127] Reproduced from ref. 127 with permission from the Royal Society of Chemistry, Copyright©2012.

(**bpp**)[124] and 2,2′:6,2″-terpyridine (**terpy**).[120,125] In this review, we will present different examples of Ln^{3+}-derived self-assemblies from ligands containing these tridentate motifs, emphasising the properties and range of applications of the resulting structures and self-assemblies.

2.1. Lanthanide self-assemblies based on a H_2dpa motif

Lanthanide self-assemblies derived from **dpa** cores or binding units have attracted significant attention in recent years.[79] The **dpa** motif facilitates the formation of stable tris Ln^{3+} complexes with high binding constants and excellent luminescent quantum yields that exist as Δ- and Λ-[Ln(**dpa**)$_3$]$^{3-}$ enantiomers (Fig. 1).[126–128] Additionally, it can be easily modified *via* amide coupling reactions, as well as modification on the pyridine unit itself, which explains why the **dpa** motif is now used widespread in contemporary lanthanide-based supramolecular assembly formation.

Recently, Sørensen and co-workers have further investigated the coordination chemistry of **dpa** ligands using a range of lanthanide ions. For example, they explored the luminescence properties of two **dpa**-derived Eu^{3+} complexes synthesised with the same reagents but varying the pH of the media during crystallisation. Under acidic conditions, the [Eu(**dpa**)(**Hdpa**)$(H_2O)_2$]·4H_2O complex was found to be the predominant species, while in basic media the Na_3[Eu(**dpa**)$_3$]·14H_2O complex dominated. They found that the lower symmetry on Na_3[Eu(**dpa**)$_3$]·14H_2O resulted in a more complex emission spectrum, thus being an example of pH-dependent luminescence behaviour.[121] Similarly, they observed the same behaviour for Sm^{3+} **dpa**-derived complexes.[108] These complexes again exhibit pH-dependent colour changes where their luminescence was reversibly affected by pH, opening a possibility for pH sensing applications. A similar pH-dependent behaviour had previously been demonstrated for tetra-substituted 1,4,7,10-tetraazacylcododecane (**cyclen**)-based Eu-complexes by Gunnlaugsson.[129] Following this line, a range of lanthanide complexes (Ln = Eu^{3+}, Tb^{3+} and Dy^{3+}) with **H_2dpa** have been obtained through a hydrothermal method, again showing pH-dependent emissions.[130]

These complexes were also explored for other applications. For example, the effect of the incorporation of the [Eu(**dpa**)$_3$]$^{3-}$ complex into a mesoporous silica matrix through incipient wetness impregnation was explored and the photophysical properties probed. Their results indicate that this finding enhances the luminescence properties of the materials, being an important approach for the development of advanced luminescent materials.[131,132]

Over the years, the Gunnlaugsson group (as well as the Leigh group, see discussion later) has done extensive research on Ln(III)-directed self-assemblies using the **dpa** moiety, in combination with chiral naphthalene arms.[133–135] The developed ligands showed effective sensitisation of lanthanide emission,[136,137] and as mentioned before, the presence of the chiral centres within the organic ligands allowed for the transfer of chirality to Ln^{3+} centres, leading to well-resolved CPL emissions with 'good' luminescence dissymmetry factors (g_{lum}).[127,138–141]

Recently, Taniguchi *et al.* have shown that Tb^{3+} complexes synthesised from these chiral naphthalene-derived ligands also showed strong magnetochiral dichroism.[142] Gunnlaugsson's research group then also demonstrated the use of circular dichroism (CD) and CPL spectroscopy to confirm the chirality of luminescent monometallic Ln^{3+} complexes derived from 'half helicate' ligands.[133,135] The result allowed the identification of different binding stoichiometries and binding affinities and, importantly, enabled the determination of the unique (chiral) CD fingerprint for each of these stoichiometries.[133,135]

While previous studies focused primarily on the fundamental behaviour of Ln^{3+} self-assembly systems in solution, our group has extended this work towards the development of Ln^{3+}-directed self-assemblies as functional materials. Recent examples include the use of previously reported **dpa**-based naphthalene-derived chiral ligands.[134,143,144] Further modifications to the aforementioned 'half-helicate' ligand, by simply incorporating long alkyl chains at the free carboxylic acid side, were designed to enhance its material properties with the aim of forming Langmuir–Blodgett monolayers. Particularly, the Eu^{3+} complexes were the first examples of amphiphilic self-assembles exhibiting Eu(III)-centred CPL.[143] More recently, the authors developed luminescent Langmuir–Blodgett (LB) films containing discrete Ln(**1**)$_3$ chiral amphiphilic complexes (Ln^{3+} = Sm^{3+}, Tb^{3+}, Dy^{3+} and Lu^{3+}) derived from ligand **1** (Fig. 2).[145]

The effect of immobilisation of these complexes into LB films on their luminescence properties was also investigated. Although Ln^{3+}-centred luminescence was observed along with CPL in the solution for all the complexes, unfortunately, no CPL emission could be detected from single-monolayer LB films of the Tb(**1**)$_3$ and Sm(**1**)$_3$ systems, possibly due to low concentration effects.[145] With the aim of overcoming this challenge, the authors are working on improving the current system.

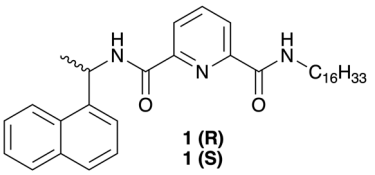

Fig. 2 Chiral **dpa** asymmetrical 'half-helicate' ligands with long chains **1(*R*)** and **1(*S*)**.[145] Reproduced from ref. 145 with permission from the Royal Society of Chemistry, Copyright©2012.

Recently, Kitchen and co-workers reported the synthesis and study of lanthanide amphiphiles using **2(*R*)** and **2(*S*)** ligands (Fig. 3), where Ln^{3+} = La^{3+}, Sm^{3+}, Eu^{3+}, Tb^{3+} and Dy^{3+}.[146] They incorporated complexes of Eu^{3+}, Tb^{3+}, Dy^{3+} and Sm^{3+} in a 1/1/10/50 ratio to create quadruple-emitting thin films. This study opens the door for their use in a range of sensing applications, as four distinct receptors for sensing can be functionalised to each respective Ln^{3+} complex within the films.

Kitchen *et al.* also reported the synthesis of the asymmetric ligand **3** (Fig. 4), a **dpa**-based ligand that has been functionalised with the 1,8-naphthalimide chromophore (**Nap**).[147] It was found that the resulting Eu^{3+} complex, Eu(**3**)$_3$, was multi-emissive, displaying colour-tuneable emission windows by changing the excitation wavelength in both the solid and solution states; the phenomenon arising from the mixing of the blue-centred emission of 1,8-naphthalimide and the Eu(III)-centred red emission. The complex retained these photophysical properties when spin-coated onto quartz slides, yielding thin films that were further analysed.[147] Researchers in the Kitchen group are currently investigating the potential of the application of these systems for use in self-calibrating ratiometric oxygen sensors.

Besides modifying the 'arms' of these monotopic systems, many research groups have explored variations at the *para*-position of the central pyridyl ring to introduce a functionality. Gunnlaugsson, in collaboration with Pal and co-workers, has recently expanded on their designs and developed various **dpa**-based ligands (**4a–d**) with different functionalities at the back of the pyridine unit *via* an ether linkage. These, as evidenced before,[148] have been shown to enhance solubility in competitive solvents, such as alcohols (Fig. 5).[149]

The crystal structures of Eu^{3+} complexes with these chiral ligands have been resolved, as demonstrated in Fig. 5 for the complexes formed from the (*R*,*R*) and (*S*,*S*) ligands of **4c**, which give rise to the formation of either Λ for Eu(**4c**(***R*,*R***))$_3$ or Δ stereochemistry around the Eu^{3+} centre within such complexes. The packing of the complexes within the structure also demonstrated that the helical nature of the complexes was extended into the three dimensions for both systems. The chiral nature of the complexes in the solid state was also confirmed by recording the CPL emission from both systems in their solid state using conventional CPL spectroscopy and the newly developed CPL laser scanning confocal microscopy (CPL-LSCM). The latter method opens a new and unexplored means

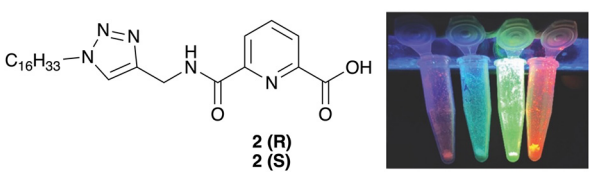

Fig. 3 Asymmetrical carboxylate **dpa** 'half-helicate' ligands with long chains **2(*R*)** and **2(*S*)** and lanthanide complexes under UV light (λ_{ex} = 254 nm): left to right Sm(**2**)$_3$, Dy(**2**)$_3$, Tb(**2**)$_3$ and Eu(**2**)$_3$.[146] Adapted from ref. 146 with permission from the Royal Society of Chemistry, Copyright©2021 (CC BY 3.0).

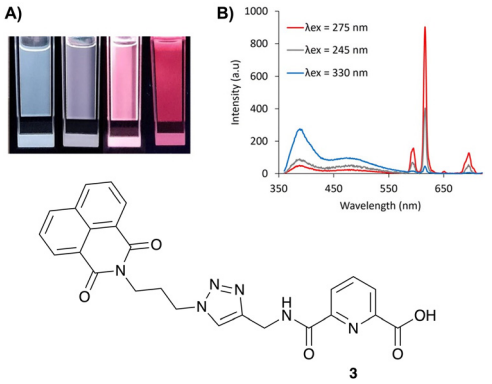

Fig. 4 (A) Eu(**3**)$_3$ solutions depicted under a UV light (λ_{ex} = 254 nm) at different concentrations (10, 5, 1, and 0.01 mM from left to right) in MeOH. (B) Fluorescence emission spectra of Eu(**3**)$_3$ at different excitation wavelengths showing different intensities of Eu^{3+}-centred emission *versus* **Nap** emission.[147] Adapted from ref. 147 with permission from the Royal Society of Chemistry, Copyright©2023.

of probing chirality of such lanthanide complexes in the solid state, in addition to conventional solution state studies.[149]

In related studies, Signore *et al.*[150] reported the **H$_2$dpa** derivative ligands, **5** and **6**, which were functionalised with coumarin at the 4-pyridyl position (Fig. 6). The addition of iodine in compound **6** resulted in the appearance of a second absorption shoulder at *ca.* 375 nm, which, in theory, should enhance the luminescence of the resulting tris Eu^{3+} complexes. However, negligible differences in the quantum yield were observed between Eu(**5**)$_3$ and Eu(**6**)$_3$, with both complexes displaying low quantum yields, suggesting that the presence of other non-radiative pathways were responsible for the quenching of the lanthanide luminescence. These results show that the introduction of iodine (*via* the heavy atom effect) is not enough (alone) to enhance the luminescence of the complexes in this instance.

In another study, Pal and colleagues reported the use of the related chiral ligands **7(*R*,*R*)** and **7(*S*,*S*)** (Fig. 6).[151] The resulting Eu(III) enantiomeric complexes, Eu(**7(*R*,*R***))$_3$Cl$_3$ and Eu(**7(*S*,*S***))$_3$Cl$_3$, demonstrated stability in solutions over a period of several months, with no alterations to g_{lum} values. The aforementioned g_{lum} value quantifies the degree of circular polarization in the emitted light, and is a key parameter in CPL studies. The authors reported that the stability of these values indicates that the chiral environment around the Eu^{3+} centre remains unchanged over time (*i.e.* no racemisation). Consequently, this property rendered Eu(**7**)$_3$Cl$_3$ as an ideal candidate for use as a standard reference in the calibration of CPL spectrometers.

The interest to the development of the ligand's derivatives of **H$_2$dpa** for their coordination to the Ln ions has been ongoing, and recently, de Bettencourt-Dias and colleagues have carried out extensive research on luminescent lanthanide complexes derived from this motif centred on their potential biological properties/applications. Particularly, some of their research studies have focused on luminescent lanthanide complexes capable of generating cytotoxic single oxygen ($^1O_2$). This interest stems from their potential therapeutic applications such as MRI contrast agents, among others, due to their selective

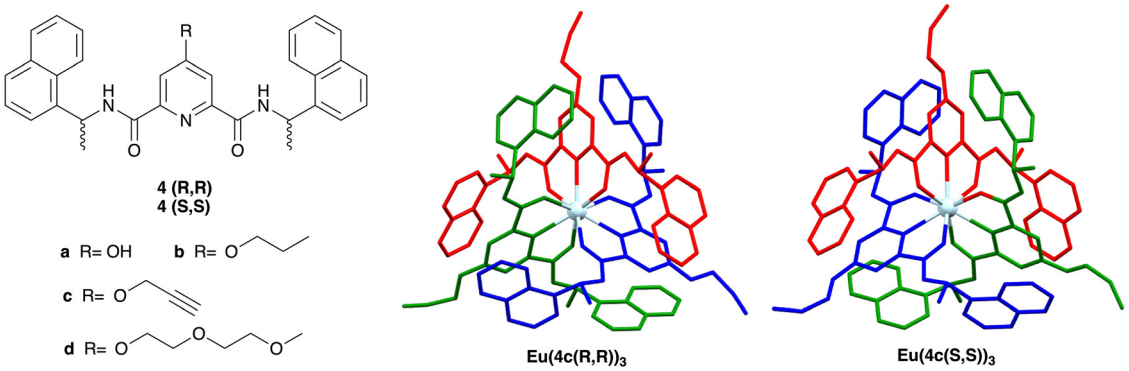

Fig. 5 Chiral ligands **4(*R,R*)/(*S,S*)** that possess different functionalities at the 4-position of the pyridine ring (**4a–d**); corresponding crystal structures of the Eu^{3+} complexes Eu(**4c**)3 formed from the (*S,S*) and the (*R,R*) enantiomers of the propargyl derivative **4c**.[149] Adapted from ref. 149 with permission from the Royal Society of Chemistry, Copyright©2024.

accumulation in tumour tissues. They developed **dpa**-derived ligands functionalized with a 1,8-napthalamide moiety, **8** and **9** (Fig. 7) and their corresponding Nd^{3+}, Eu^{3+} and Yb^{3+} complexes $Ln(\mathbf{8})_3$ and $Ln(\mathbf{9})_3$, which showed the capability of generating $^1O_2$ with high efficiency.[152]

Later, the de Bettencourt-Dias group has studied ligand **10** (Fig. 8) and its complexes $Nd(\mathbf{10})_2$, $Er(\mathbf{10})_2$ and $Yb(\mathbf{10})_2$. These were the first examples to show the ability to control $^1O_2$ generation through the excitation wavelength attributed to the presence of multiple sensitisation pathways from **10** to the Ln^{3+} ions due to the presence of 2,2′:5′,2″-terthiophene within the ligand.[153] Following the same ligand design, ligand **11** (Fig. 8) was found to be capable of sensitising Ln^{3+} ions (Ln = Nd^{3+}, Eu^{3+}, Gd^{3+}, Er^{3+} and Yb^{3+}), also leading to the excitation wavelength-dependent $^1O_2$ generation in $Ln(\mathbf{11})_2$ complexes.[154] However, all these complexes were found to be insoluble in water, which renders them useful for therapeutic applications, but providing a new route for the formation of this type of systems.

Recently, the same group has reported ligands **12** and **13** (Fig. 8), and their respective $Ln(\mathbf{12})_3$ and $Ln(\mathbf{13})_3$ complexes

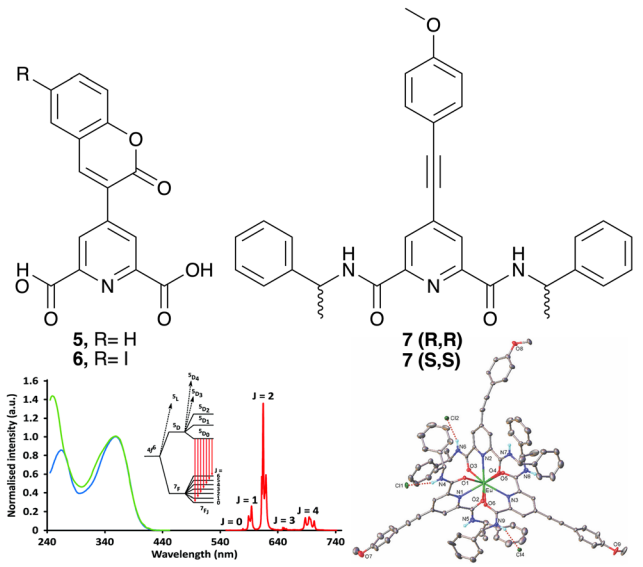

Fig. 6 (A) **H_2dpa** derivatives functionalised with coumarin at the 4-pyridine position (**5**, **6**),[150] chiral ligand based on the **dpa** motif functionalised at the 4-pyridine position (**7**).[151] (B) Absorption (green) and excitation (blue, λ_{em} = 615 nm) spectra normalised at 365 nm and emission (red, λ_{exc} = 365 nm) spectra of $[Eu(\mathbf{7})_3]^{3+}$ complexes ($c = 16 \times 10^{-6}$ M) in acetonitrile. (C) X-ray structure of the Λ-$[Eu(\mathbf{R\text{-}7})_3]Cl_3$ complex.[151] Adapted from ref. 151 with permission from the Royal Society of Chemistry, Copyright©2019.

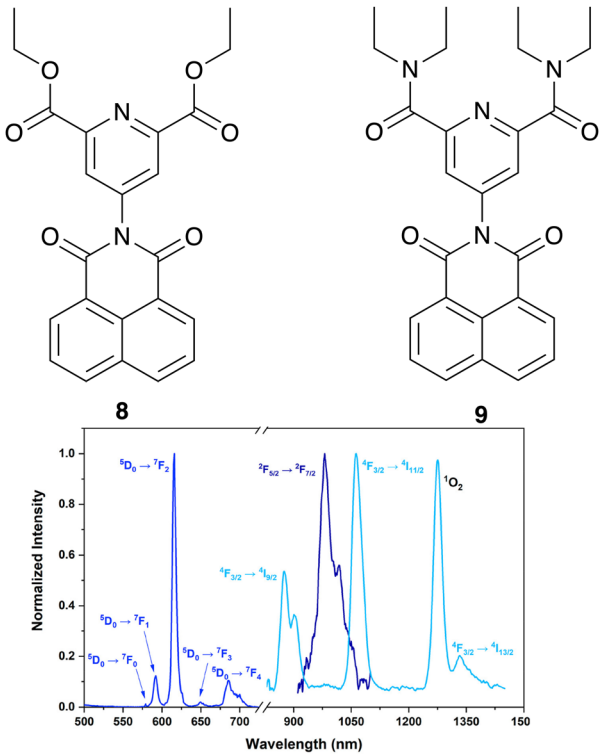

Fig. 7 (A) Derivatives of **H_2dpa** ligand functionalized with 1,8-napthalamide (**8**, **9**). (B) Normalized emission spectra of the $[Ln(\mathbf{9})_3]^{3+}$ complexes [Ln = Eu^{3+} (blue), Nd^{3+} (light blue), or Yb^{3+} (navy)].[152] Adapted from ref. 152 with permission from the American Chemical Society, Copyright©2019.

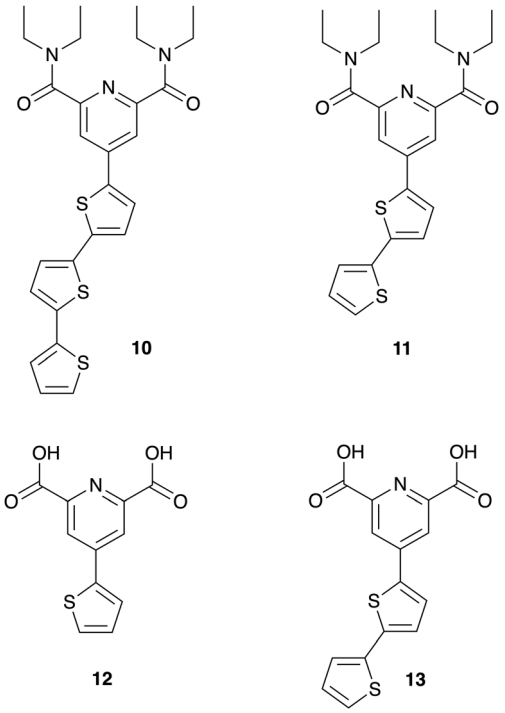

Fig. 8 Ligands (**10–13**) synthesised by de Bettencourt-Dias and coworkers.[153–155]

where Ln = Eu^{3+}, Gd^{3+} and Yb^{3+}. These complexes displayed improved water solubility and luminescence properties, and excitation wavelength-dependent $^1O_2$ generation was also observed, which is more efficient for the complexes with ligand **13**. Moreover, all the compounds showed interesting photocytotoxic activity against HeLa cells making them attractive for application in photodynamic therapy.[155]

The research group of de Bettencourt-Dias also reported a **dpa**-derived ligand functionalised with an amino group at the 4-pyridyl position and their [Ln(**L**)$_3$], where Ln = La^{3+}, Eu^{3+}, Gd^{3+}, and Tb^{3+}, showing luminescence and stability under physiological pH conditions. The cytotoxicity of these complexes was also studied against different tumour cells showing high values of cytotoxic activity. The authors highlight the strong red luminescence of [Eu(**L**)$_3$] and its ability to penetrate cancer cells, which is effective for use as luminescent dye. This complex was also able to cross a simulated blood–brain barrier, and hence, it is a potential theragnostic agent.[156]

De Bettencourt-Dias's group has also developed lanthanide complexes derived from **dpa** ligands possessing carbazole groups. In these studies, they found that both the Eu(**L**)$_3$ and the Yb(**L**)$_3$ complexes display viscosity-dependent emission under both one-photon and two-photon excitation. Moreover, the Yb(**L**)$_3$ complex is the second example reported of viscosity sensing based on the NIR-emitting Ln^{3+} compound.[157] They expanded this study by performing the synthesis of a new **dpa** ligand functionalized with carbazole and its Eu(**L**)$_3$ and Yb(**L**)$_3$ complexes, finding a viscosity- and temperature-dependent behaviour.[158] These results highlight carbazole-functionalized **dpa** ligands as promising in the fields of imaging, sensing, and diagnosis.

In line with the potential biological applications of **dpa**-derived lanthanide complexes, Byrne and colleagues reported the synthesis of terbium complexes derived from different glycoconjugate ligands.[159] These systems showed enhancement of terbium-centred emissions in solutions in the presence of carbohydrate-binding protein LecA, a lectin associated with *Pseudomonas aeruginosa*, a Gram-negative bacterium responsible for numerous infections. This sensing ability was also demonstrated in the presence of competitors, opening a path to develop more complexes with this characteristic for use as a diagnostic tool.

Lately, Daumann and coworkers studied the influence of the presence of lanthanide ions on the activity of methanol dehydrogenases (MDH), crucial enzymes in both microbial metabolism and environmental applications.[160,161] The enzyme activity was monitored using two different assays: dye-coupled and protein-coupled assays. The results displayed that the MDH activity was higher in the presence of La^{3+}, Ce^{3+} and Pr^{3+}, demonstrating the importance of lanthanides in enhancing the MDH enzyme activity.[160]

2.2. Lanthanide self-assemblies derived from pybox

Another class of ligands that have been extensively used in Ln(III)-directed self-assemblies over the years are **pybox** motifs.[162,163] Often **pybox**-derived ligands have been used in combination with β-diketonates to form stable Ln^{3+} complexes. Lanthanide β-diketonates are a widely studied class of complexes because many of these ligands are commercially available and their corresponding complexes are highly luminescent.[164–169]

Di Bari's group has carried out intensive research with lanthanide complexes derived from the **pybox** motif. For example, they reported the formation of Ln^{3+} complexes (Ln^{3+} = Eu^{3+} or Tb^{3+}) using **14**(***R,R***), **14**(***S,S***), **15**(***R,R***) or **15**(***S,S***) (Fig. 9) and studied their luminescent and chiroptical properties.[122]

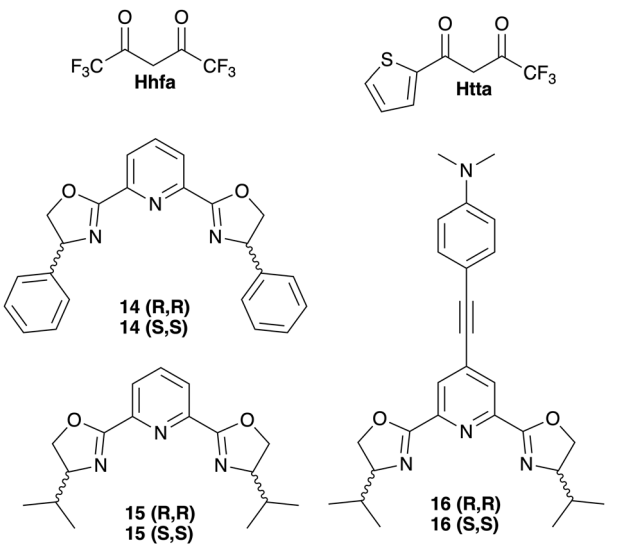

Fig. 9 Structural formulas of β-diketones hexafluoroacetylacetone (**Hhfa**), 2-thenoyltrifluoroacetone (**Htta**) and pyridine bis-oxazoline (**pybox**)-derived chiral ligands **14–16**.[122,170]

Their studies have shown that the stoichiometry of these Ln complexes was influenced by the substituents of the **pybox** oxazoline ring, with **15** forming the typical tris complexes with Ln^{3+}, whereas **14** preferred a 2 : 1 (L : M) stoichiometry where the coordination environment of the Ln ion is not fully saturated, giving the possibility of ancillary ligand coordination, leading to the potential application of these complexes as a 'probe' for the detection of chiral analytes or as an emissive layer in organic light-emitting devices (OLEDs). This study also demonstrates the importance of the ligand design and how it then influences the corresponding lanthanide complexes.[122]

Di Bari's research group also reported a series of Ln(hfa)$_3$(**L**) and Ln(**tta**)$_3$(**L**) complexes (Ln^{3+} = La^{3+}, Sm^{3+}, Eu^{3+}, Gd^{3+}, Tm^{3+} and Yb^{3+}) synthesized combining the chiral **pybox** derivatives **14**(***R*,*R***), **14**(***S*,*S***), **15**(***R*,*R***) or **15**(***S*,*S***) with the achiral β-diketones such as hexafluoroacetylacetone (**Hhfa**) or 2-thenoyltrifluoroacetone (**Htta**) (Fig. 9).[171] The resulting complexes exhibited strong CPL emissions. Using chiroptical, CD, CPL and vibrational CD spectroscopy, and a range of optical measurements, a 'super-spectrum' was elucidated by the authors, indicating that all the complexes shared a homogeneous structural environment. Additionally, in this study, vibrational circular dichroism (VCD) was highlighted as an alternative and promising method for probing the structures of the lanthanide complexes in solutions. These findings contribute to the advancement of characterisation and design of functional lanthanide-based (chiral) materials.[171] Lately, the authors have further explored the properties of the reported Yb(**hfa**)$_3$(**L**) and Yb(**tta**)$_3$(**L**) complexes also derived from **14**(***R*,*R***), **14**(***S*,*S***), **15**(***R*,*R***) and **15**(***S*,*S***). These complexes were found to exhibit a NIR-CPL emission, a phenomenon that is only recently beginning to be suited for such lanthanide systmes.[172] This was followed up by the incorporation of a conjugated substituent through the pyridine 4-position of **15**, resulting in ligand **16** (Fig. 9). Upon coordination with Er^{3+}, the Er(**16**)$_2$ complex was obtained.[127] This complex exhibited efficient NIR-CPL emission in the 1400–1600 nm region, achieved by the extended π-conjugation of the ligand system, known to sensitise the low-energy Er^{3+} levels.[170] These findings highlight their potential for applications in NIR-CPL bioassays or chiral NIR optoelectronics.

Yuasa *et al.* reported complexes of Eu^{3+} with asymmetric chiral **pybox** ligands **17**(***R***) or **17**(***S***) combined with three chelating units of β-diketonate **hfa**, as shown in Fig. 10.[173] The resulting Eu(**17**(***R***))(**hfa**)$_3$ complex was observed to switch CPL handedness upon binding of a trifluoroacetic anion (CF_3COO^-). Furthermore, the CPL emission for Eu(**17**(***R***))(**hfa**)$_3$ was unaffected in the presence of competing anions, making the complex a 'target-identifiable probe'.

More recently, de Bettencourt-Dias and co-workers have reported two different and efficient lanthanide ion sensitizers derived from the *para*-substituted **pybox** motif, **18** and **19**, Fig. 11. The complexes derived from these ligands result in high quantum yields of emission in the case of Eu(**18**)(NO$_3$)$_3$, Tb(**18**)(NO$_3$)$_3$, and Eu(**19**)(NO$_3$)$_3$, but showed a lack of sensitisation for the Tb^{3+} ion, in the case of ligand **19** due to its low triplet state energy level. This study emphasises how the

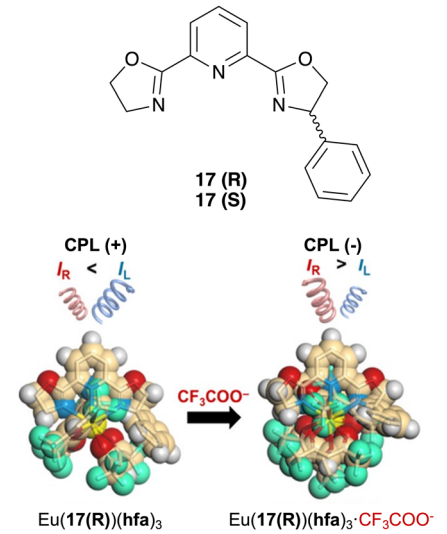

Fig. 10 Schematic of the CF_3COO^- anion coordinated to Eu(**R-17**)(**hfa**)$_3$, resulting in a switch in the CPL handedness. Adapted from ref. 173 with permission from the American Chemical Society, Copyright©2022 (CC BY 4.0).[173]

photophysical properties of luminescent Ln^{3+} complexes can be enhanced by carefully tuning the substituents on the ligand.[174]

Miao *et al.* prepared a series of mononuclear lanthanide-derived complexes, Ln^{3+} (Ln^{3+} = La^{3+}, Gd^{3+}, and Tb^{3+}).[134] They reported the first example of CPL-active Tb^{3+} complexes containing three coumarin-derived ligands along with the **pybox**-derived chiral ligand, **20**(***R*,*R***) or **20**(***S*,*S***) (Fig. 12). The resulting single diastereomer Eu(**20**)(**coum**)$_3$ complex demonstrates that the chiral ligands lead to the formation of a unique structure, enhancing the luminescence properties of Tb^{3+} enantiomers.[175] These findings establish a new pathway for the development of chiroptical organo-Tb^{3+} luminophores.[175] Later, they extended this work by replacing coumarin (**coum**) ligands with 1-phenyl-3-methyl-4-(isobutyryl)-5-pyrazolone (**pmip**) as the ancillary ligand, achieving similar results.[176]

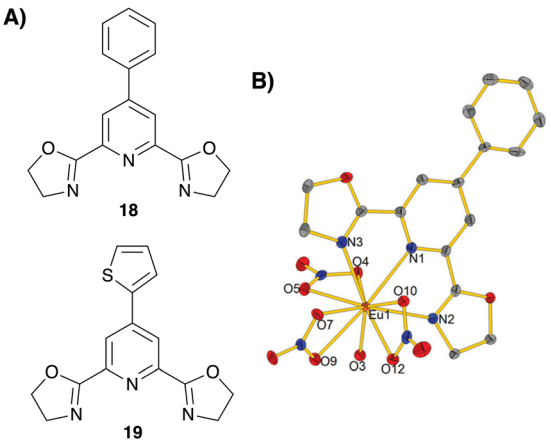

Fig. 11 (A) Structural formulas of **pybox**-derived ligands **18** and **19**. (B) Single crystal structure of Eu(**19**)(NO$_3$)$_3$·H$_2$O.[174] Adapted from ref. 174 with permission from the Royal Society of Chemistry, Copyright©2020.

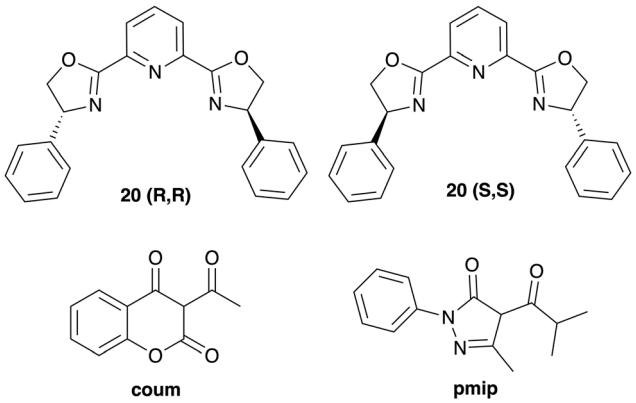

Fig. 12 **Pybox**-derived chiral ligands **20(*R*,*R*)** and **20(*S*,*S*)**, coumarin (**coum**) and 1-phenyl-3-methyl-4-(isobutyryl)-5-pyrazolone (**pmip**) ligands.[175,176]

2.3. Lanthanide self-assemblies with ligands containing tridentate nitrogen-donor ligands

Another class of binding motifs used to obtain mononuclear complexes involves ligands containing only nitrogen heterocycles for Ln^{3+} coordination.[75,177] Recently, Trifonov and co-workers reported the synthesis of Ln(**21**)$_3$ complexes (Ln^{3+} = Eu^{3+}, Gd^{3+}, Tb^{3+}, Dy^{3+}, Er^{3+} and Yb^{3+}) derived from the monotopic tridentate ligand **21** (Fig. 13).[178]

All the chiral complexes formed exhibited Ln(III)-centred luminescence, except in the case of the erbium(III) complex Er(**21**)$_3$. In particular, Eu(**21**)$_3$ and Tb(**21**)$_3$ exhibited high quantum yields for Eu^{3+} complex, 57%, and a moderate quantum yield for Tb^{3+}, 17%, in the solid state. Consequently, the researchers investigated whether mixing Eu(**21**)$_3$ and Tb(**21**)$_3$ at different ratios in the solid state would have potential temperature-sensing properties. The study revealed that a mixture of Eu(**21**)$_3$:Tb(**21**)$_3$ yielded optimal performance as a ratiometric thermometer within the temperature range of 130–220 K, representing one of the first examples of three-blade propeller Ln(III)-compounds designed for luminescence thermometry.[178]

Avarvari and colleagues have recently designed an enantiopure helicene-based tridentate ligand **22** (Fig. 14), containing an extended π-conjugated system. This ligand leads to the formation of luminescent Eu^{3+}- and Yb^{3+}-derived complexes, Eu(**22**)(**tta**)$_3$ and Yb(**22**)(**tta**)$_3$. Both complexes exhibit luminescence properties, with the β-diketone **tta** ancillary ligands

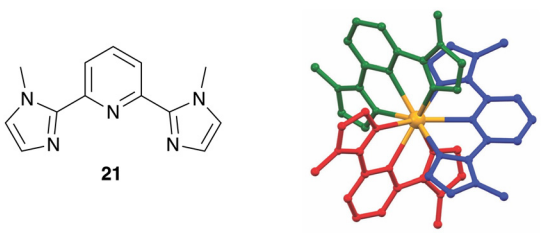

Fig. 13 Structural formula of ligand **21** (left) and single crystal structure of its dysprosium complex, Dy(**21**)$_3$(ClO$_4$)$_3$ (right).[178] Adapted from ref. 178 with permission from the Royal Society of Chemistry, Copyright©2022.

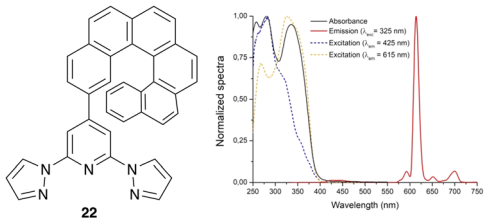

Fig. 14 (A) Structural formula of helicene-derived tridentate ligand **22** synthesised as *M* and *P* enantiomers. (B) Normalized absorption, emission, and excitation spectra of [Eu(**tta**)$_3$(**22M**)].[179] Adapted from ref. 179 with permission from Wiley-VCH GmbH, Copyright©2022.

completing the coordination sphere. These **tta** ligands play a crucial role in the antenna effect, sensitizing the luminescence of lanthanide centres. The Eu^{3+} complex showed typical red luminescence, while the Yb^{3+} complex exhibited near-infrared emissions. This study highlights the influence of the helicene unit on the chiroptical and luminescence properties of both complexes, demonstrating how structural modifications in the ligand can fine-tune the CPL activity and emission efficiency of lanthanide complexes, and to the best of our knowledge, this is the first example of such CPL system that is not formed on the use of point chirality in the ligand design.[179]

Piguet and collaborators have carried out an extensive work on lanthanide complexes derived from tridentate-nitrogen ligands. For example, they designed ligands **23–25** (Fig. 15) to further explore their coordination to a La(β-diketonate)$_3$(diglyme) complex. They also conducted investigations to address the limited light absorption of Yb^{3+} and Er^{3+} ions, which limits their effectiveness in luminescent upconversion systems.[180] For example, they generated ligand **26**, which was functionalised with a cyanine antenna (Fig. 15), and the resulting Er(**hfa**)$_3$(**26**) complex showed improved absorption of light, enhancing the efficiency of the upconversion. This approach addresses the typical low quantum yields seen in lanthanide-based molecular upconversion systems.[181]

Lately, this ligand was further modified to give ligand **27** (Fig. 15). The coordination with Er(**hfa**)$_3$ resulted in the formation of the [Er(**hfa**)$_3$(**27**)]$^+$ cationic complexes, which showed quantum yields and brightness that were two to three times higher than those of Er(**hfa**)$_3$(**26**).[182] Further theoretical[183] and experimental studies in this topic were performed within the group to optimize the energy transfer mechanisms by introducing extended π-electron delocalization, flexibility and heavy atoms on the ligand skeleton.[184]

Additionally, they focused on the rational design of the nitrogen-tridentate ligands to improve the efficiency of lanthanide complexation. The authors found an enhanced affinity when using preorganized ligands by performing thermodynamic studies. The study revealed that the presence of rigid, planar and extended π-conjugated systems, as well as steric hindrance, is a crucial factor for binding trivalent lanthanide containers such as La(β-diketonate)$_3$.[187,188] Moreover, they reported that ligand **28** (Fig. 15), obtained by metal-templated synthesis using a Grubbs catalyst and neutral Ln(β-diketonate)$_3$ where Ln = La^{3+}, Eu^{3+}, Gd^{3+}, Y^{3+}, and Er^{3+}, is more efficient with

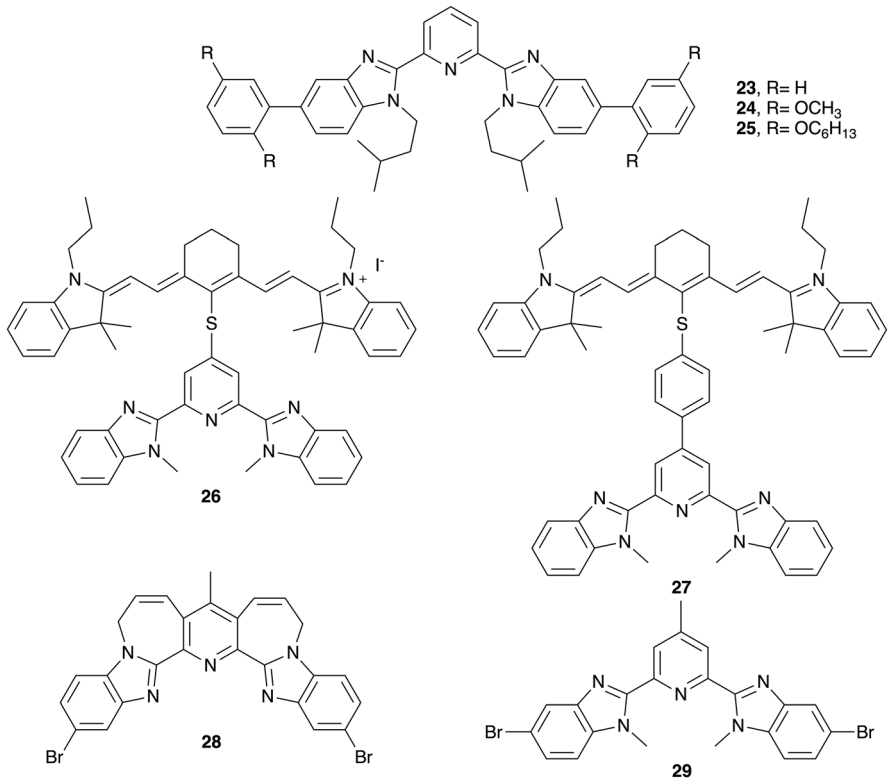

Fig. 15 Structural formulas of tridentate ligands **23–29**.[181,182,185,186]

the larger lanthanides. The metal complexes obtained Ln(β-diketonate)$_3$ (**28**), which displayed better thermodynamic stability than those obtained with the precursor **29** due to the removal of the energy penalty associated with *trans–trans* to *cis–cis* reorganisation. The unique design of **28** opens a route to explore it as an Er-based upconversion system in soluble polymers.[186]

Although not as ubiquitous as **dpa** derivatives, the 2,6-bis(1,2,3-triazol-4-yl)pyridine (**btp**) moiety has also been used in developing monometallic Ln^{3+} complexes over the years.[119,123] Monotopic **btp** derivatives exhibit strong chelating properties due to their rigid structure and were found to form highly stable tris complexes with a range of Ln^{3+} ions.[119,189–191] The Gunnlaugsson group expanded upon previous research of the **btp** moiety by incorporating chiral 'arms' to yield compounds **30–32** (Fig. 16).[192] The resulting Ln(**L**)$_3$ (Ln^{3+} = Eu^{3+}, and Tb^{3+}) complexes gave rise to CPL spectra being mirror images of each other and confirming that the complexes were also enantiopure. A high quantum yield was obtained for the Tb(**30**)$_3$ complex (Φ = 67%), whereas the analogous Eu(**30**)$_3$ complex was significantly less emissive (Φ = 0.8%), suggesting that the antenna is a more efficient sensitiser for Tb^{3+}.[192]

Lately, Gunnlaugsson and colleagues developed three chiral **tzpa** ligands by combining **btp** and the **dpa** motifs, **33–35** (Fig. 17). They studied the complexation with Tb^{3+} ions giving rise to mononuclear complexes in all cases.[193] It was found that ligands **33** and **34** form highly luminescent complexes Tb(**L**)$_3$ under thermodynamic control exhibiting visible green emission, while under kinetic control, the Tb(**L**)$_2$ complexes were obtained. These outcomes differed from previous studies with

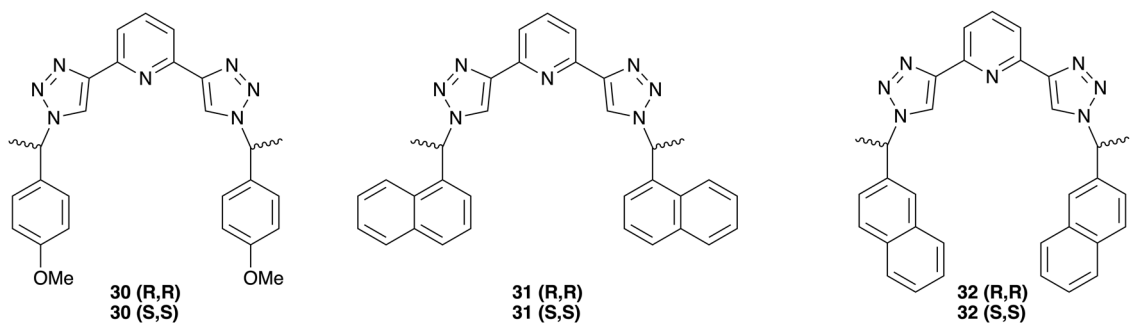

Fig. 16 Structural formulas of chiral **btp**-derived ligands **30–32**.[192]

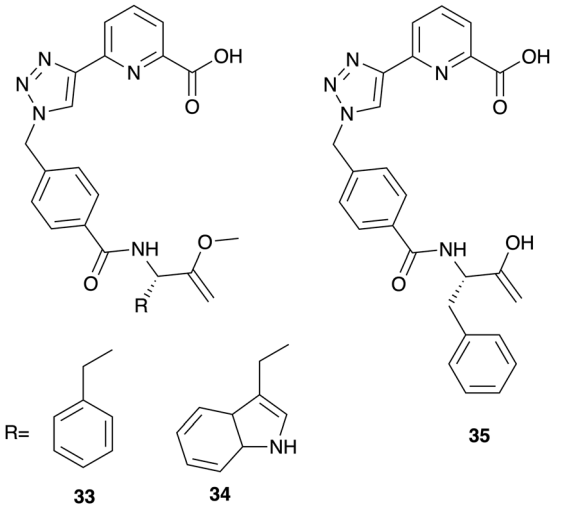

Fig. 17 Structural formulas of ligands **33**, **34** and **35**.[193]

btp and **dpa** ligands, where the complexes showed the formation of an $M(\mathbf{L})_3$ stoichiometry in both cases. Upon complexation with ligand **35**, the formation of $Tb(\mathbf{35})_3$ was found in acetonitrile. Moreover, it was observed that the *q*-value (number of water molecules directly coordinated to the lanthanide ions) was *ca.* 0, indicating full saturation of the Tb^{3+} coordination environment with ligand donor atoms. However, upon the addition of water, these complexes underwent dissociation. Nevertheless, these ligands offer a platform to explore **tzpa**-derived self-assemblies by performing structural changes on the **btp** and **dpa** cores to develop ligands with multiple binding sites to further obtain polymetallic supramolecular structures, something that the group has been actively working on in recent times (see discussion later on).

Recently, Patra and coworkers have reported the synthesis of two different bioprobes designed for the selective recognition of nucleoside phosphates (ATP, ADP or AMP), and for the detection of extremely toxic organophosphates (nerve agents such as DCP). These probes are based on Eu^{3+} complexes derived from ligands **36** and **37** (Fig. 18), and exhibit unique photophysical properties that can be modulated *via* their interactions with phosphate-derived molecules. Upon binding to these analytes, the complexes undergo changes in their emission intensities and lifetimes, giving rise to the modulation of luminescence responses.[194]

2.4. Lanthanide self-assemblies derived from non-tridentate nitrogen-donor ligands

Although pyridine-centred tridentate motifs are widely used due to their ability to readily fulfil Ln^{3+} high-coordination requirements, other nitrogen donor ligand designs are also frequently employed within such designs.[111,165,195–199] The Ung research group have done extensive research within the coordination chemistry of these types of ligands, for example, they designed the hexadentate ligand **38** (Fig. 19) and synthesised the derived lanthanide complexes of formula $Ln(\mathbf{38})(OTf)_3$, Ln = Nd^{3+}, Sm^{3+}, Eu^{3+}, Tb^{3+}, Dy^{3+}, and Yb^{3+}. They found that the Ln coordination environment differed depending on the Ln^{3+} ionic radius. All the complexes exhibited metal-centred emissions from visible (Sm^{3+}, Eu^{3+}, Tb^{3+}, and Dy^{3+}) to near-infrared (Nd^{3+} and Yb^{3+}) regions, showing moderate to low quantum yields. Additionally, it was found that the $Eu(\mathbf{38})(OTf)_3$ complex exhibits a C_2 symmetry in solutions.[200] They continued working to improve the sensitization for near-infrared emitting lanthanides by modifying the pyridine units of the ligand. The authors also reported enantiopure Sm^{3+}, Eu^{3+}, Tb^{3+}, and Dy^{3+} lanthanide complexes derived from chiral ligands **39** and **40** $Ln(\mathbf{L})(OTf)_3$ (Fig. 19), which were found to exhibit CPL with high dissymmetry factors.[201,202]

Recently, Piccinelli and co-workers have used β-diketone **Htta** together with ligand **41** (Fig. 20) to explore the effect of the counterion used in Ln^{3+} assemblies (Ln^{3+} = Sm^{3+} and Eu^{3+}) on their resulting CPL signals.[203] For the $Eu(\mathbf{41})(\mathbf{tta})_2$ complex, the triflate counterion displayed a higher g_{lum} value than that of its nitrate counterparts. It was proposed that the observed CPL was the result of the difference in bond lengths between isomers. Moreover, they reported a series of water-soluble $Eu(\mathbf{42})_3$ and $Tb(\mathbf{42})_3$ complexes. Enantiopure ligand **42** (Fig. 20) was designed to provide a dissymmetric environment

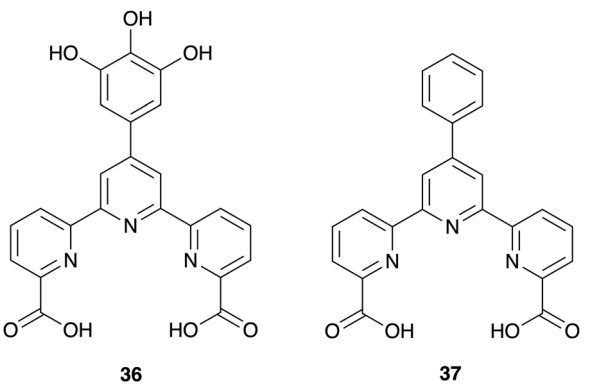

Fig. 18 Structural formulas of ligands **36** and **37**.[194]

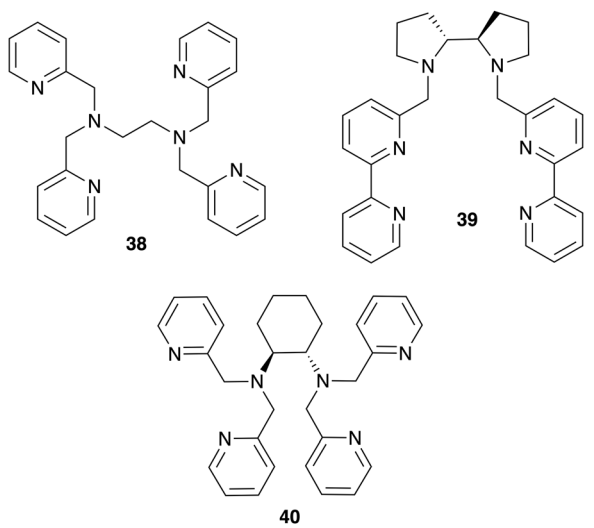

Fig. 19 Structural formulas of ligands **38**, **39** and **40**.[200–202]

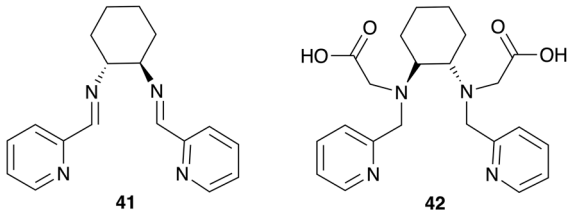

Fig. 20 Structural formulas of chiral ligands **41** and **42**.[203,204]

with the aim of exhibiting chiroptical features, whilst allowing further coordination from ancillary ligands. Notably, Tb(**42**)$_3$ exhibited pronounced CPL activity, resulting in a g_{lum} value of 0.1 for the $^5D_4 \rightarrow {}^7F_5$ transition, and is thus being studied as a potential CPL bioprobe in aqueous media.[204]

Li and colleagues used the bidentate ligands **43**(***R***) or **43**(***S***) (Fig. 21) and β-diketonate **Hbtfa** to form homochiral complexes with Sm^{3+} and Eu^{3+}.[205,206] The ligand design was based on previously reported work by Mamula *et al.*[207,208] Both of the Ln(**43**)(**btfa**)$_3$ complexes were emissive due to mechanical actions, known as triboluminescence (TL), as well as having CPL. Notably, the dissymmetry factors for the Sm^{3+} complex were found to be higher than those for Eu^{3+}, which is a rare phenomenon, given that Sm^{3+} typically exhibits lower emission in CPL-active complexes.[205] Moreover, they extended the work by synthesizing two chiral Pr^{3+}- and Ho^{3+}-derived complexes by combining ligands **43** with β-diketone **Hdbm**.

These Pr^{3+} and Ho^{3+} complexes were found to exhibit NIR luminescence upon excitation at 410 nm. They also showed non-linear optical properties due to their non-centrosymmetric self-assemblies, displaying second-harmonic generation (SHG) and high third-harmonic generation (THG) responses; these are the first examples of NIR-emissive lanthanide-derived complexes showing such activities.[206] Vomiero and co-workers used asymmetric bidentate ligand **44** with dibenzoylmethane (**Hdbm**) (Fig. 22) to obtain Eu^{3+} and Tb^{3+} complexes. The Eu^{3+} complex of formula Eu(**44**)(**dbm**)$_3$ displays a quantum yield of 25% in the solid state. The complex was then incorporated into poly(methyl methacrylate) (PMMA) matrix for the preparation of luminescent plastic materials.[209]

Moreover, de Bettencourt-Dias and coworkers expanded on their study (see Section 2.1) of the ability of generating cytotoxic single oxygen ($^1O_2$) of lanthanide complexes derived from oligothienyl-functionalized ligands **45–47** (Fig. 23). The lanthanide-derived

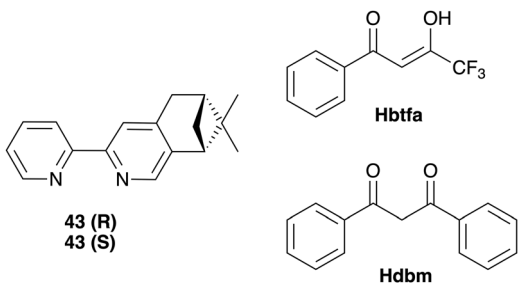

Fig. 21 Structural formulas of bidentate ligands **43**(***R***)/**43**(***S***) and β-diketones **Hbtfa** and **Hdbm**.[205,206]

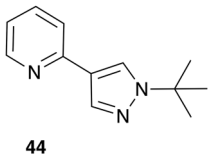

Fig. 22 Structural formula of asymmetric bidentate ligand **44**.[209]

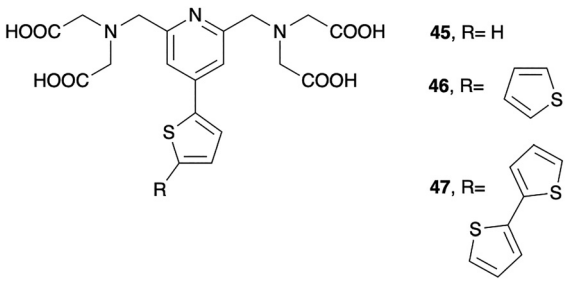

Fig. 23 Structural formulas of ligands **45–47**.[210]

complexes, $[Ln(\mathbf{L})(COO)_4]^-$ (Ln = Nd^{3+}, Eu^{3+} and Yb^{3+}), showed good IC_{50} phototoxicity values against HeLa tumour cells upon UV irradiation, the Nd^{3+} complex $[Nd(\mathbf{46})(COO)_4]^-$ being the most promising of these.[210]

Within this class of ligands Charbonnière and colleagues have focused their recent effort on the development of supramolecular complexes with the ability of generating upconversion. They extended upon a previous study performed with ligand **48** (R = H) considering the promising photophysical properties that the Yb^{3+}-derived complexes showed in water (Fig. 24),[211] developing ligand **49** by using deuterium, with the aim of decreasing any nonradiative vibrational quenching due to the presence of C–H oscillators within the structure. The resulting complex, Yb(**49**), exhibited high luminescence and long lifetime (65 μs) in D_2O, which is one of the longest reported to date. They also prepared polynuclear complexes in water, $[(Yb\mathbf{48})_2Tb_x]$ or $[(Yb\mathbf{49})_2Tb_x]$ (where x = 1–3), where the Tb^{3+}-centred emission was observed for both complexes. These complexes were found to exhibit ytterbium to terbium upconversion sensitisation upon excitation at 980 nm.[212] This work was further developed by the team when preparing $[Ru(\mathbf{bpm})_3(LnL_3)_3](BAr^F{}_4)_2$ hetero-tetrametallic complexes, where Ln = Lu^{3+} and Yb^{3+}. These complexes were obtained by using the $[Ru(\mathbf{bpm})_3]^{2+}$ core, where **bpm** is 2,2′-bipyrimidine, together with Ln(**tta**)$(H_2O)_3$ fragments. Particularly, the authors found that upon excitation at 980 nm, the Yb^{3+} complexes exhibited upconverted emission of the ^{3}MLCT state of the central Ru(II) core at 636 nm. This represents the first example

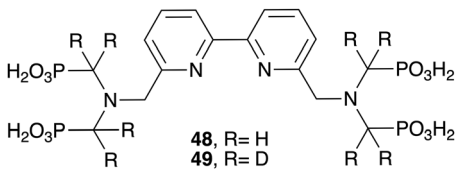

Fig. 24 Structural formulas of ligands **48** and **49**.[211–213]

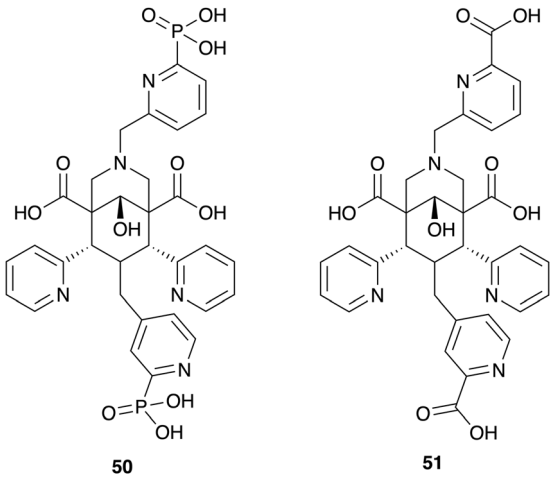

50 51

Fig. 25 Structural formulas of ligands **50** and **51**.[214]

of an f → d molecular upconversion, offering new ways for the development of efficient upconverting molecular devices using heterometallic complexes.[213]

More recently, Nonat and collaborators have reported two bispidine-based ligands containing chiral centres **50** and **51** (Fig. 25) and their Tb^{3+} complexes. The modifications in the ligand structure led to different complexation and luminescence properties, where the Tb(**51**) complex exhibited a higher luminescent quantum yield and stronger kinetic inertness, making it promising to future applications as a chiral luminescent probe.[214]

An alternative approach to enhancing the functionality of supramolecular architectures involves the incorporation of multiple binding sites within the ligand design. By incorporating multiple sites for Ln^{3+} coordination within a ligand, the scope for the potential self-assemblies to be formed is increased. Therefore, the following sections will discuss in detail ligands with more than one binding site for Ln^{3+} ions and their resulting self-assemblies.

3. Recent advances in polymetallic Ln^{3+}-derived self-assemblies

The formation of more complex intricate self-assemblies, as functional and responsive architectures, and higher order structures, remains one of the main objectives of supramolecular self-assembly chemistry. The use of lanthanides is particularly attractive in the design of such systems due to their unique coordination and physical properties, as discussed above. This section will focus on the development of such systems. Besides the increase in complexity of their resulting self-assemblies, the reported polynuclear Ln^{3+} systems developed to date have demonstrated to be promising in a range of applications such as in sensing,[215–219] and hence, host–guest chemistry,[220] imaging,[221] single molecular magnets,[222–224] and in the formation of other types of stimuli-responsive materials.[28,29,57,96,225] The development of polymetallic Ln^{3+}-directed self-assemblies over recent times is noteworthy and, as mentioned before, there are several in-depth reviews that provide some detailed insights into this fast emerging area of research within lanthanide chemistry.[57,75,226–228]

It is well known that the development of different lanthanide self-assembled architectures depends on multiple factors, making the prediction of the final architecture both complex and challenging.[93] Moreover, the properties of the resulting complexes are highly dependent on their architecture. Thus, understanding the factors that control the formation of a specific supramolecular architecture, as well as the pathways through which these assemblies are formed is crucial to control their properties.

Normally, the formation of a supramolecular architecture can be concentration-dependent due to the labile non-covalent interactions between the ligands and the metal ions. In most cases, higher order supramolecular structures are obtained by increasing the overall concentration of both the metal ions and the ligands. Moreover, it was found that the stoichiometry of the complexes, as well as the architecture, could be metal ion-dependent. Furthermore, counter-anions and solvents are also factors that influence the local environment of the self-assembly, and hence, the final self-assembled architecture, as they can act as templates within the self-assembly process. Thus, a small modification in the reaction conditions (*e.g.* solvent polarity or metal salt used) can result in different supramolecular structures with diverse properties. Additionally, small changes in the ligand design and a variation in the metal ion used have shown a high effect on the final self-assembly architecture.[227] In the next section, we will discuss in some detail the examples reported in recent years, highlighting the key advances and emerging trends within this field.

3.1. Lanthanide-derived helicates

The term 'helicate' was first introduced by Jean-Marie Lehn in 1987 to describe a class of self-assembled supramolecular copper compounds (linear polypyridyl ligands), exhibiting a helical-type architecture with similar characteristics to the double-helix structure of DNA.[229] A supramolecular helicate consists of one or more organic ligands that are wrapped helically around a series of metal ions that define the axis of helicity. Since Piguet and co-workers reported the first dinuclear triple-stranded helicate with lanthanide metal ions in 1997,[230] a vast array of lanthanide-derived helicate complexes has been described. Indeed, Bünzli and Piguet research groups, pioneered the field, and both researchers have carried out an extensive work on studying multimetallic Ln^{3+}-directed (as well as using mixed d- and f-metal) assemblies throughout the years, providing key insights that have contributed significantly to the current state of the field.[8]

As mentioned above, recent studies have demonstrated that slight alterations to parameters such as the ligand : metal ratio (L : M), solvent, ligand design or concentration can significantly impact the architectures achieved in ditopic tridentate ligands, as well as their resulting photophysical properties.[227,231,232] To achieve helicates, the ligand should fulfil specific requirements,

such as, possessing flexibility, to enable to form stable helicoidal architectures upon metal ion coordination.[13,233] Raymond and co-workers have showed that the use of C_2-symmetric bis-bidentate ligands enables the achievement of M_2L_3 helicates. In addition, depending on the nature of the metal ion this could be more challenging, for example in the case of lanthanides, this is dictated by their large and variable coordination numbers. However, recent studies have demonstrated that small changes in the spacer length can be a key factor to achieve a specific architecture.[58,234] Inspired by the architecture and structural characteristics of biological macromolecules, ditopic tridentate ligands are frequently used in designing polymetallic helicoidal Ln^{3+}-derived self-assemblies. These systems possess two distinct binding sites for Ln^{3+} coordination, thus increasing the complexity of the self-assembly process, leading to the formation of 3 : 2 (L : M) supramolecular complexes, such as helicates. Among the wide variety of tridentate ligands, the dpa motif is one of the most extensively used, due to its versatility in developing both monometallic and polymetallic Ln^{3+}-derived assemblies.

Over the years, the Gunnlaugsson group has synthesised many examples of ditopic **dpa** ligands featuring chiral naphthalene arms for the development of Ln^{3+}-derived helicates.[235–237]

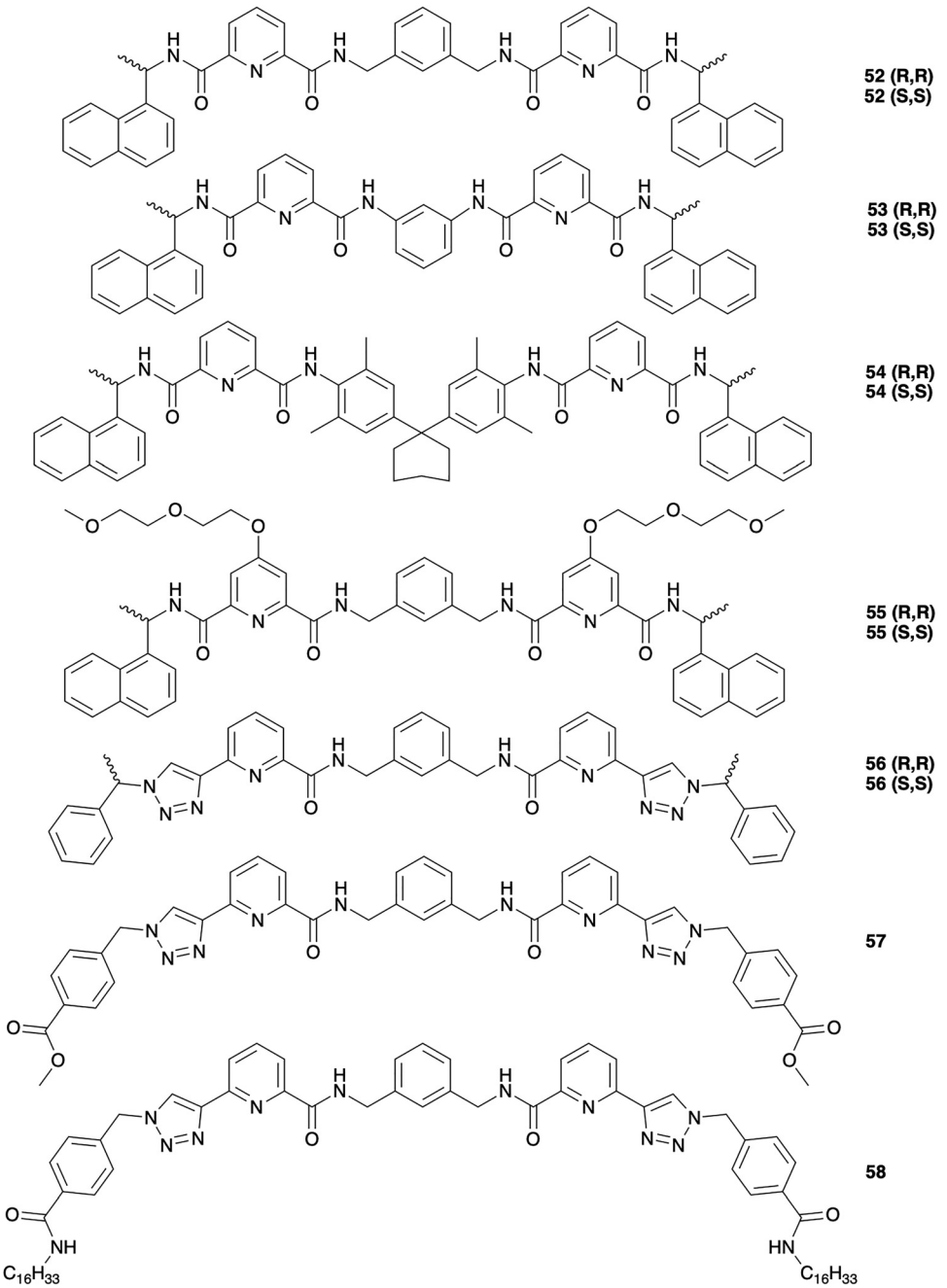

Fig. 26 Structural formulas of chiral **dpa**-derived ligands **52–58**.[231,239,240]

These chiral arms act as an antennae alongside the **dpa** binding units and play a key role in sensitising and enabling the CPL of the Ln^{3+} ions. More recently, Kotova *et al.* have investigated how differences in spacer sizes in ditopic **dpa**-based symmetric ligands affect the overall photophysical properties of the resulting $Eu_2(\mathbf{L})_3$ (L = **52–54**) (Fig. 26) complexes through *in situ* studies.[231]

For these examples, ligands **52** and **53** feature a short aryl spacer, while the ligand **54** displays a bulkier spacer possessing a cyclohexane ring. The examination of the spectroscopic titration data (*i.e.* carried out under kinetic control), where the UV-Vis, the fluorescence of the ligand and the delayed lanthanide emission were monitored and fitted using non-linear regression analysis software, showed that **52–54** all formed species $Eu(\mathbf{L})_2$, $Eu_2(\mathbf{L})_2$ and $Eu_2(\mathbf{L})_3$, with $Eu_2(\mathbf{L})_3$ being the dominant species (normally formed in *ca.* 90–95% yield) upon the addition of 0.67 equivalents of the metal ions, with slightly higher binding constants when the linker between the **dpa** moieties was shorter (**52** and **53**), and the other species being formed at higher Ln-ion equivalents.

Furthermore, further photophysical studies of the $Eu_2(\mathbf{L})_3$ complexes revealed negligible differences in their luminescence lifetimes. However, the quantum yield decreased with 'increasing' the hindrance of the linker, which was also accompanied by a decrease in the corresponding η_{sens} (the sensitisation efficiency) value of the Eu^{3+} centers within the self-assembly structures.

The Gunnlaugsson group has further expanded on their ditopic **dpa** ligand designs, reporting compounds **55(*R*,*R*)** and **55(*S*,*S*)** (Fig. 26) and their self-assembly with Eu^{3+} in protic polar solvents.[238,239] The resulting helicates $Eu_2(\mathbf{55(\mathit{R},\mathit{R})})_3$ and $Eu_2(\mathbf{55(\mathit{S},\mathit{S})})_3$ were obtained in high yields (78% and 71%, respectively, under thermodynamic control), with Eu(III)-quantum yields of 3.5% and 3.2% in methanol and 4.1% and 4.4% in acetonitrile, respectively.[238] These values were again lower than their previously reported mononuclear trinuclear 'sliotar' counterparts, which could be attributed to the lower efficiency of sensitisation between the ligand antenna and the Eu^{3+} core, and increased quenching pathways within Ln_2L_3 structures compared to LnL_3 ones.[137] The studies of higher order assemblies using $Eu_2(\mathbf{55(\mathit{R},\mathit{R})})_3$ showed that their thin LB films were formed only when using acetonitrile, while exclusive formation of monodisperse spherical aggregates was observed from methanol or methanol/water mixtures.

Recently, researchers in the Gunnlaugsson group have also reported the *in situ* formation of dimetallic triple stranded helicates using the **tzpa** ligands **56(*R*,*R*)** and **56(*S*,*S*)** (Fig. 26).[239] As triazol ligands show higher sensitisation of Tb^{3+}-centred emissions, these were formed (under thermodynamic control) as $Tb_2(\mathbf{56})_3$, and the subsequent self-assembly studies (under kinetic control) between **56** and Tb^{3+} in solution suggested the formation of 2:2 and 2:3 M:L dimetallic helicates, where $Tb_2(\mathbf{56})_2$ stoichiometry was the dominant.

More recently, the group has expanded its research by modifying the **tzpa** motif and synthesizing the first examples of **tzpa** ligands with carboxylic methyl ester (**57**) and long hydrophobic alkyl chains (**58**). It was anticipated that the incorporation of hydrophobic chains into the ligand would facilitate the formation of higher order self-assembly architectures.

They also performed the synthesis of the derived luminescent di-metallic triple-stranded Tb^{3+} helicates $[Tb_2(\mathbf{L})_3]$, under both thermodynamic and kinetic control. The material features of the helicates were investigated using SEM imaging in a range of solvents, where it was established that they exhibited different morphological features, not only when compared to the ligands, but also between both types of helicates (*e.g.* short *vs* long alkyl chains).

Recent examples of the **dpa** motif employed in ditopic ligands included the incorporation of the moiety into ligand **59** (Fig. 27(A)), as reported by Yan and co-workers, which also featured a photochromic diarylethene spacer.[241] The presence of the photochromic diarylethene spacer plays a key role in this design, as it enables light-driven control over metal coordination, this being of particular interest for developing light-driven molecular switches. Self-assembly with Eu^{3+} resulted in the formation of the chiral $Eu_2(\mathbf{59})_3$ helicate, which displayed conformational changes when exposed to UV irradiation at 275 nm. This process was reversible, as when $Eu_2(\mathbf{59})_3$ was exposed to visible light irradiation at 526 nm, the switching was returned to its original form (Fig. 27(A)) with concomitant changes in the spectroscopic readout. Interestingly, in the closed-ring state, the complex exhibited a decrease in the Eu^{3+} luminescence, as well as a decrease in the CPL g_{lum} values, thus establishing $Eu_2(\mathbf{59})_3$ as a reversible optical and chiroptical switch.

Sun and co-workers reported compound $Eu_2(\mathbf{60(\mathit{R},\mathit{R})})_3$, which is the first example of a chiral photoresponsive helicate derived from a dithienylethene ligand **60**.[242] As for the previous example, both **60** and its resulting Eu^{3+} helicate exhibited a UV-induced conformation. Furthermore, the study revealed a transfer of chirality from **60** to the Eu^{3+} centre, resulting in the formation of *P* or *M* diastereomers, respectively (Fig. 27(B)).

The authors also developed the hexameric lanthanide-organic capsule derived from **tzpa** ligands **61** and **62(*R*,*R*)/(*S*,*S*)** (Fig. 28).[220] Upon complexation of ligand **61** with $Eu(OTf)_3$, a $Eu_2(\mathbf{61})_3$ triple-stranded helicate was isolated. However, when the ligand underwent complexation with $Eu(ClO_4)_3$, a concentration-dependent formation of a new species occurred, which became the dominant species at concentrations above 72.6 mM, mimicking the self-assembly process of the R_6 insulin hexamer. Through ESI-TOF-MS, the new concentration-triggered species, $[Eu_2(\mathbf{61})_3]_6(ClO_4)_{36}$, were elucidated. The hexamerisation of $Eu_2(\mathbf{61})_3(OTf)_6$ was also achieved by adding ClO_4^- to a solution of this species, as confirmed using ^1H NMR titration studies. A solvent-triggered helicate-to-hexamer transformation was observed by adding THF-d_8 to a solution of $[Eu_2(\mathbf{61})_3]_6(ClO_4)_6$ in a CD_3CN:CD_3OD (c = 0.02 mM) mixture, leading to the appearance of $[Eu_2(\mathbf{61})_3]_6(ClO_4)_{36}$. During this process, aggregation-induced emission (AIE) behaviour was also observed, with a decrease in the Eu(III)-centred emission initially, followed by a 2.5 times enhancement as the THF content increased, together with an increase in the Eu^{3+} quantum yield from 22.8% to 46.2%. Furthermore, excited-state

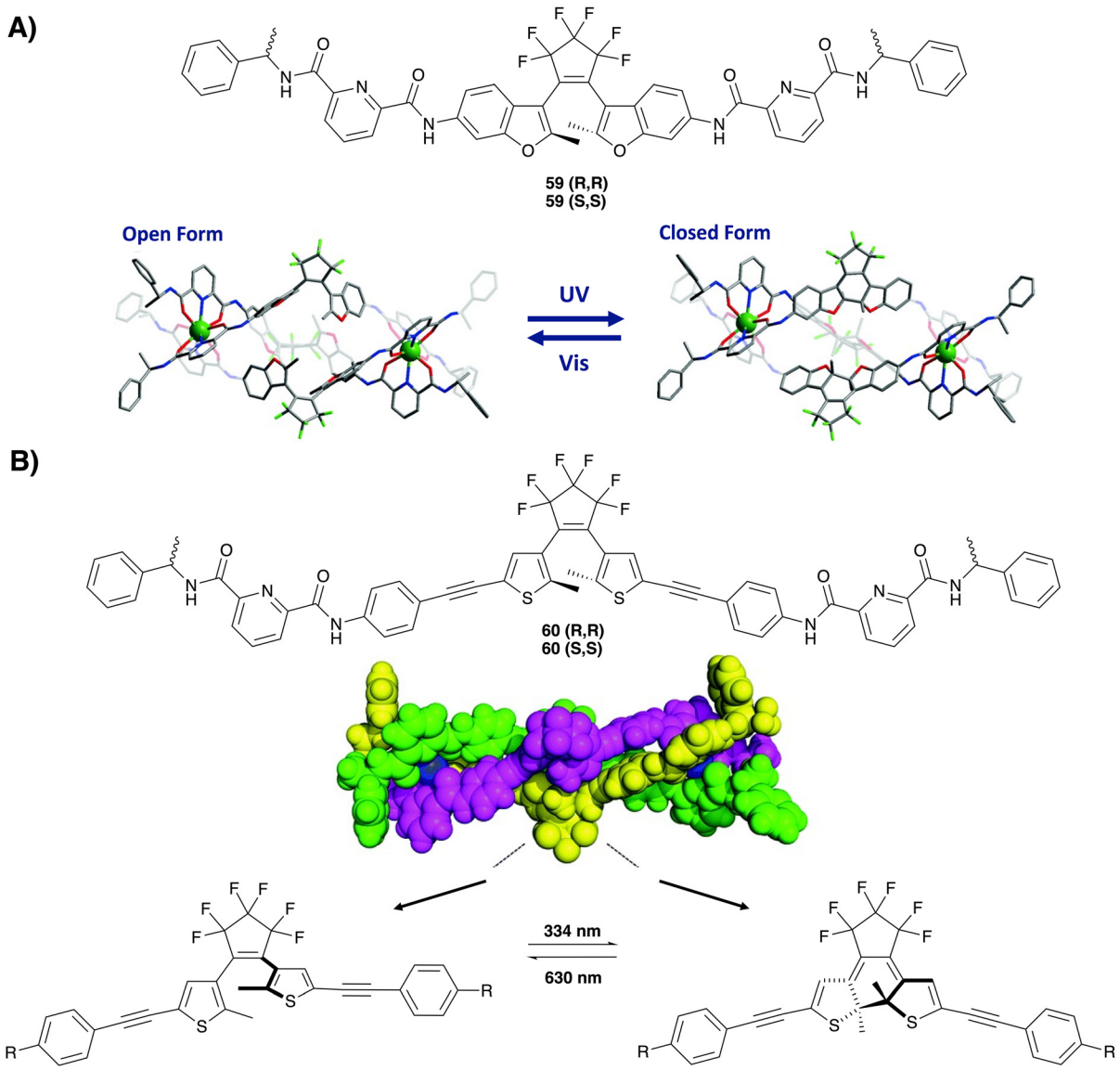

Fig. 27 (A) Structural formula of ligand **59** and structural reversible change of the Eu_2(**59**)$_3$$(OTf)_6$ helicate upon alternating UV and visible light irradiation.[241] (B) Ligand **60** and optimized structure of the *M*-(ΛΛ)-Eu_2(**60**(***R,R***))$_3$ helicate. Photoirradiation at 334 nm transforms the open form of the diarylethene moiety into a closed form and can be reversed back upon irradiation at 630 nm.[242] Adapted from ref. 242 with permission from the Royal Society of Chemistry, Copyright©2018.

lifetime measurements showed the presence of a longer decay in CH_3CN : THF (1 : 29) compared to that measured in CH_3CN alone.[220] This outcome confirms a complete helicate-to-hexamer transformation triggered by solvent conditions. The hexameric $[Eu_2(\mathbf{61})_3]_6(ClO_4)_{36}$ assembly also displayed aggregation-induced water stability, which is a highly favourable property owing to many polynuclear Ln^{3+} assemblies dissociating under aqueous conditions. Further host–guest studies on this system have demonstrated that the $[Eu_2(\mathbf{61})_3]_6(ClO_4)_{36}$ system exhibits encapsulation and selectivity towards terpene drugs within the central cavity of the hexamer. The chiral analogue ligands, **62**(***R***,*R*)/(*S*,*S*), formed enantiopure $Eu_2(\mathbf{62})_3$ complexes, which subsequently resulted in the formation of enantiopure $[Eu_2(\mathbf{62})_3]_6(ClO_4)_{36}$ hexamers. This was confirmed through CD and CPL studies.[220]

A similar type of linker was used by Sun and co-workers who reported the self-assembly of **63**(***R,R***)/(***S,S***) with La^{3+}, where a 2/3 M/L ratio resulted in a bimetallic triple-stranded helicate $La_2(\mathbf{63})_3$. By changing the M/L ratio to 1/1, the resulting self-assembly changed to a mononuclear pincer complex, La(**63**) (Fig. 29). CD studies revealed that both supramolecular structures were found to be enantiomeric. Subsequently, the catalytic properties of both complexes were investigated in relation to asymmetric Friedel–Crafts alkylation reactions. In these reactions, $La_2(\mathbf{63})_3$ showed a lower yield but higher enantiomeric excess products compared to La(**63**).[243]

The authors completed this work by changing the chiral naphthalene groups for an achiral isopropyl amine, giving rise to the ligand **64** (Fig. 29). This modification of the ligand design

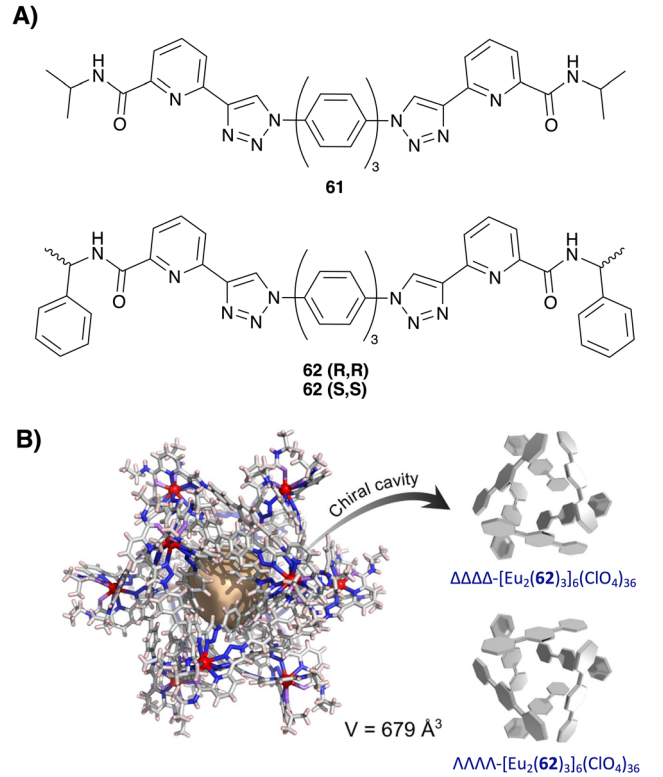

Fig. 28 (A) Structural formulas of the ligands **61**, **62(*R*,*R*)** and **62(*S*,*S*)**. (B) Cavity volume and enantiopure chiral cavities of $[Eu_2(\mathbf{61})_3]_6(ClO_4)_{36}$.[220] Adapted from ref. 220 with permission from the American Chemical Society, Copyright©2021.

resulted in the formation of mono-ligand bridged dinuclear La^{3+} complex $La_2(\mathbf{64})_3$ when the M/L ratio is 2/3, while when the ratio was 1/1, a La^{3+}-derived polymer, $[La_2(\mathbf{64})_2]_n$, was obtained.

It has been shown that by adding ligands or lanthanide ions between these structures, the reversible formation of both structures could be achieved. Moreover, the authors added the chiral ligand **20** to the self-assembly to induce chirality into the complexes, leading to the mononuclear La(**64**)(**20**) self-assembly, which exhibits a CD signal and can be used to determine the enantiomeric excess. This strategy demonstrates the versatility of lanthanide-derived self-assemblies and provides a new method for enantiomeric excess sensing.[244]

Sun and co-workers extended their research by synthesising enantiopure bis-tridentate ligands, featuring both an axial and a point chirality, having reported the stereo-controlled self-assembly process of a family of both homochiral and mesomeric La^{3+} and Eu^{3+} triple-stranded helicates. Using CD and CPL spectroscopy, it was revealed that axial chirality was a key factor in determining the configuration of the metal ion centre, controlling the helicity of the supramolecular architecture. The resulting homochiral helicates demonstrated enhanced enantioselectivity in the luminescent detection of D/L-leucinol, highlighting the importance of precise stereochemical control for optimizing the applications of the functional materials.[245]

As mentioned above, Piguet and colleagues have also carried out extensive research within the field of helicates derived from lanthanides.[246,247] For example, they reported a study revealing the possibility of the thermodynamic self-assembly formation of luminescent heterodimetallic helicates, by using the hexadentate gallium-based tripodal ligands **65** and **66** (Fig. 30).[248] Kinetic analysis showed that the $[GaLn(\mathbf{L})_3]^{6+}$ helicates (where Ln = Y^{3+}, Eu^{3+}, and Er^{3+}) retain the triple-stranded helical structure even when exposed to lanthanide exchange conditions. They also reported that the attachment of a second ligand slows down the metal exchange process, allowing the closed–shell $[GaYGa(\mathbf{66})_3]^{9+}$ to be used as an inactive matrix for diluting the open–shell $[CrErCr(\mathbf{66})_3]^{9+}$ structural isomer. This leads to the detection of molecular upconversion at room temperature, opening up the way for optimizing processable, NIR to visible upconverting materials.[233] They further extended their investigations to heterometallic helicates derived from d- and f-metal ions, although these are not discussed in this review.[249–251]

Riddell and co-workers investigated the effect of the ligand backbone symmetry on polynuclear lanthanide self-assemblies. By changing a symmetric ethylene linker with an asymmetric amide (Fig. 31), they discovered the formation of a $Ln_6(\mathbf{67})_6$ complex (Ln = Sm^{3+}, Eu^{3+}, Gd^{3+}, and Tb^{3+}), with unsaturated metal centres. Moreover, the counter-ions and the ionic radii of Ln ions were found to be a key factor in the final architecture of the complex.[252] It was found that when the central amide moiety in ligand **67** was changed for an ethylene bridge, ligand **68**, a $Ln_2(\mathbf{68})_3$ complex, was obtained, indicating the formation of a helicate. These complexes showed different luminescence properties, with $Eu_6(\mathbf{67})_6$ exhibiting shorter luminescence lifetimes and lower quantum yields, than $Eu_2(\mathbf{68})_3$. This demonstrates the role of the ligand design on the self-assembly process and on the luminescence properties of the complexes.[252]

3.2. Lanthanide-derived metallocages

Besides the study of helicate systems, there has been a recent focus on the employment of the ditopic tridentate motif to achieve other higher-order assemblies. Lanthanide metallo-cages are interesting self-assembled architectures with potential applications in different fields such as catalysis, sensing, host–guest, imaging or magnetism.[253–255] Metallocages are three-dimensional architectures formed by the coordination of multidentate ligands to metal ions positioned at the vertices of the cage. It is well known that the design of the ligand influences the final architecture of the metallo-supramolecular structure, and thus, on its functionality. Different characteristics such as the size, or the flexibility of the ligands employed, are known to be key factors for the self-assembly of metallocages. Thus, a flexible ligand usually leads to metal complexes with low nuclearity, while rigid ligands used to favour polynuclear compounds. Hence, the size and shape of the final architecture of the complex can be controlled by the distance and the orientation of the donor atoms.[256] Moreover, the presence of bulky groups, as well as the length-to-width ratio of a ligand, or the metal ion size, can be used to control the self-assembly process.[253,257,258]

The Sun group has been particularly active in developing this topic, with their effort leading to significant research in

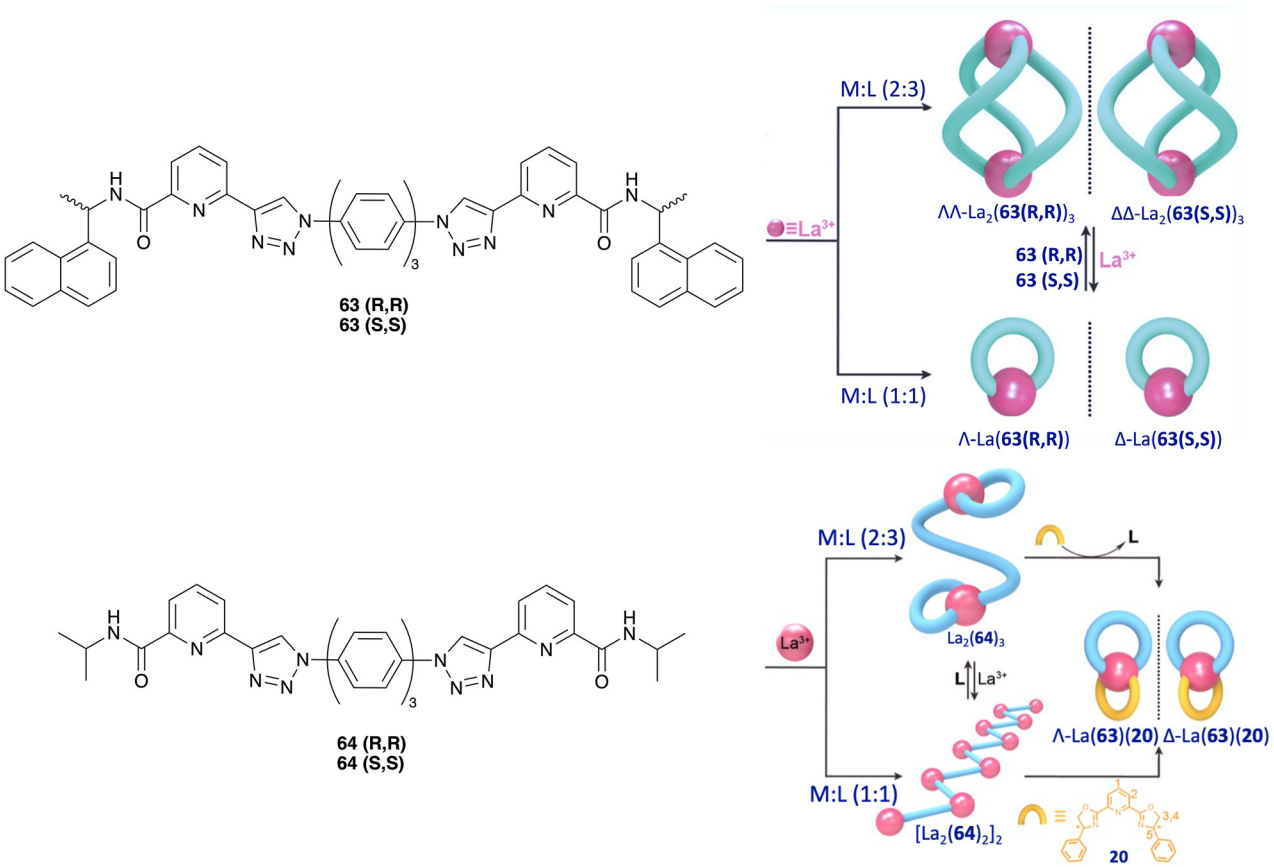

Fig. 29 Coordination-directed stereo-controlled self-assemblies derived from ligands **63(*R*,*R*)/(*S*,*S*)** and **64(*R*,*R*)/(*S*,*S*)** by varying the metal/ligand ratio.[243,244] Adapted from ref. 243 and 244 with permission from the Royal Society of Chemistry, Copyright©2021 and 2022.

recent years on Ln^{3+}-directed polymetallic assemblies, including the design of low-symmetry lanthanide metallocages that can distinguish and bind selectively to higher fullerene isomers.[259]

As an example of the metallocages prepared by Sun and co-workers, then they reported ligands **69–72** for the purpose of exploring how increasing the distance of the linker between **dpa** moieties affects the self-assembly process with Ln^{3+} ions (Fig. 32).[260]

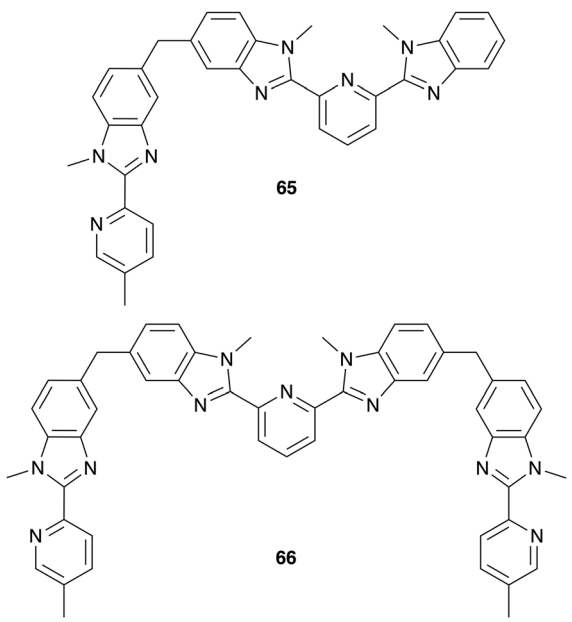

Fig. 30 Structural formulas of ligands **65** and **66** synthesised by Piguet and colleagues.[248]

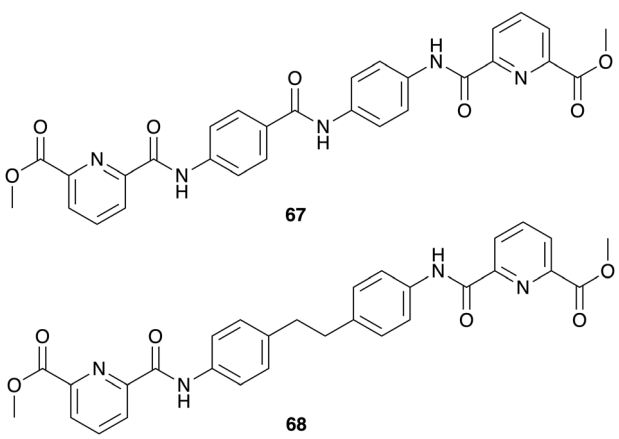

Fig. 31 Structural formulas of ligands **67** and **68** synthesised by Riddell and co-workers.[252]

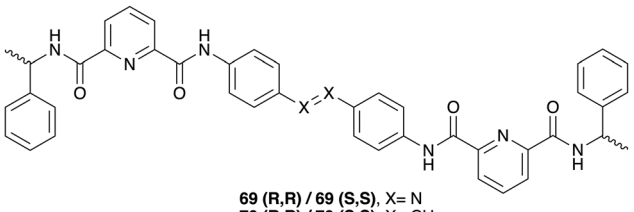

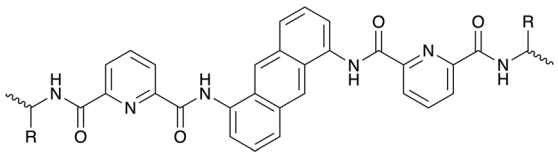

Fig. 32 Structural formulas of ligands **69–72** synthesised by Sun's research group.[260]

The Sun group found that when the spacers are flexible (*e.g.* ligands **69** and **70**), a mixture of helicates $Ln_2(\mathbf{L})_3$ and metallo-cages $Ln_4(\mathbf{L})_6$ are formed. However, by using rigid spacers (*e.g.* ligands **71** and **72**), a mixture of a helicate $Ln_2(\mathbf{L})_3$ and a cubic complex with the formula $Ln_8(\mathbf{L})_{12}$ are formed, as shown in Fig. 33, the formation of which depends on the concentration. These cubic-derived complexes were found to have potential as 'switch-off' sensors towards explosives, with high selectivity and sensitivity for the electron-deficient nitroaromatic compound picric acid.[260] This study further confirmed how small changes in the ligand structure can have influence on the outcome of the supramolecular architecture of the complexes, and thus on their properties.

The authors also designed ligands **73** and **74** (Fig. 34), where the tridentate moiety combines the carboxamide unit of **dpa** and the oxazoline of **pybox**.[232]

Upon self-assembly with Eu^{3+}, it was observed that both ligands formed $Eu_2(\mathbf{L})_3$ helicates (L = **73**, **74**). However, when **73** underwent self-assembly with Eu^{3+} at a high concentration (4.8×10^{-1} M), the tetrahedral cage $Eu_4(\mathbf{73})_6$ was shown to be formed. This represents the first reported example of a

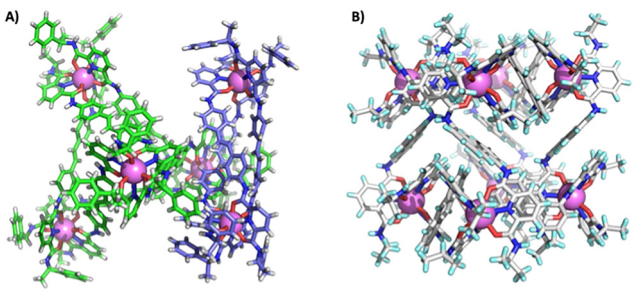

Fig. 33 X-Ray crystal structure of the mixture of $Eu_2(\mathbf{70}(\mathbf{R},\mathbf{R}))_3$ and $Eu_4(\mathbf{70}(\mathbf{R},\mathbf{R}))_6$, with only one helicate (left) and one tetrahedron shown for clarity (highlighted blue and green, respectively), and $Nd_8(\mathbf{72})_{12}$, where Nd = purple; C = white; N = dark blue; O = red; H = cyan (right).[260] Adapted from ref. 260 with permission from the American Chemical Society, Copyright©2017.

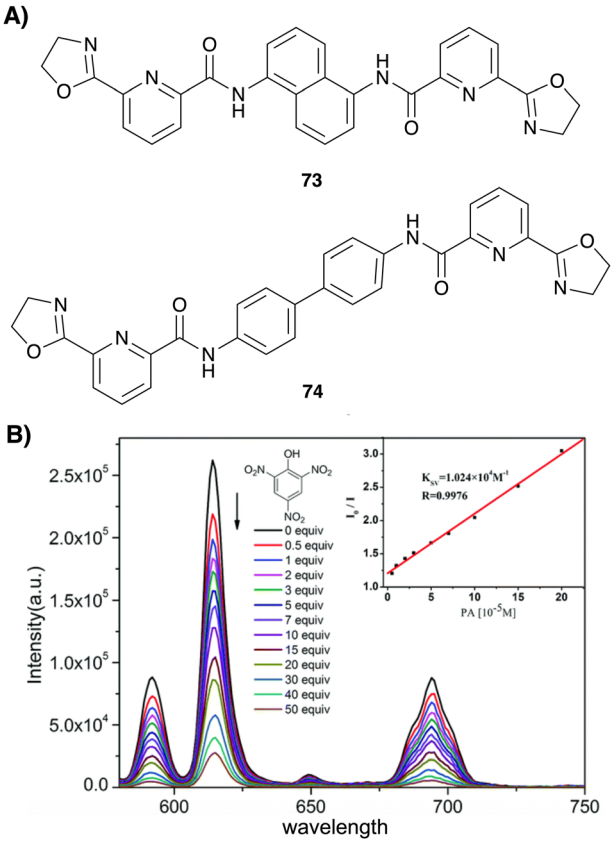

Fig. 34 (A) Structural formulas of ligands **73** and **74**. (B) Fluorescence emission spectra of $Eu_4(\mathbf{73})_6(OTf)_{12}$ (c = 1×10^{-5} M) in CH_3CN upon addition of picric acid (λ_{ex} = 350 nm), Inset: Stern-Volmer plot, reported by Sun and colleagues.[232] Adapted from ref. 232 with permission from the Royal Society of Chemistry, Copyright©2017.

transformation induced by concentration. This complex exhibited high stability and did not reassemble into the $Eu_2(\mathbf{73})_3$ species upon dilution. Furthermore, the ability to detect electron-deficient nitroaromatics was demonstrated, with a notable selectivity towards picric acid at the pbb level. In contrast, the $Eu_4(\mathbf{74})_6$ species were not observed under the same high-concentration conditions and only the $Eu_2(\mathbf{74})_3$ helicates were present. This outcome is attributable to the less sterically constrained nature of the linker, which favours the formation of a helicate.[232]

Later, the authors reported an attractive new approach towards polynuclear water-stable Ln^{3+}-directed self-assemblies with potential applications for bioimaging and drug delivery.[261] The rationale behind the ligand design, which involved the joining of both tridentate motifs through the 4-pyridyl position (Fig. 35), was to develop a more rigid ligand that would in turn aid in the formation of more stable polynuclear structures with Ln^{3+}.

When ligand **75** reacted with $Ln(OTf)_3$ (Ln^{3+} = Eu^{3+}, Gd^{3+}, and Tb^{3+}) in a 3/2 L/M ratio alongside 12 equivalents Et_4NOH in DMSO ($[(Et_4N)_4(\mathbf{75})]$ = 1.44×10^{-5} M in DMSO), a mixture of self-assemblies with the stoichiometry $Ln_4(\mathbf{75})_6$ and $Ln_6(\mathbf{75})_9$ were obtained. Moreover, an increase in ligand concentration resulted in the formation of more complex structures such as $Ln_6(\mathbf{75})_9$. It was also observed that the existence of the $Ln_4(\mathbf{75})_6$

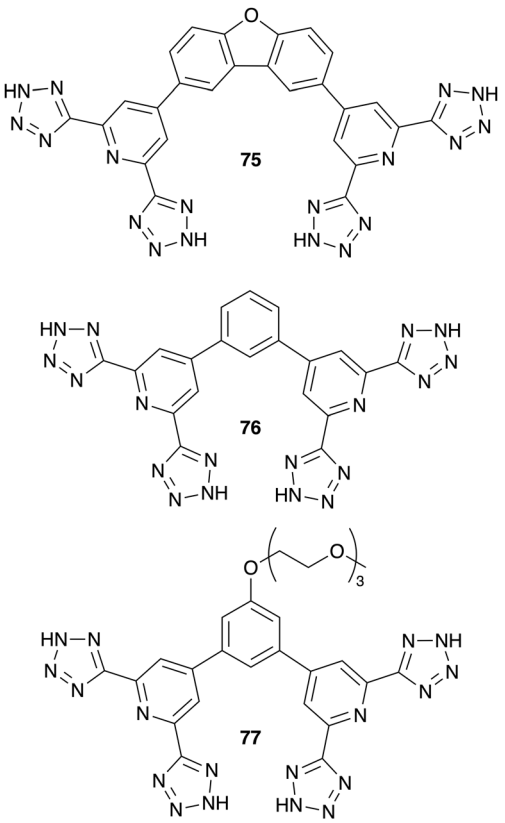

Fig. 35 Structural formulas of ligands **75–77** reported by Sun and colleagues.[261]

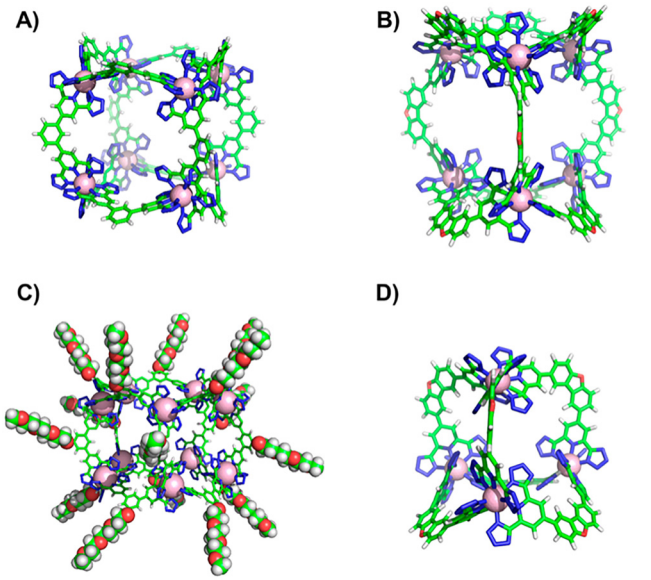

Fig. 36 Crystal structures of (A) $K_{24}Eu_8$(**76**)$_{12}$, (B) $K_{18}Eu_6$(**75**)$_9$, and energy optimised structures of (C) $K_{30}Eu_{10}$(**77**)$_{15}$, and (D) $K_{12}Eu_4$(**75**)$_6$.[261] Adapted from ref. 261 with permission from the American Chemical Society, Copyright©2020.

complex was not a result of the dissolution of the Ln_6(**75**)$_9$ complex. When **76** or **77** underwent identical complexation conditions, the predominant self-assembly was Ln_8(**L**)$_{12}$.[261] When the base was switched from Et_4NOH to KOH, then this resulted in the formation of crystals with the chemical formula $K_{18}Eu_6$(**75**)$_9$, which were obtained by slow diffusion of acetone into DMSO. Upon dilution of the solution to the concentration of 10^{-4} M, a total transformation of $K_{18}Eu_6$(**75**)$_9$ to $K_{12}Eu_4$(**75**)$_6$ was achieved.

In the case of **76**, the use of KOH as the base resulted in the observation of a mixture of both $K_{24}Eu_8$(**76**)$_{12}$ and $K_{30}Eu_{10}$(**76**)$_{15}$. Furthermore, treatment of **77** with $EuCl_3$ and KOH in water at lower concentrations ($\sim 10^{-6}$ M) resulted in the formation of $K_{30}Eu_{10}$(**77**)$_{15}$ self-assembly. The attempts to crystallize $K_{30}Eu_{10}$(**77**)$_{15}$ resulted in a gradual transformation of this assembly to the octanuclear $K_{24}Eu_8$(**77**)$_{12}$ complex, suggesting that its formation was the thermodynamic product (Fig. 36). This investigation illustrates the intricate effects that the choice of Ln^{3+} salt, solvent, base and concentration conditions have on the resulting self-assemblies formed.[261] Furthermore, it was later shown that the stability and luminescence performance of such systems can be increased through embedding them into mesoporous silica using a "ship-in-a-bottle" synthetic strategy.[284]

Photophysical studies on these systems demonstrated the attractive luminescence properties of Tb_8(**76**)$_{12}$ and Eu_8(**77**)$_{12}$ complexes, exhibiting high quantum yields in DMSO and water. Moreover, the Gd_8(**77**)$_{12}$ complex exhibited a considerably prolonged retention time in tumour sites in comparison to commercially available Gd^{3+}-containing contrast agents, suggesting its potential application as a magnetic resonance imaging contrast agent. The mixed Gd^{3+}/Eu^{3+} cages have potential as dual-mode imaging agents, making these complexes unique in nature.[261]

Sun's group has continued its effort within this area of research and reported a series of Ln^{3+}–Pt^{3+} (Ln^{3+} = Nd^{3+}, Eu^{3+}, Yb^{3+}, and Lu^{3+}) cages based on **dpa**-containing ligands **78** and **79** (Fig. 37).[262] The Pt^{3+}–acetylide unit was specifically chosen for its use in photo-functional complexes as well as its ability to efficiently sensitise Ln^{3+} *via* metal-to-ligand charge transfer (MLCT). This property allowed the excitation to the visible region in the case of Nd^{3+}- and Yb^{3+}-based cages. Furthermore, it was observed that the Ln_4(**79**)$_6$ (Ln^{3+} = Eu^{3+} and Yb^{3+}) assembly showed temperature-dependent red and near-infrared emission properties. Therefore, the resulting Ln_4(**79**)$_6$ complexes were tested as potential temperature sensors. The different angles of the ligands resulted in either helicates or tetrahedral cages upon self-assembly with Ln^{3+}.

In a related study, the Sun group designed C_2-symmetric triazole-derived ligands with different linear lengths in the spacer with the aim of obtaining multinuclear luminescent Eu^{3+}-derived metallo-cages. They found that by increasing the length of the spacer, the self-assembly process was indeed modulated. In the case of the shorter spacer (with one phenyl ring), a tetranuclear Eu_4L_6 metallo-cage was obtained, while with the larger spacer (three phenyl rings) the 'classical' dinuclear Eu_2L_3 helicate was formed. In the case of the ligand with two phenyl rings in the spacer, a mixture of a helicate and a metallo-cage was obtained. However, when the concentration of this ligand was increased, the complete transformation of

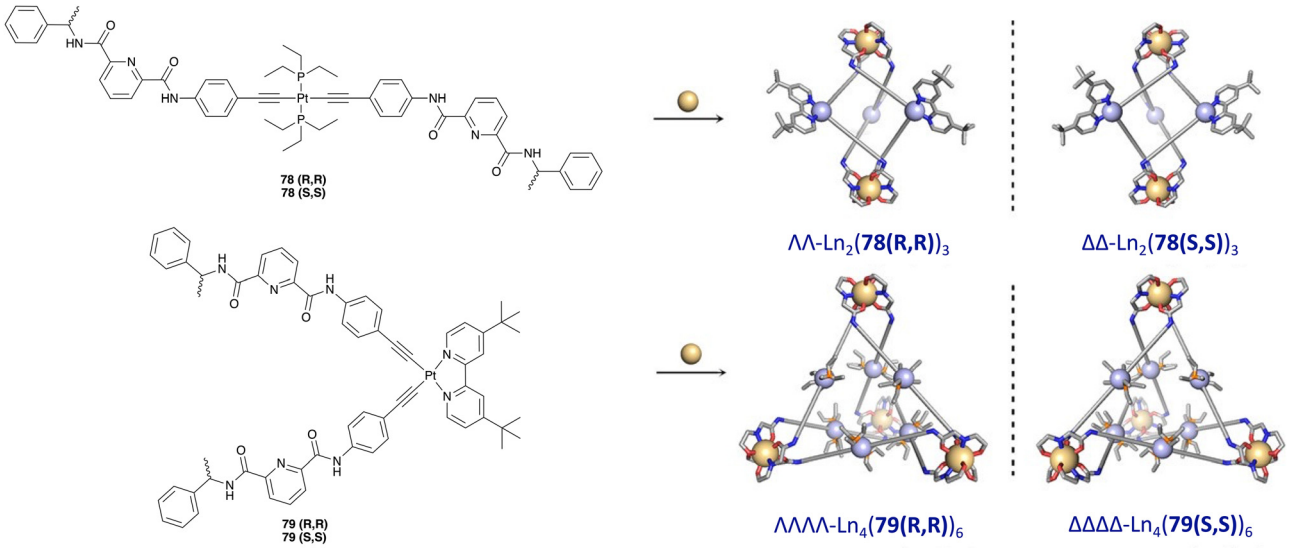

Fig. 37 Stereo-controlled self-assembly of heterometallic cages derived from **78** and **79**.[262] Adapted from ref. 262 with permission from the American Chemical Society, Copyright©2022.

the helicate to the cage compound occurs, in a similar manner to that described above. The resulting Eu-based cages exhibited high luminescence and also gave rise to CPL. This study is another approach for the development of lanthanide-based cages.[263]

Lately, the authors have designed stereoselective self-assembly ligands **80(*R*,*R*)**/**80(*S*,*S*)** (Fig. 38), to achieve enantiopure tetrahedral complexes derived from Sm^{3+}, Eu^{3+} and Yb^{3+}.[264] The authors achieved the formation of enantiopure tetranuclear metallo-cages, Ln_4(**80**)$_6$, with the metal stereochemistry defined by using the C_2-symmetric ligands **80(*R*,*R*)**/**80(*S*,*S*)**. In the cases of $YbEu_4$(**80**)$_6$ and $YbSm_4$(**80**)$_6$, these tetrahedral complexes exhibited the ability of emitting upconverted circularly polarized luminescence (UCCPL), being the first example of UCCPL in lanthanide supramolecular complexes.

In addition to concentration-triggered helicate to other higher-order structural transformations, Law and co-workers have reported ditopic **dpa**-based ligands **81–83** (Fig. 39), where the use of rigid 2,6-diaminoanthraquinone as a linker was shown to favour the formation of tetrahedral cages when undergoing Ln^{3+}-directed self-assembly.[265] The arms of these ligands, although similar, contained different point chiralities with the aim to investigate how these small differences affect the self-assembly process with Eu^{3+}.

The differences observed in the CPL and the CD, as shown in Fig. 40, and in the ^{1}H NMR spectra of the resulting Eu^{3+} tetrahedral complexes can be attributed to the varying degrees of stereoisomerism within each system, where the complexation of **81(*R*,*R*)** or **81(*S*,*S*)** with $Eu(OTf)_3$ leads to a highly stereoselective formation of either ΛΛΛΛ-[Eu_4(**81(*R*,*R*)**)$_6$](OTf)$_{12}$ or ΔΔΔΔ-[Eu_4(**81(*S*,*S*)**)$_6$](OTf)$_{12}$.

Conversely, the use of either enantiomer of **82** or **83** under the same reaction conditions resulted in a formation of a mixture of both isomers. Intriguingly, compound **83** exhibited slightly better selective stereocontrol in comparison to **82**, despite the location of its point chirality being further away from the coordination site. This finding suggests that steric effects may have a more significant influence on the diastereoselectivity of the resulting Eu^{3+} cages than that of point chirality.[265]

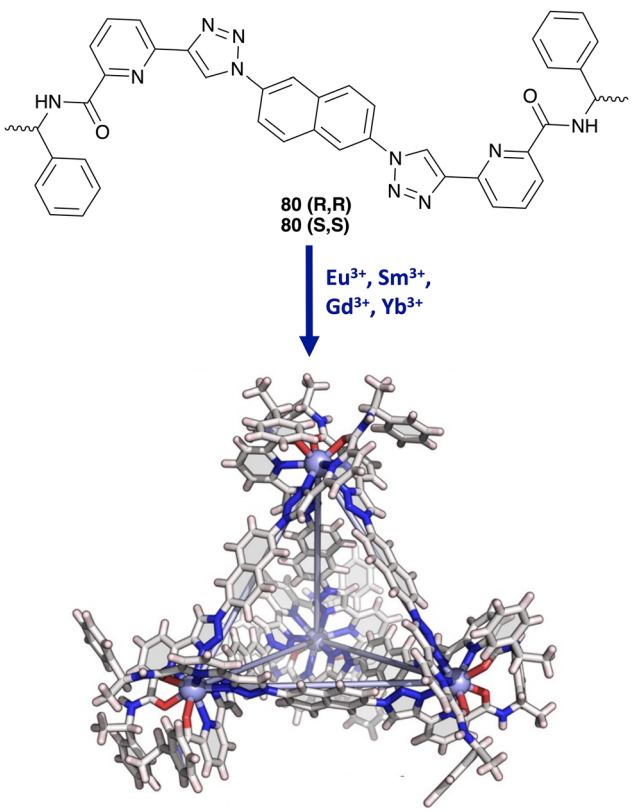

Fig. 38 Self-assembly of metallo-cages derived from **80(*R*,*R*)**/**80(*S*,*S*)**.[264] Adapted from ref. 264 with permission from the Chinese Chemical Society, Copyright©2025.

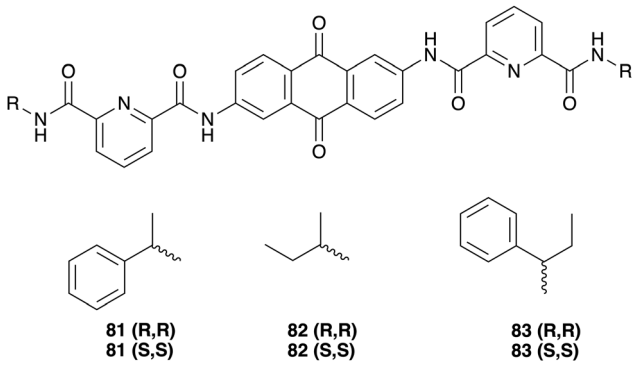

Fig. 39 Structural formulas of ditopic **dpa**-based ligands **81–83**.[265]

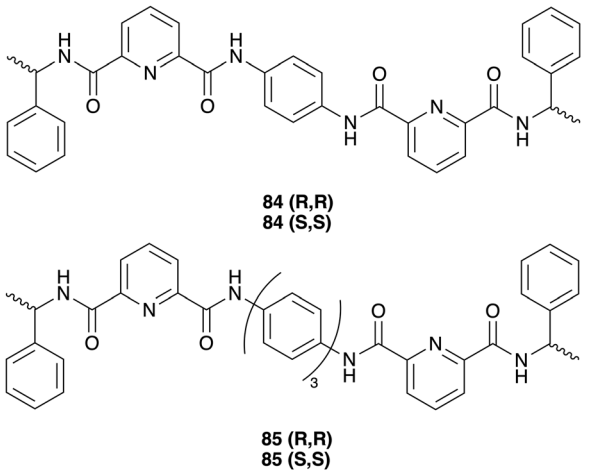

Fig. 41 Structural formulas of ditopic **dpa**-based ligands **84** and **85**.[234]

More recently, the authors have demonstrated that the linker length and ionic radii of the Ln^{3+} ion employed in the formation of such self-assemblies may influence the helicate-tetrahedral transformation of ditopic **dpa**-based ligands **L**,[266] such as in the case of **84** and **85** (Fig. 41).[234]

A tetrahedral single-crystal structure $Eu_4(\mathbf{84}(\boldsymbol{S},\boldsymbol{S}))_6$ was obtained by diisopropyl ether diffusion into the solution of $Eu_2(\mathbf{84}(\boldsymbol{S},\boldsymbol{S}))_3$ helicate in a CH_3CN solution. Remarkably, only the helical species were observed when using the analogous ligand containing the linker with two aromatic rings[266] and ligand **85** containing three aromatic rings (Fig. 42).

This behaviour can be attributed to the linkers of both ligands being longer with more rotational freedom, suggesting that the length and flexibility of the chosen linker affect the self-assembly process. Thus, it was observed that by increasing the length of the spacer, the helicoidal structure was favoured, as was seen with **85**, while the shorter linker in **84** gave rise to a tetrahedral architecture. Moreover, the larger Ln^{3+} ions tend to form dimetallic helicates while smaller ones form

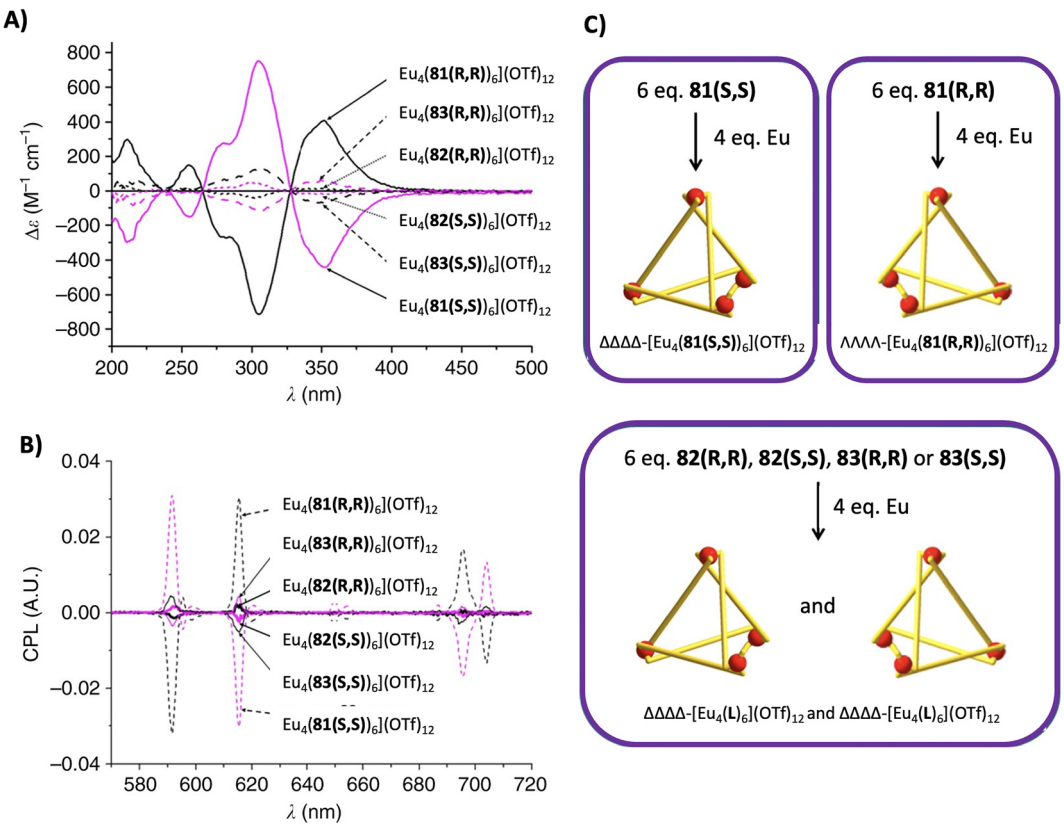

Fig. 40 (A) Circular dichroism spectra of $Eu_4(\mathbf{L})_6$ (L = **81–83**). (B) Circularly polarised luminescence spectra of $Eu_4(\mathbf{L})_6$. (C) Scheme depicting the reasoning behind the differences observed in chiroptical intensity.[265] Adapted from ref. 265 with permission from Springer Nature, Copyright©2017.

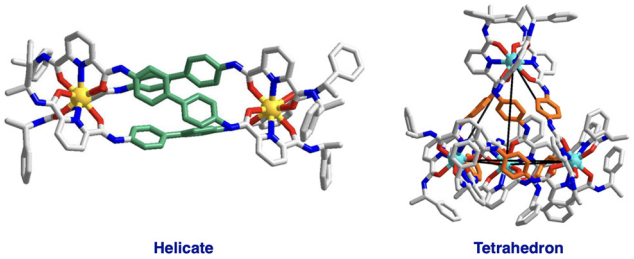

Fig. 42 Single-crystal X-ray structures showing the formation of helical or tetrahedral (Eu_4(**84(*S*,*S*)**)$_6$) structures, respectively.[234] Adapted from ref. 234 with permission from Springer Nature, Copyright©2021.

tetrahedral cages, where Lu_4(**L**)$_6$ was shown to be the most stable one.[234]

The authors further expanded these studies and reported the formation of heterometallic Ln_nLn_{4-n}(**70**)$_6$ (n = 0–4) tetrahedral complexes.[267] The mixture of Eu_2(**70**)$_3$ and Ln_2(**70**)$_3$ (Ln^{3+} = Gd^{3+}, Tb^{3+}, and Dy^{3+}) helicates in a 1/1 ratio resulted in single crystals suitable for X-ray analysis *via* slow ether diffusion into CH_3CN. It was found that upon crystallization of a mixture of Eu_2(**84**)$_3$ and Gd_2(**84**)$_3$ in a ratio of 1/1, a heterometallic cage was obtained with the formula Eu_nGd_{4-n}(**84**)$_6$ (n = 0–4). Differentiation between Eu^{3+} and Gd^{3+} by X-ray crystallography was not possible due to their similar electron densities. However, the use of mass spectrometry convolution studies enabled the differentiation of the ratio of Gd^{3+} to Eu^{3+} in the tetrahedral complexes, where Eu_2Gd_2(**84**)$_6$ was identified as the predominant species, being formed in 46% yield, and the unique heterometallic species were detected. A similar result was obtained for a mixture containing both Eu_2(**84**)$_3$ and Tb_2(**84**)$_3$ complexes.[267]

3.3. Multimetallic lanthanide cages from tripodal ligands

Another approach allowing for the formation of multimetallic Ln^{3+} assemblies, such as cages, involves the use of tripodal ligands. Their rigid design, with three distinct binding sites for Ln^{3+} ions, allows for greater control over the 'pre-organization' of ditopic tridentate ligands, as the competing self-assembly of helicate systems is absent. The Sun research group have carried out work on this topic, describing the formation of tetrahedral cages from the self-assembly of the tripodal ligands **86** or **87** (Fig. 43), bearing the pybox coordination moiety, with Eu^{3+} ions.[268] Interestingly, it was observed that the quantum yield (in acetonitrile) of Eu_4(**86**)$_4$ was considerably higher than that of Eu_4(**87**)$_4$ being 10.2% *vs.* 0.24%, respectively. This phenomenon can be attributed to the intraligand charge transfer (ILCT) sensitization of the Eu^{3+} core, which contrasts with the conventional T^1 sensitization process typically employed in Ln^{3+} self-assemblies. Furthermore, the Eu_4(**86**)$_4$ complex was found to have promising sensing properties towards inorganic ions, exhibiting a 'turn-off' of the Eu^{3+}-centred luminescence upon addition of I^- ions and an enhancement in Eu^{3+}-centred luminescence in the presence of Cu^+ cations.[268]

The authors have also incorporated the **tzpa** moiety into tripodal systems, **88** and **89** (Fig. 44), with the aim of forming

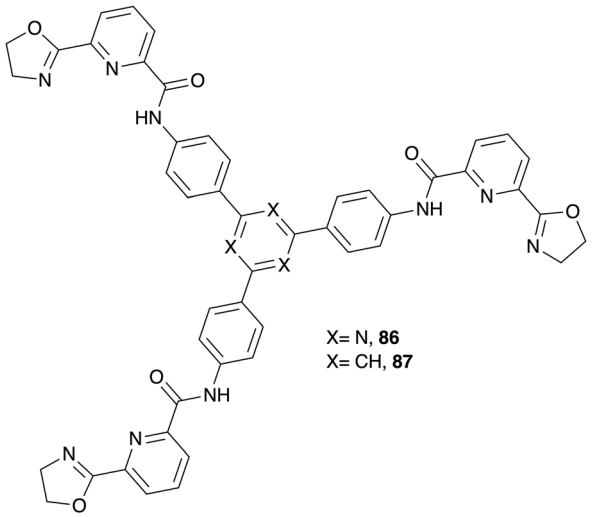

Fig. 43 Structural formulas of tripodal ligands **86** or **87**.[268]

cages.[269] The self-assembly of either of these ligands with $Ln(OTf)_3$ (Ln^{3+} = Sm^{3+}, Eu^{3+}, Tb^{3+}, Dy^{3+}, and Er^{3+}) yielded Ln_4(**L**)$_4$ cages. High quantum yields were obtained for Tb_4(**89**)$_4$ (50.8%), as well as for Eu_4(**88**)$_4$ (51%) and Eu_4(**89**)$_4$ (56.6%) in an acetonitrile solution. As compound **89** was shown to efficiently sensitise both Eu^{3+} and Tb^{3+}, mixed heterometallic cages were formed by reacting **89** with Eu^{3+} and Tb^{3+} in a 1/1 ratio, resulting in the formation of the self-assembly Eu_xTb_{4-x}(**89**)$_4$$(OTf)_{12}$ (x = 0–4). The potential of these mixed lanthanide cages to act as radiometric luminescent thermometers was investigated by examining the luminescence of the Eu_xTb_{4-x}(**89**)$_4$$(OTf)_{12}$ (x = 0–4) cages in the temperature range from 80 to 400 K. An increase in temperature (from 200 to 360 K) resulted in a significant decrease in the Tb^{3+}-centred emission at 545 nm ($^5D_4 \rightarrow {}^7F_5$), accompanied by an enhancement in the Eu^{3+}-centred luminescence at 616 nm ($^5D_0 \rightarrow {}^7F_2$) owing to an energy transfer process from Tb^{3+} to Eu^{3+}. This temperature-dependent luminescence change could also be observed by the naked eye, as a colour change from green to red was observed in the solution.[269]

More recently, the authors have expanded on this work by using analogous tripodal systems based on ligands **90** and **91**, where the angle between the spacer and the chelating **tzpa** moiety is 120°, in contrast to the 180° observed for tripodal ligands **88**, **89**, **92** and **93** (Fig. 44).[270] This small change in ligand design resulted in the first example of the formation of Eu_3L_3 'sandwich' structures upon self-assembly with Eu^{3+}, in contrast to the more prevalent Eu_4L_4 tetrahedral cage structures. The findings of the self-assembly studies indicated that while **91** solely formed the Eu_3(**91**)$_3$ complex, the solvent-triggered transformation between Eu_3(**90**)$_3$ or Eu_4(**90**)$_4$ complexes was also observed.

Sun and co-workers have also introduced the **tzpa** moiety with an external triazole unit into ligand **92** and the **btp** motif with compound **93** (Fig. 44). It was found that **93** was able to efficiently sensitise the luminescence of all emitting Ln^{3+} ions spanning both the visible and NIR regions (Ln^{3+} = Pr^{3+}, Nd^{3+},

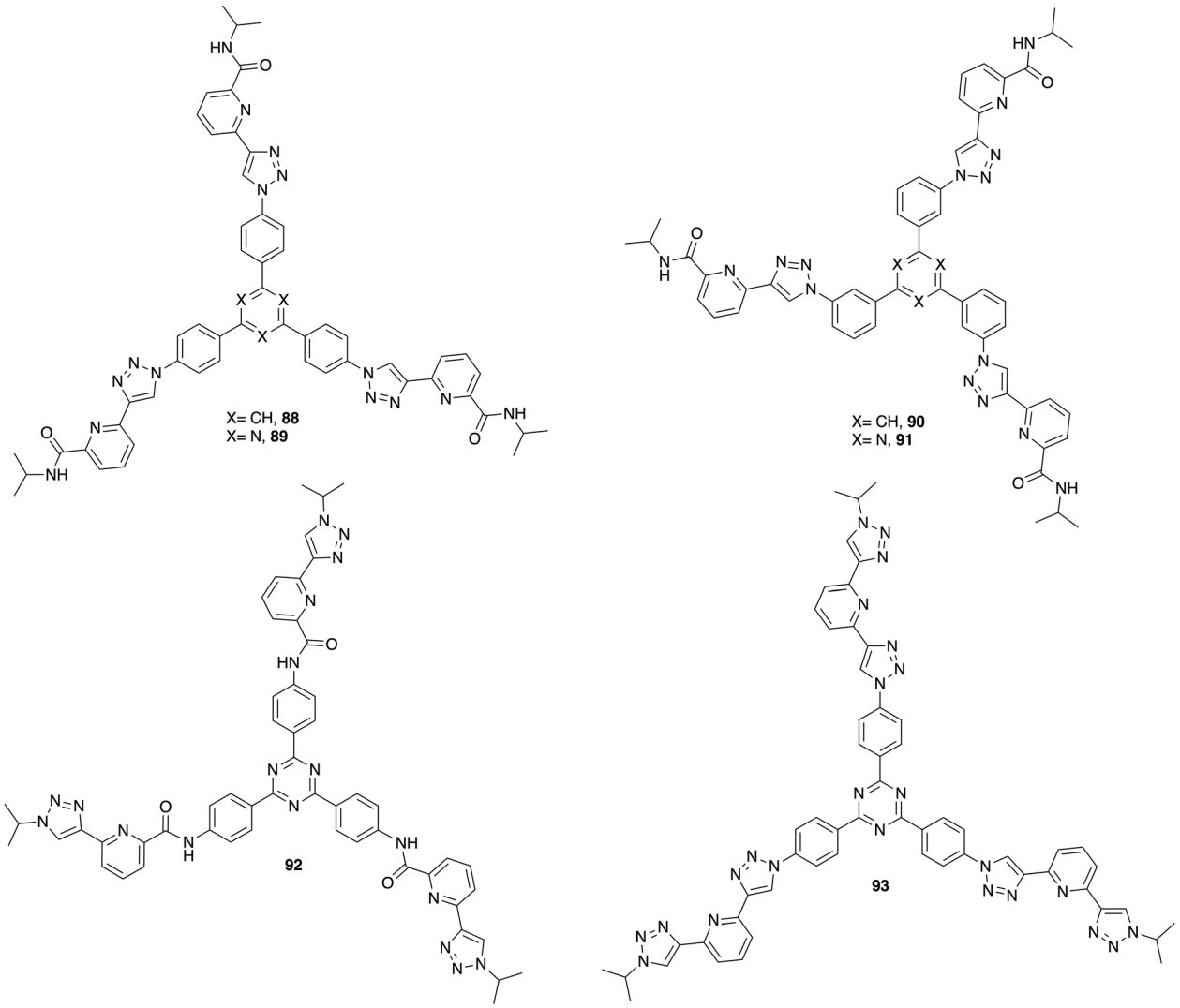

Fig. 44 Structural formulas of tripodal ligands **88–93**.[269–271]

Sm^{3+}, Eu^{3+}, Tb^{3+}, Dy^{3+}, Ho^{3+}, Er^{3+}, Tm^{3+}, and Yb^{3+}), with a record high quantum yield obtained for $Tb_4(\mathbf{93})_4$ (Φ = 82%) in the acetonitrile solution. The high quantum yield exhibited by these lanthanide organic polyhedra (LOPs), particularly those employing **89** and **93**, prompted an investigation into their potential as white light emitters (WLEs). It was established that the International Commission on Illumination (CIE) chromaticity coordinates for $[Eu_4(\mathbf{89})_4]_2[Tb_4(\mathbf{89})_4][\mathbf{89}]_{35}$ (0.33, 0.33) in a DCM/MeOH (1/1 v/v) solution excited at 374 nm, or $[Eu_4(\mathbf{93})_4]_2$-$[Tb_4(\mathbf{93})_4][\mathbf{93}]_{230}$ (0.33, 0.34) and $[Sm_4(\mathbf{93})_4][Dy_4(\mathbf{93})_4]_{7.5}[\mathbf{93}]_{80}$ (0.34, 0.34) by exciting at 330 nm were found to be optimal for WLE systems.[271]

The authors have also designed chiral ligands to achieve Ln_4L_4 tetrahedral cages with the aim of understanding the ionic radius-dependent kinetics and the chiral amplification during the self-assembly processes. The obtained results indicated that the complexes are formed slower when using lanthanide ions with a smaller ionic radius. They found that in the case of Ln_4L_4 cages with mixed chiral and achiral ligands, then upon using the lanthanide ions La^{3+} and Pr^{3+}, respectively, the self-assembly of the cages and their chiral amplification occur simultaneously. However, in the case of Eu_4L_4, two different steps were found to occur in the cage formation: first of these being assigned to the self-assembly followed by chiral amplification. This different kinetic behaviour could, however, also be due to the different ligand exchange rates.[272]

Lately, Sun and colleagues reported the first example of a radical-bridge lanthanide tetrahedral cages obtained by self-assembly between a radical ligand derived from triphenylamine and Ln^{3+} ions (Ln = La^{3+}, Eu^{3+}, Gd^{3+}, Tb^{3+}, and Lu^{3+}). The stability of the cages derived from paramagnetic ions (Eu^{3+}, Gd^{3+}, and Tb^{3+}) was higher, and this could be due to the magnetic interactions between these ions and the radical ligands. This study presents an approach for the development of stable radical-based systems with potential applications as lanthanide-derived smart materials.[273] Additionally, they prepared luminescent films based on Eu_4L_4 tetrahedral cages derived from two triarylborane-cored tritopic ligands. Both

films exhibited strong luminescence properties, and high sensitivity towards volatile amines with a high level of detection (sub-ppt level). Within these results, they demonstrate the potential of lanthanide cage-based films in sensing applications.[274]

In a recent study, Kotova *et al.*[275] have developed a tripodal ligand based on the **dpa** design (Fig. 45), employing a similar strategy to that shown in ligand **7**.[151] This was achieved by developing compound **94**, which possesses a 1,3,5-benzenetricarboxiamide core, joining to three **dpa** moieties through the 4-pyridyl position of the **dpa** center.[275] Titration studies of **94** with $Eu(OTf)_3$ revealed the expected formation of 1 : 1, 2 : 1 and 3 : 1 (M:L) species *in situ*, where the lanthanide emission was highly modulated depending on the nature of the speciation in the solution. This design offers the potential for the development of higher order structures through further synthetic modification of the **dpa** unit at the esters.

Despite the prevalence of the tridentate ligand motif in the formation of complex higher order self-assemblies, there have been several examples developed using non-tridentate ligand designs. Like their mononuclear counterparts, non-terdentate binding motifs are also used in the formation of polymetallic Ln(III)-directed self-assemblies. For example, Sun and co-workers have reported the formation of the tetradentate tripodal acylhydrazone ligand **95** with the ability to form self-assembled octahedral metallocages derived from Lu^{3+}, Yb^{3+} and Eu^{3+}, as shown in Fig. 46.[276] These metallocages exhibited charge-reversibility depending on the pH of the media. This enables controlling the structure of the cage and the encapsulation/release of different ionic guest molecules by changing the pH of the media, resulting in a potential candidate for the development of smart luminescent supramolecular materials.

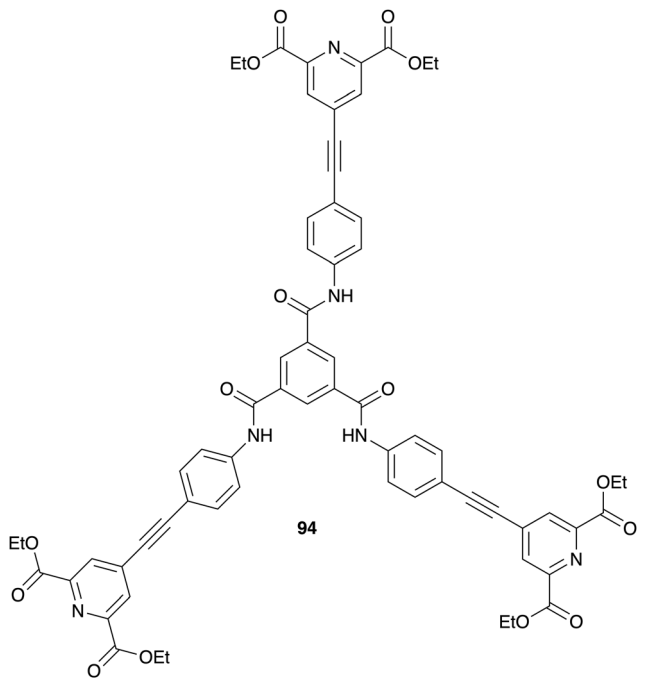

Fig. 45 Structural formula of tripodal ligand **94** based on the **dpa** design.[275]

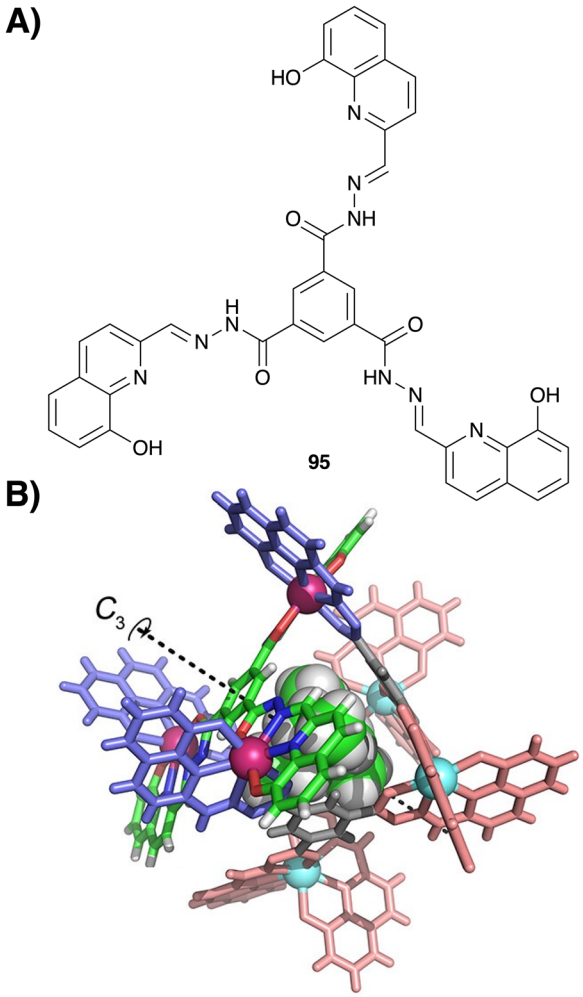

Fig. 46 (A) Structural formula of ligand **95**. (B) X-ray single-crystal structure of $\Delta_3\Lambda_3$-$(Et_4N)_6Eu_6$(**95**)$_4$.[276] Adapted from ref. 276 with permission from the American Chemical Society, Copyright©2023.

More recently, Zang and co-workers have reported two different lanthanide self-assembled octahedral metallo-cages by using Eu^{3+} and Tb^{3+} ions together with the tri(β-diketone) ligand **96** (Fig. 47).[277]

In this study, they successfully demonstrated the ability of inducing CPL by using specific amino acids that can modify the chiral environment around the Ln^{3+} ions; the chiral induction of the racemic mixture was achieved with arginine, showing the highest CPL metrics for Eu^{3+} to date (g_{lum} = 0.53, FM value = 0.323). The authors further studied the mechanism underlying this induced CPL phenomenon and suggested that the induction efficiency increases while increasing the coordination number of the amino acids or the coordination energy between amino acids and Eu^{3+}, providing a strategy for the design of luminescent materials with tuneable chiroptical characteristics.

3.4. Lanthanide-derived mechanically interlocked molecules

Mechanically interlocked molecules (MIMs) have attracted great interest for chemists in the last decades.[278] The formation of MIMs involves two or more interlocked molecules, so they

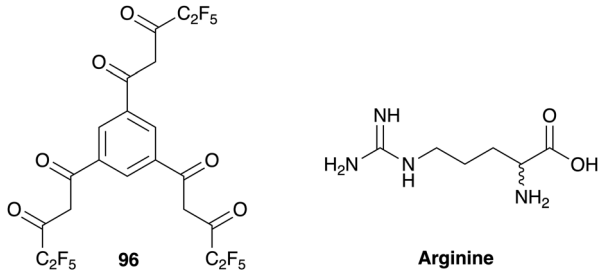

Fig. 47 Structural formulas of ligand **96** and **arginine**.[277]

cannot be separated without breaking the covalent bonds.[279] Since there are several recent reviews focused on MIMs,[21,225,280–287] in this section we will only discuss the latest examples of MIMs derived from lanthanide ions and nitrogen-donor ligands.

The first example of Ln-templated MIM was that of Gunnlaugsson and Lincheneau who in 2014 reported the formation of the [2] and [3]-catenanes using Eu^{3+}, and ring closing metathesis reactions, the ligand being based on the **dpa** motif. While not being able to obtain the crystal structures of these MIMs, the authors used both HRMS and luminescence titrations to demonstrate their formation, where the ion was placed within the closely packed **dpa** macrocyles.[288] Since then, only a relatively few examples of lanthanide-based MIMs have been reported.

In 2019 Ghosh and colleagues[289] reported the synthesis of a phenanthroline-based macrocycle **97** together with an alkene-terminated ligand **98** to achieve a multifunctional [2]catenane (Fig. 48), with the ability to bind Eu^{3+} and Gd^{3+} ions inside the supramolecular architecture. The experimental studies demonstrated that both lanthanide ions were coordinated within the host cavity, as shown by HRMS, and the authors obtained the X-ray crystal structure of Eu-[2]catenane.

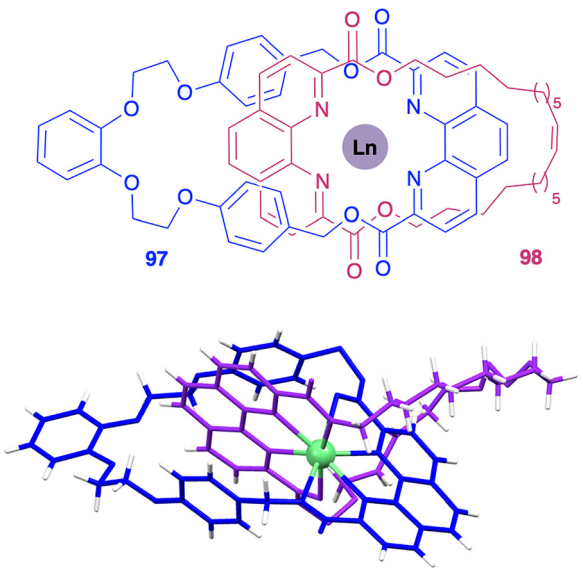

Fig. 48 Lanthanide-binding [2]catenane.[289] Adapted from ref. 289 with permission from the Royal Society of Chemistry, Copyright©2019.

Thompson and co-workers developed a series of five polyrotaxanes derived from different cyclodextrins (Fig. 49) modified with the chelating agent 1,4,7,10-tetraazacyclododecane-1,4,7,10-tetraacetic acid (DOTA) to improve the coordination of Gd^{3+} ions within the cavity.

This study focuses on the evaluation of the physicochemical and imaging properties of these rotaxanes, which display high stability, high relaxivity as MRI contrast agents, and biocompatibility.[290]

Recently, Schaufelberger and coworkers have reported how mechanical bonds can modulate lanthanide luminescence in [2]rotaxanes, providing efficient energy transfer and selectivity towards Cu^{2+} ions, acting as efficient turn-off sensors, opening a new path of bioresponsive probes and imaging applications.[292]

Many studies focused on molecular knots with d-metal ions have been published in the last few years.[293–296] In contrast, the use of lanthanides is less common, but this area has been pioneered by Leigh *et al.* The Leigh research group was the first in demonstrating the use of the Ln-ions in knot formation, and have since then, made significant efforts by studying these topologies using lanthanide ions.[297]

The design of the molecules builds on the "Trinity Sliotar" family motif derived by the Gunnlaugsson group, using the **dpa** ligands with (*R*)- or (*S*)-1-(2-naphthyl)ethylamine antennae.[137]

For example, in 2018, the Leigh group reported a rotaxane-like structure, Lu-**102–103**, obtained by tying a knot by means of lanthanide-templated synthesis. This knotting increases the steric hindrance locking a macrocycle on the thread (Fig. 50), and they observed that while removing the Lu^{3+} ion, the knot unties and the macrocycle de-threads, demonstrating that this process is reversible by introducing Lu^{3+} again.[291]

To further explore this field, the Leigh group studied the stereoselective synthesis of knots with different topologies (*e.g.* square and granny knots) through lanthanide-templated synthesis. To achieve this, they synthesized two different tris(2,6-pyridinedicarboxamide) ligands, resulting in enantiomeric granny knots and in a diastereomeric square knot.[298]

In a related study, Leigh *et al.* found that variation in the metal ion used to tie the knot can give rise to different knots using the same strand. Thus, the metal ion used can guide the folding and entanglement of the knot in the same way as chaperones during the protein folding.[33]

Furthermore, they synthesised three different Lu^{3+}-derived knots using the chiral ligands **104–106** (Fig. 51). This study has elucidated the ability of these knots to induce a twist in an achiral liquid crystal. Therefore, this modifies the pitch and inverts the chirality of the liquid crystal, modifying its macroscopic properties.[299]

In 2022, the Leigh group introduced a new approach for the synthesis of molecular knots using a Vernier template synthesis. This strategy employs coordinatively mismatching ligands and lanthanide metal ions, being more effective than the use of metal helicates to cross the strands and prepare the knots.

The Vernier approach allowed the authors to obtain specific knots with a better yield. It also allowed them to gain control over their topology by modifying the L/M ratio, hence enabling the synthesis of more complex knots and, thereby, showing specific structure and functional properties.[300] These knots

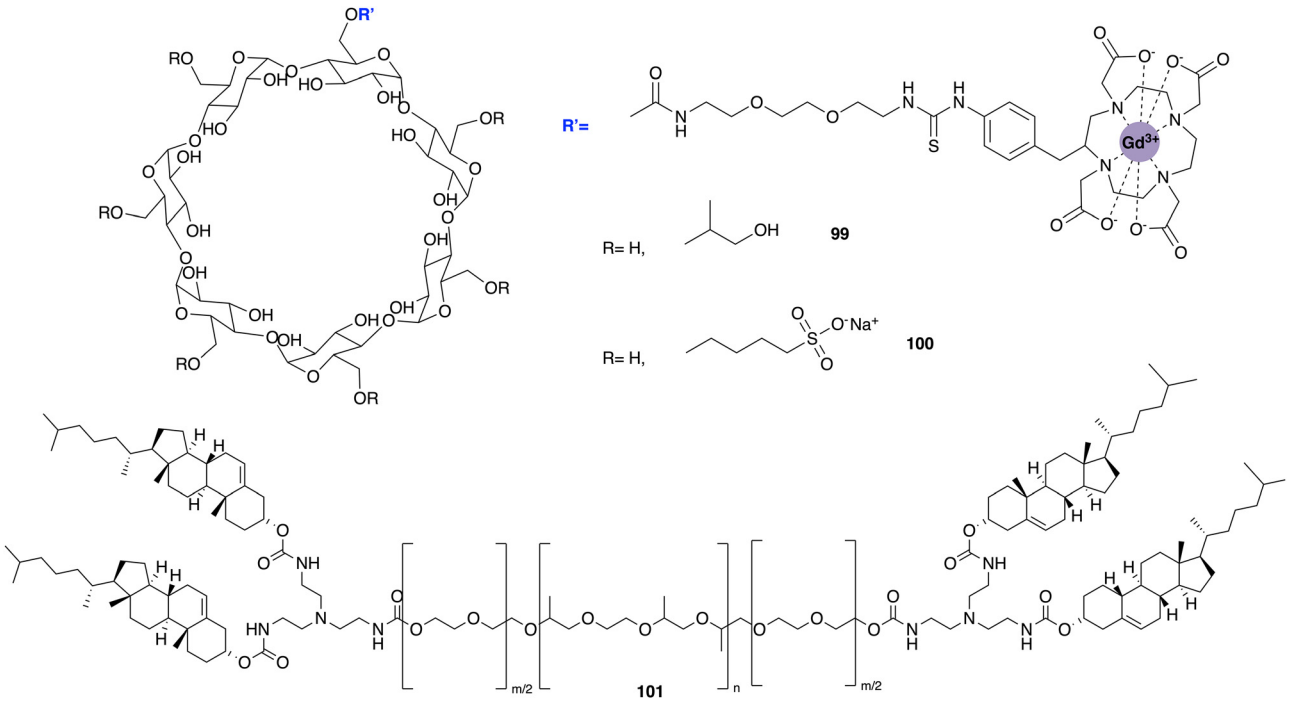

Fig. 49 Structural formulas of the ligands used for the synthesis of polyrotaxanes (**99–101**).[290]

also showed enhanced stability and different chiroptical properties. Additionally, the synthesised **dpa** or 2,6-pyridinedicarboxamide (**pdc**)-derived achiral and chiral ligands were described as precursors of different molecular knots. By means of **pdc**-Lu^{3+} social self-sorting, a derived trefoil knot was obtained by using achiral ligands in a 1 : 1 stoichiometry, while granny and square knots were achieved using chiral ligands.[301]

These findings further highlight the importance of the ligand design in guiding the self-assembly of molecular knots. From this short account, it is clear that the lanthanides can play a major role in the formation of supramolecular self-assembly-based MIM systems, an area that is only just beginning to be explored for such systems.

3.5. Metallo-supramolecular polymers

Metallo-supramolecular polymers featuring Ln^{3+} ions have emerged as promising systems for the development of gels and soft materials with improved mechanical and luminescence properties. This type of supramolecular architecture demonstrates great potential for applications in materials science, where the coordination and the range of physical properties of the lanthanides can be truly capitalised on. As several reviews have been published recently, covering all the aspects about this type of architecture, this section will only discuss the recent advancements, where the systems formed have been done so with the view of capitalising on their luminescence properties.[76,77,302,303]

Several pyridine-based metallo-supramolecular polymers with different polycarbonate backbones **BEP** (pyridine-2,6-bis(ethyl)ester) and **BDP** (pyridine-2,6-bis(diethylamide)) have been recently synthesised for such polymer formation. Upon coordination with Ln^{3+} ions (Ln = Eu and Tb), the resulting polymers exhibited an increase in glass transition temperatures and Ln^{3+}-centred emissions (Fig. 52).

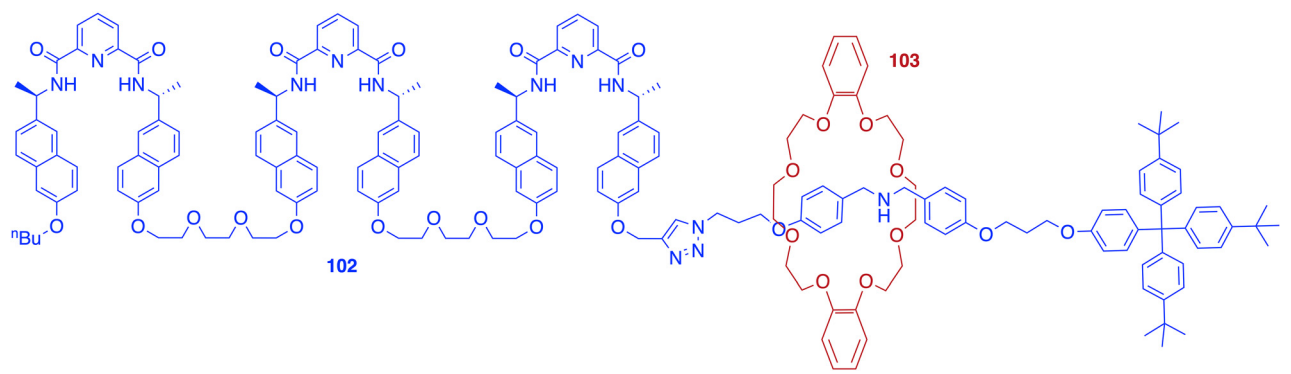

Fig. 50 Structural formulas of the ligands used to obtain the rotaxane-like structure Lu-**102–103**.[291]

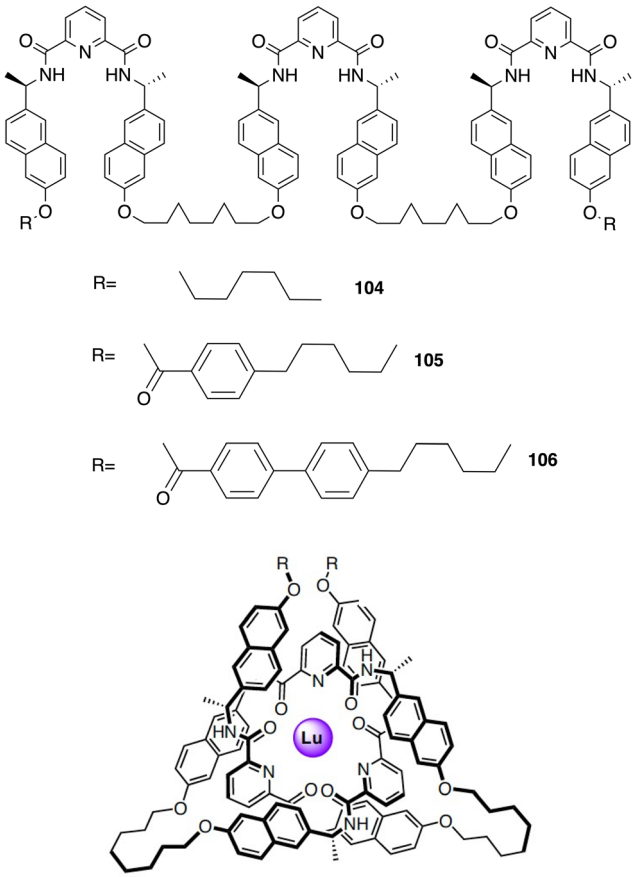

Fig. 51 Structural formulas of the ligands **104–106** and representation of the derived knots.[299] Adapted from ref. 299 with permission from Springer Nature, Copyright©2020.

The **BEP** polymer showed higher emission efficiencies for both Eu^{3+} and Tb^{3+} polymer systems, compared with the **BDP**-derived systems. Furthermore, a blue emission was observed when Tb^{3+} was used, and a white light emission was achieved by the $Eu_{1.8}Tb_{28}$(**BEP**)$_1$ system. This type of functional materials can be used in multicolour displays or in combination for white light generation.[304]

The synthesis of metallosupramolecular multiblock copolymers using Eu^{3+} and Tb^{3+} complexes as building blocks (Fig. 53) was successfully achieved by a seeded living polymerization technique. Two different aggregates were developed

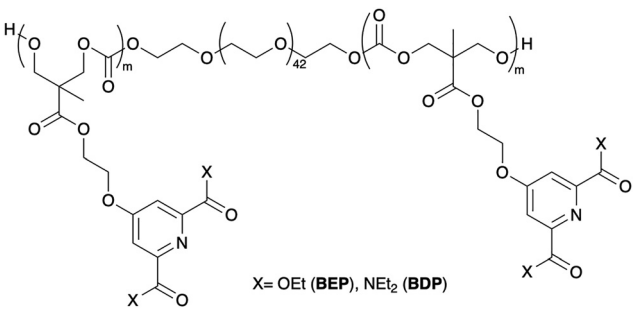

Fig. 52 Polycarbonate backbones **BEP** and **BDP**.[304]

from the Eu^{3+} complexes: the kinetic spheric aggregate rises from the [Eu(**107**(***R,R***))$(NO_3)_3$] complex (1 : 1), and the thermodynamic fibre aggregate rises from the [Eu_2(**107**(***R,R***))$(NO_3)_6$] complex (2 : 1) *via* π–π stacking and hydrogen bond formation. The polymerization of [Eu_2(**107**$(NO_3)_6$] was kinetically controlled by changing the concentration of the metallic salt. This resulted in a metallosupramolecular polymer with controlled length. By means of copolymerizing the kinetically formed Tb^{3+} complex with a seed derived from the Eu^{3+} complex, they developed metallosupramolecular tri- and penta-block copolymers *via* a seed-end chain-growth mechanism. [Eu(**108**(***R***))] was also successfully used as a seed to obtain tri-block copolymers.[305]

Lately, a new route to obtain polymer hydrogels that are highly stretchable and luminescent with magnetic resonance relaxation properties was developed by using a small amount of lanthanide-derived cages as cross-linkers. To achieve this, the ligand **109** (Fig. 54) was synthesised and coordinated to Eu^{3+} and/or Gd^{3+} ions to form the cages [$K_{24}Ln_8$(**109**)$_{12}$].

After this, the cages were used as cross-linkers for the free radical polymerization with acrylamide, to obtain polymeric hydrogels. The hydrogels exhibited superior stretchability and tensile stress, strong luminescence in the case of Eu^{3+}-derived hydrogels and efficient magnetic resonance relaxation properties for Gd^{3+}-derived hydrogels. Notably, both ions could co-assemble with the ligand **109**, giving rise to the [$K_{24}Eu_xGd_{8-x}$(**109**)$_{12}$] cage offering potential applications in biomedical imaging.[306]

Piguet and co-workers have recently reported the synthesis of the ligands **110–115** assisted by metal ions (Fig. 55), with the aim of modulating the luminescence properties of the corresponding Eu^{3+} complexes.[307] Their investigation revealed that a dimer **114** and a polymer **115**, both derived from ligand **110**, were obtained through the acyclic diene metathesis polymerization (ADMET), an essential methodology in the design of polymer architectures in supramolecular chemistry.

However, it was found that the Ru-based Grubbs catalyst activity was hindered by the coordination of **110** to [Eu(**hfac**)$_3$], preventing an efficient polymerisation, thus precoordination with [Eu(**hfac**)$_3$] was achieved before polymerisation, guaranteeing the success of the reaction. The resulting dimer **114** and polymer **115** exhibited extended π-conjugation, where the number of conjugated π-electrons in the ligand has crucial influence on the luminescence properties of the derived Eu^{3+} complexes. It was observed that the ligand-sensitised photoluminescence quantum yields for Eu^{3+} complexes decreased with the extension of π-conjugation due to quenching through unfavourable europium-to-ligand back energy transfers [Eu(**113**)(**hfac**)$_3$ > Eu(**112**)(**hfac**)$_3$ > Eu(**111**)(**hfac**)$_3$ > Eu(**110**)(**hfac**)$_3$ > Eu_2(**114**)(**hfac**)$_6$ > Eu_{18}(**115**)$_{18}$(**hfac**)$_{54}$].[307]

Gunnlaugsson and co-workers have also explored the field of lanthanide-based/crosslinked metallosupramolecular polymers. For example, they developed the **btp** ligands **116–118** (Fig. 56) by incorporating a methyacrylamide unit in these structures, with the aim of obtaining polymeric hydrogels.[308]

Compound **118** was made with the intention to be incorporated into a polymeric film using 2-hydroxyethyl methacrylate (HEMA), ethylene glycol dimethacrylate (EGDMA) and methylmethacrylate

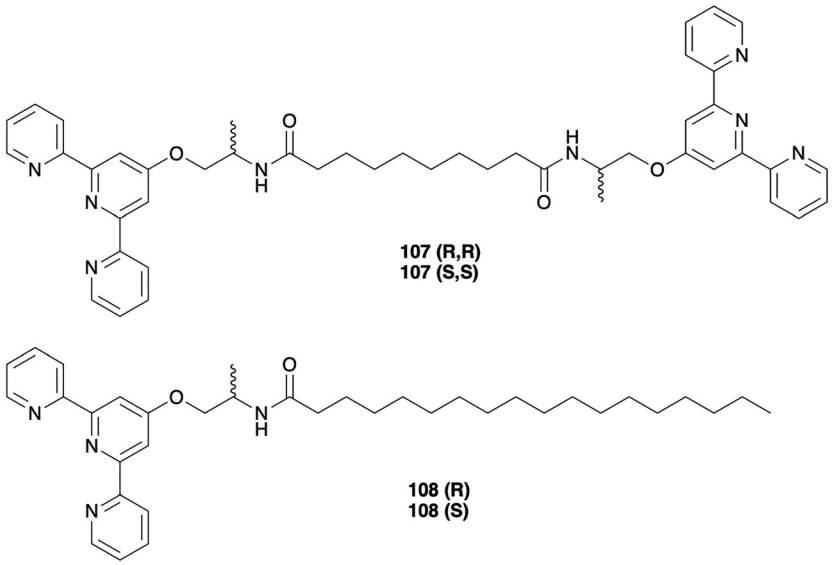

Fig. 53 Terpyridine-based ligands **107** and **108**.[305]

(MMA), while **117** was used as a 'model compound' to compare how the incorporation of **118** into a polymeric backbone affects its photophysical properties upon Ln^{3+} coordination. The $Tb(\mathbf{117})_3$ complex showed long lifetimes and a high quantum yield in solutions (Φ = 72%). A fiber supramolecular hydrogel was also developed upon interactions of **116** with Tb^{3+}.

Two luminescent polymers were developed in this work, showing metal ion-mediated cross-linking upon interaction with Ln^{3+}. These materials also showed no metal leakage after long-term water exposure, showing that the Tb^{3+} emission was stable over a long period of time. Furthermore, the hydrogels remain highly luminescent in aqueous media, indicating no dissociation, which is a significant improvement over the previous system. This work is ongoing using the ligands incorporating conjugated receptor sites to develop responsive polymers for use in luminescence sensing applications.[308]

To further explore the use of the **btp** ligands in such material chemistry, Gunnlaugsson and co-workers employed ligand **116** combined with poly(ethylene-*alt*-maleic anhydride)[P(E-*alt*-MA)] as a precursor of two polymers that are soluble in water and methanol (P1 and P2). The resulting cross-linked polymers coordinated to the Tb^{3+} ions showed strong green luminescence, which was clearly visible to the naked eye.[309]

The results of the titration studies, where the interaction between the **btp** ligands upon gradual addition of Tb^{3+} revealed the predominant formation of 1 : 2 (M : L) species in solution, suggested that two ligands from the polymer backbone can coordinate to one Tb^{3+} ion, enabling cross-linking. However, within the polymer structures, other stoichiometries could also occur; this is more difficult to quantify *vs.* that done in solutions for such **btp**-based ligands. In this system the backbone itself most likely also plays an important role in coordinating to metal ions.[309]

Following their previous work with chiral naphthyl-derived ligands, the Gunnlaugsson group also synthesised Eu^{3+} complexes derived from the monotopic asymmetric **dpa** ligand **119** and the symmetric **dpa** ligand **120** (Fig. 57), with the aim of studying how the symmetry of the ligand affects the properties of the resulting hydrogels, and how this was translated into the polymer photophysical properties.

These two monomers were employed in the co-polymerisation to form supramolecular hydrogels, where the lanthanide ion acts as a crosslinking agent enabling Eu^{3+}-centred luminescence of the resulting material.[310] These monomers were incorporated as additional crosslinkers in HEMA-based hydrogels. The authors demonstrated that in the case of the asymmetric ligand **119(*S*)**, the dominant stoichiometry within the polymer was found to be $Eu(\mathbf{119})_2$, resulting in less emissive materials. In contrast, the hydrogel derived from the ligand **120(*R*,*R*)** revealed the formation of more stable $Eu(\mathbf{120})_3$ with a higher red luminescence intensity, which was clearly visible to the naked eye. These findings demonstrate the role of the ligand design on the final photophysical properties of lanthanide-derived hydrogels.

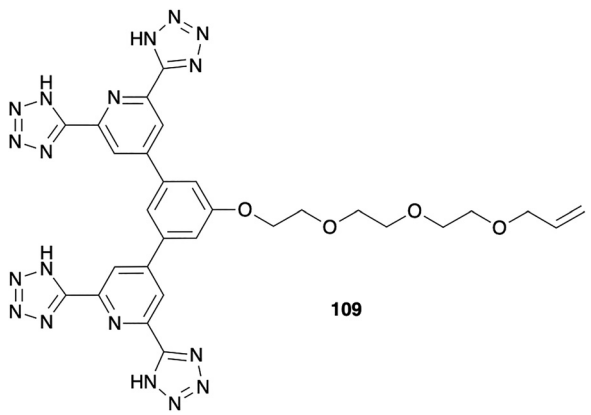

Fig. 54 Structural formula of ligand **109**.[306]

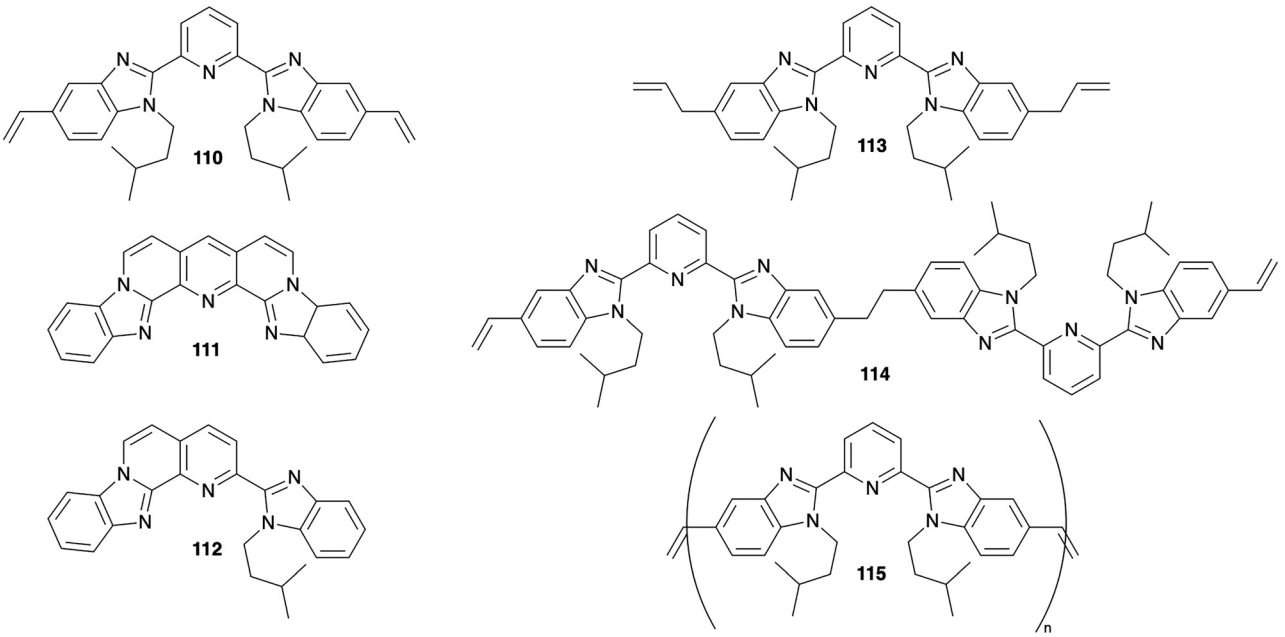

Fig. 55 Structural formulas of ligands **110–115**.[307]

Kotova *et al.* have recently designed and utilised compound **121** (Fig. 58), a mannose-derived **dpa** ligand conjugated to K^+-stabilised guanosine quadruplexes (**G4**), with the aim of developing bio-inspired healable luminescent hydrogels using Eu^{3+} ions.[311]

In this study, hydrogels of **G4-121** were prepared in a 1/1 ratio (**121** : Eu^{3+}), resulting in materials with Eu^{3+}-centred CPL emissions. The authors also explored rheological and morphological properties of the hydrogels (Fig. 58). This study is particularly relevant in view of exploring and understanding the mechanisms of induced CPL and the recent discovery of the biological activity of lanthanide ions, as these gels could be used as models for studying biological processes.

Following the line of the studies incorporating biologically related molecules, a series of tripodal ligands containing amino acids were developed using the benzene-1,3,5-tricarboxamide (**BTA**) motif, **122–125** (Fig. 59A).

The developed molecules showed the formation of self-assembly structures with different morphologies. For example, the glycine derivative of the ligand **122** assembles in a robust gel (Fig. 59(B)), whereas monodisperse solid microspheres were obtained in the cases of alanine-, phenylalanine- and leucine-derived ligands (Fig. 59(C)). The addition of Eu^{3+} and Tb^{3+} ions resulted in further morphological changes of the ligand assemblies: from a fibrous gel to nanospheres in the case of glycine derivatives, while in the other cases, hierarchical crosslinked superstructures were formed. Notably, the inherent chirality of the self-assemblies influences the chirality of the microspheres functionalised with lanthanide ions, resulting in CPL.[312]

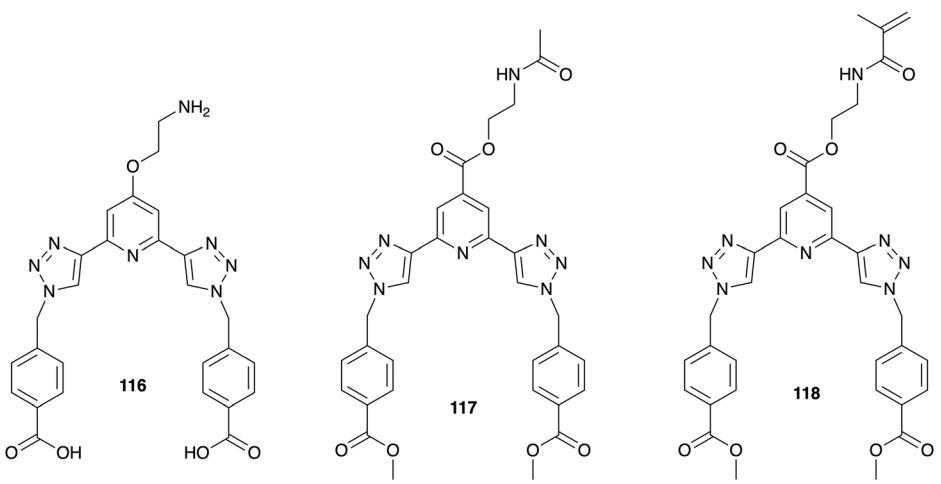

Fig. 56 Structural formulas of **btp**-derived ligands **116–118**.[308,309]

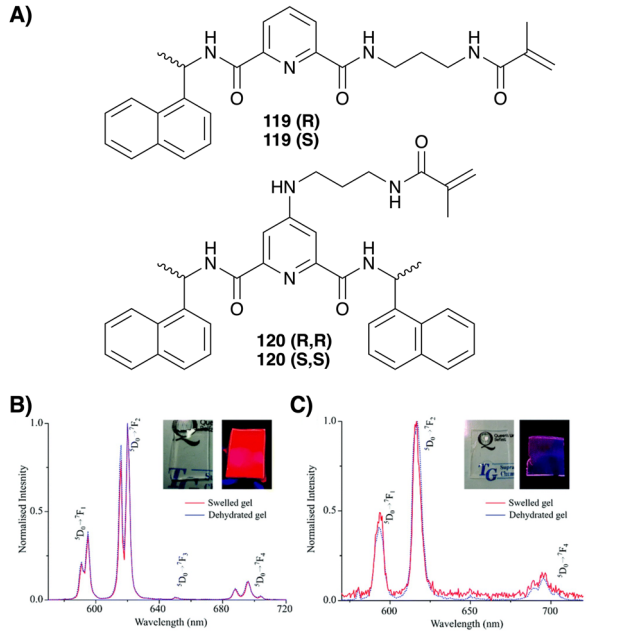

Fig. 57 (A) Structural formulas of **119(*R*)**, **119(*S*)**, **120(*R*,*R*)** and **120(*S*,*S*)** and normalised time-gated emission spectra of (B) p(HEMA-*co*-EGDMA-*co*-**120(*S*,*S*)**) and (C) p(HEMA-*co*-EGDMA-*co*-**119(*S*)**) hydrogels that swelled in the presence of 0.33 equiv. of Eu^{3+} (red line) and the corresponding dehydrated gel (blue line). Insets represent the photographs of the corresponding materials swelled in the presence of Eu^{3+} under ambient and UV light.[310] Adapted from ref. 310 with permission from the Royal Society of Chemistry, Copyright©2019.

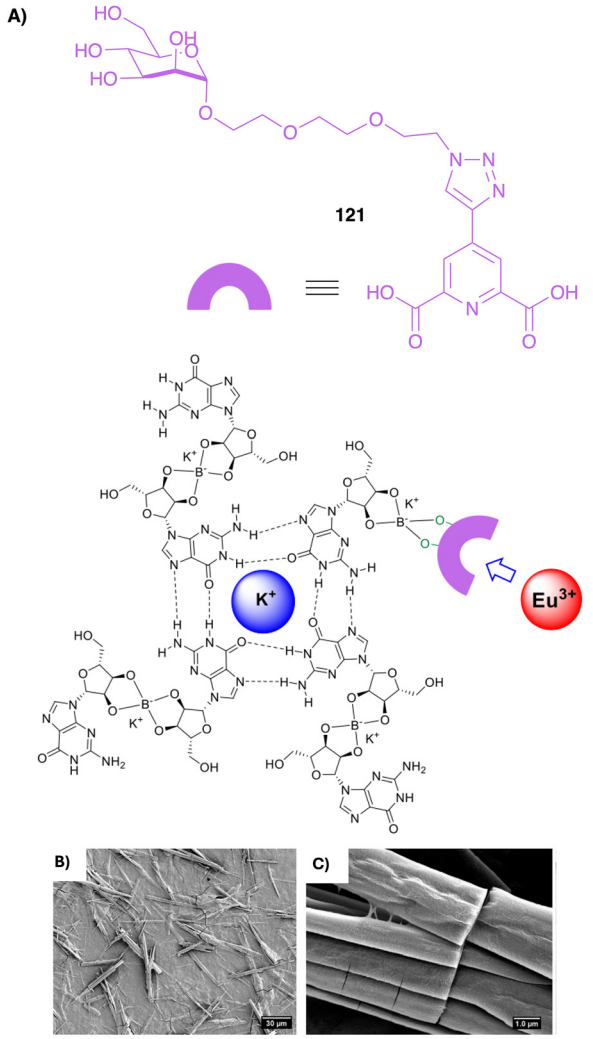

Fig. 58 (A) Structural formula of **121** and the schematic of the guanosine quadruplexes (**G4**) functionalised with **121** (**G4-121**) comprising the hydrogel. The binding site of Eu^{3+} ion is depicted schematically. (B) and (C) SEM images of dried hydrogel **G4-121**.[311] Adapted from ref. 311 with permission from Elsevier B.V., Copyright©2022.

Lately, the Gunnlaugsson group have further reported the use of tripodal **BTA**-derived ligands functionalized with terpyridine units acting as a low-molecular weight gelator (LMWG) molecules forming supramolecular gels. They found that these ligands **126** and **127** (Fig. 60) form gels in different organic solvents, and that upon addition of d- or f-metal ions, the cross-linking of the gel fibres occurred, leading to modified morphological and rheological properties of the gels while bringing the photophysical functionality to the newly formed system.[313,314]

One of the latest examples of fluorescent hydrogels was developed by Liao and colleagues *via* a one-pot synthetic methodology, combining a red-light-emitting dpa-derived Eu^{3+} complex $Eu(\mathbf{dpa})_3$, together with a blue light-emitting AIE molecule.

These molecules were introduced into a poly(vinyl alcohol) (PVA) hydrogel to obtain a multicolour tuneable fluorescence hydrogel. The resulting hydrogel exhibited stimuli response to different changes, such as pH, excitation wavelength or the presence of Fe^{3+} ions (Fig. 61). This approach opens a new path for the design and synthesis of novel multifunctional materials.[315]

4. Conclusions and future perspectives

The development of novel lanthanide-derived self-assemblies has increased in the last few years, driven by the interesting luminescence properties and potential applications of these systems. Of particular interest is understanding how these self-assemblies are formed, thus controlling the factors that have influence on the final stoichiometry, architecture and properties of the resulting lanthanide complexes has become the focus of research to date. Herein, we provided an update and comprehensive overview of luminescent lanthanide self-assemblies derived from non-macrocyclic nitrogen-donor ligands, covering studies reported from 2017 to date. All these systems show promising properties including temperature- or pH-dependent luminescence, upconversion, circularly polarized luminescence or biological activity. These properties highlight their potential for different applications of such self-assemblies as smart supramolecular materials: pH- or temperature-sensors, biological probes for use in sensing, imaging or diagnosis, optical sensors, switchable molecules or luminescent plastic materials.

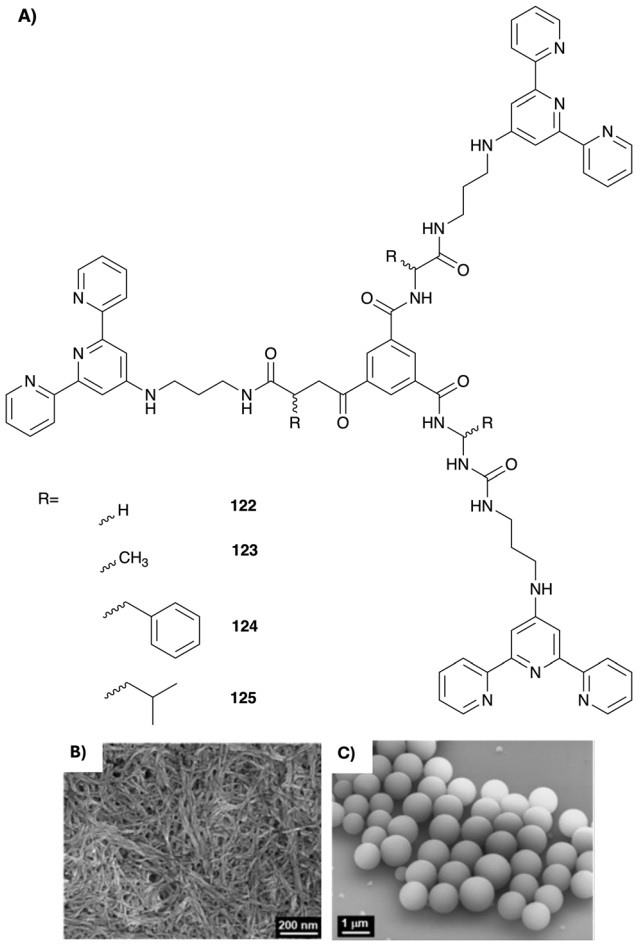

Fig. 59 (A) Structural formulas of the ligands **122–125**. (B) SEM image of the xerogels formed from **122**. (C) SEM image of the microspheres formed from **123**.[312] Adapted from ref. 312 with permission from Elsevier B.V., Copyright©2024.

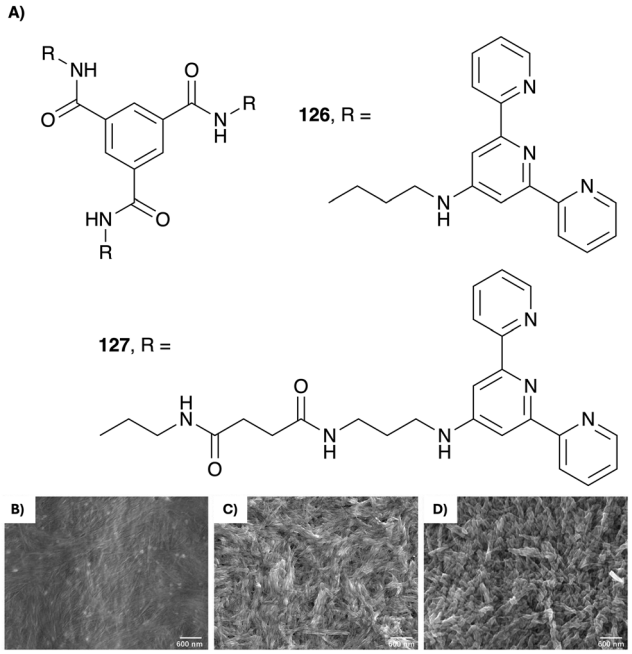

Fig. 60 (A) Structural formulas of ligands **126** and **127**; SEM images of organogel (B) **126** (0.6 wt%), and its corresponding metallogels with (C) La^{3+} and (D) Sm^{3+}. Adapted from references (CC-BY-4.0).[313,314] Adapted from ref. 313 and 314 with permission from Wiley-VCH, Copyright©2025.

Despite the aforementioned advancements, there remains much to explore within this field of research. One particularly fascinating area for future research is the exploration of their biological and bio-materials properties.[316–319] For instance, lanthanides have been shown to play an important role in bacterial metabolism,[316] as demonstrated by the finding of a lanthanide-binding molecule produced by *Methylobacterium extorquens*. This discovery provides insights into how microbes interact and sense lanthanide ions.[319] New insights into the potential of gadolinium-derived complexes as promising contrast agents were also reported.[320] Moreover, as the use of lanthanides increases, the toxicity of lanthanides emerges as an important topic of investigation. Lately, different novel functional genomics techniques have been used to identify potential therapeutic targets to mitigate the toxic effects of lanthanides.[321]

Additionally, the urgent need to recover lanthanides by using chelating ligands is another area to be explored, as lanthanides are essential in everyday technological materials.[322–327] Recently, the development of 2D protein layers as chelating agents for lanthanide ions has been reported, representing a promising approach for their recovery.[325] It is very likely that supramolecular self-assembly structures from lanthanides can also be used for such applications.

While some of the examples presented herein have demonstrated some selectively of one lanthanide ion over the other, their efficient separation remains a challenge due to their chemical similarity.[328,329] Recently, a machine learning approach has been developed to predict lanthanide extraction behaviour, screening a large number of ligands for accurate separation.[330] Once again, the idea of 'selective lanthanide' self-assembly can be employed to distinguish between such closely related ions! Some progress has

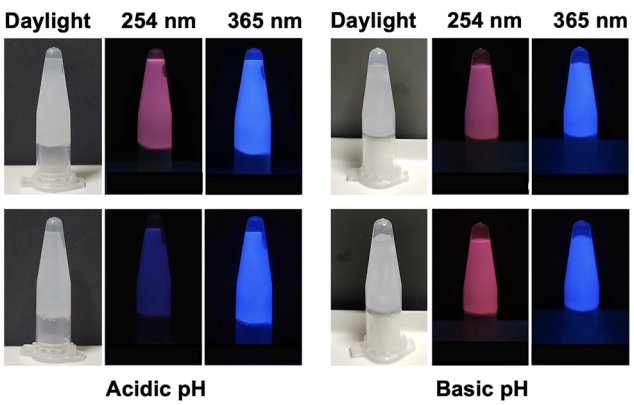

Fig. 61 PVA hydrogels containing Eu(**dpa**)$_3$ and blue-emitting AIE molecule at acidic and basic pH under daylight or a 254/365 nm excitation source. Adapted from reference.[315] Adapted from ref. 315 with permission from the American Chemical Society, Copyright©2025.

been made on this, as the synthesis of a two-ligand system combining lipophilic and hydrophilic behaviours with opposing Ln selectivity has recently been reported, leading to the selective separation of lanthanide ions.[331] Similarly, modifications in the connectivity and preorganization of tetradentate $[N_2O_2]$ ligands have demonstrated changes in their selectivity for lanthanide ions.[332]

With all these in mind, these challenges open the possibility to continue exploring within the field of lanthanide self-assemblies, providing new knowledge, advancements and interesting applications. It is clear that the future of supramolecular lanthanide chemistry is very bright, and we hope that this review, in addition to giving an overview of the recent progress in the area, can be an inspiration to newcomers to the field to tackle such challenges with new views and ideas, where the lanthanides take on a central role in supramolecular self-assembly chemistry.

Author contributions

All the authors took part in reviewing the area, gathering information and examples from the literature and writing this manuscript. S. F-F. is the lead writer of this review, supervised the writing along with S. O. D. and O. K. and edited the first draft. T. G. supervised the project and edited the final draft of the manuscript.

Conflicts of interest

There are no conflicts to declare.

Data availability

No primary research results, software or code have been included, and no new data were generated or analysed as part of this review.

Acknowledgements

We would like to thank the Irish Research Council (IRC Post-graduate funding to S.D. GOIPG/2018/2993) and Xunta de Galicia for the postdoctoral fellowship (S.F.-F. Ref. ED481B_044/2024). TG would like to thank Science Foundation Ireland (SFI, now renamed Research Ireland) and the SFI Synthesis and Solid-State Pharmaceutical Center (SSPC) for Research Centres Phase 2 Funding (12/RC/2275_P2).

Notes and references

1 J.-M. Lehn, *Angew. Chem., Int. Ed. Engl.*, 1988, **27**, 89–112.
2 C. J. Pedersen, *Angew. Chem., Int. Ed. Engl.*, 1988, **27**, 1021–1027.
3 D. J. Cram, *Angew. Chem., Int. Ed. Engl.*, 1988, **27**, 1009–1112.
4 J. Sauvage, *Angew. Chem., Int. Ed.*, 2017, **56**, 1–15.
5 J. F. Stoddart, *Angew. Chem., Int. Ed.*, 2017, **56**, 2–34.
6 B. L. Feringa, *Angew. Chem., Int. Ed.*, 2017, **56**, 1–20.
7 S. Thoonen, K. L. Tuck and D. R. Turner, *Coord. Chem. Rev.*, 2025, **522**, 216203.
8 J. C. G. Bünzli and C. Piguet, *Chem. Soc. Rev.*, 2005, **34**, 1048–1077.
9 J. L. Greenfield and J. R. Nitschke, *Acc. Chem. Res.*, 2022, **55**, 391–401.
10 R. Chakrabarty, P. S. Mukherjee and P. J. Stang, *Chem. Rev.*, 2011, **111**, 6810–6918.
11 C. Piguet, M. Borkovec, J. Hamacek and K. Zeckert, *Coord. Chem. Rev.*, 2005, **249**, 705–726.
12 A. P. Paneerselvam, S. S. Mishra and D. K. Chand, *J. Chem. Sci.*, 2018, **130**, 96.
13 M. Albrecht, *Chem. Rev.*, 2001, **101**, 3457–3497.
14 E. G. Percástegui, T. K. Ronson and J. R. Nitschke, *Chem. Rev.*, 2020, **120**, 13480–13544.
15 A. J. McConnell, *Chem. Soc. Rev.*, 2022, **51**, 2957–2971.
16 X. Wang, Y. Jiang, A. Tissot and C. Serre, *Coord. Chem. Rev.*, 2023, **497**, 215454.
17 Y. Zhang, S. Liu, Z. S. Zhao, Z. Wang, R. Zhang, L. Liu and Z. B. Han, *Inorg. Chem. Front.*, 2021, **8**, 590–619.
18 J. L. Obeso, C. V. Flores, R. A. Peralta, M. Viniegra, N. Martín-Guaregua, M. T. Huxley, D. Solis-Ibarra, I. A. Ibarra and C. Janiak, *Chem. Soc. Rev.*, 2025, **54**, 4135–4163.
19 S. Sahoo, S. Mondal and D. Sarma, *Coord. Chem. Rev.*, 2022, **470**, 214707.
20 G. Gil-Ramírez, D. A. Leigh and A. J. Stephens, *Angew. Chem., Int. Ed.*, 2015, **127**, 6208–6249.
21 E. M. G. Jamieson, F. Modicom and S. M. Goldup, *Chem. Soc. Rev.*, 2018, **47**, 5266–5311.
22 V. N. Vukotic and S. J. Loeb, *Chem. Soc. Rev.*, 2012, **41**, 5896–5906.
23 H. Y. Zhou, Q. S. Zong, Y. Han and C. F. Chen, *Chem. Commun.*, 2020, **56**, 9916–9936.
24 Z. Ashbridge, S. D. P. Fielden, D. A. Leigh, L. Pirvu, F. Schaufelberger and L. Zhang, *Chem. Soc. Rev.*, 2022, **51**, 7779–7809.
25 O. Lukin and F. Vögtle, *Angew. Chem., Int. Ed.*, 2005, **44**, 1456–1477.
26 J. F. Ayme, J. E. Beves, C. J. Campbell and D. A. Leigh, *Chem. Soc. Rev.*, 2013, **42**, 1700–1712.
27 S. D. P. Fielden, D. A. Leigh and S. L. Woltering, *Angew. Chem., Int. Ed.*, 2017, **56**, 11166–11194.
28 S. Panja and D. J. Adams, *Chem. Soc. Rev.*, 2021, **50**, 5165–5200.
29 B. C. Roy, A. Kundu, P. Biswas, S. Roy and T. S. Mahapatra, *ChemistrySelect*, 2024, **9**, e202304755.
30 W. W. Qin, B. F. Long, Z. H. Zhu, H. L. Wang, F. P. Liang and H. H. Zou, *Dalton Trans.*, 2024, **53**, 3675–3684.
31 M. I. Bardot, C. W. Weyhrich, Z. Shi, M. Traxler, C. L. Stern, J. Cui, D. A. Muller, M. L. Becker and W. R. Dichtel, *Science*, 2025, **387**, 264–269.
32 J. H. May, J. M. Fehr, J. C. Lorenz, L. N. Zakharov and R. Jasti, *Angew. Chem., Int. Ed.*, 2024, **63**, e202401823.

33 D. A. Leigh, F. Schaufelberger, L. Pirvu, J. H. Stenlid, D. P. August and J. Segard, *Nature*, 2020, **584**, 562–568.
34 K. M. Bąk, B. Trzaskowski and M. J. Chmielewski, *Chem. Sci.*, 2024, **15**, 1796–1809.
35 M. Zhang, S. Chen and L. Zhang, *J. Chem. Ed.*, 2025, **102**, 338–347.
36 M. Cirulli, A. Kaur, J. E. M. Lewis, Z. Zhang, J. A. Kitchen, S. M. Goldup and M. M. Roessler, *J. Am. Chem. Soc.*, 2019, **141**, 879–889.
37 S. Bernhard and M. W. Tibbitt, *Adv. Drug Delivery Rev.*, 2021, **171**, 240–256.
38 M. J. Webber and R. Langer, *Chem. Soc. Rev.*, 2017, **46**, 6600–6620.
39 H. Xu, R. Chen, Q. Sun, W. Lai, Q. Su, W. Huang and X. Liu, *Chem. Soc. Rev.*, 2014, **43**, 3259–3302.
40 H. Chen and J. Fraser Stoddart, *Nat. Rev. Mater.*, 2021, **6**, 804–828.
41 M. Kataria and S. Seki, *Chem. – Eur. J.*, 2025, **31**, e202403460.
42 A. Pöthig and A. Casini, *Theranostics*, 2019, **9**, 3150–3169.
43 I. V. Kolesnichenko and E. V. Anslyn, *Chem. Soc. Rev.*, 2017, **46**, 2385–2390.
44 C. Alexander, Z. Guo, P. B. Glover, S. Faulkner and Z. Pikramenou, *Chem. Rev.*, 2025, **125**, 2269–2370.
45 T. L. Mako, J. M. Racicot and M. Levine, *Chem. Rev.*, 2019, **119**, 322–477.
46 D. Wu, A. C. Sedgwick, T. Gunnlaugsson, E. U. Akkaya, J. Yoon and T. D. James, *Chem. Soc. Rev.*, 2017, **46**, 7105–7123.
47 G. Moreno-Alcántar, M. Drexler and A. Casini, *Nat. Rev. Chem.*, 2024, **8**, 893–914.
48 M. V. Ramakrishnam Raju, S. M. Harris and V. C. Pierre, *Chem. Soc. Rev.*, 2020, **49**, 1090–1108.
49 S. J. Butler and D. Parker, *Chem. Soc. Rev.*, 2013, **42**, 1652–1666.
50 S. E. Bodman and S. J. Butler, *Chem. Sci.*, 2021, **12**, 2716–2734.
51 E. Yashima, N. Ousaka, D. Taura, K. Shimomura, T. Ikai and K. Maeda, *Chem. Rev.*, 2016, **116**, 13752–13990.
52 A. V. Virovets, E. Peresypkina and M. Scheer, *Chem. Rev.*, 2021, **121**, 14485–14554.
53 L. J. Chen, H. B. Yang and M. Shionoya, *Chem. Soc. Rev.*, 2017, **46**, 2555–2576.
54 V. V. Utochnikova, *Coord. Chem. Rev.*, 2019, **398**, 113006.
55 W. Thor, A. N. Carneiro Neto, R. T. Moura, K. L. Wong and P. A. Tanner, *Coord. Chem. Rev.*, 2024, **517**, 215927.
56 S. Pullen, J. Tessarolo and G. H. Clever, *Chem. Sci.*, 2021, **12**, 7269–7293.
57 X. Z. Li, C. Bin Tian and Q. F. Sun, *Chem. Rev.*, 2022, **122**, 6374–6458.
58 M. Meyer, B. Kersting, R. E. Powers and K. N. Raymond, *Inorg. Chem.*, 1997, **36**, 5179–5191.
59 C. Piguet, A. F. Williams, G. Bernardiuelli, E. Moret and J.-C. G. Bünzli, *Helv. Chim. Acta*, 1992, **75**, 1697.
60 M. Elhabiri, R. Scopelliti, J.-C. G. Bünzli and C. Piguet, *Chem. Commun.*, 1998, 2347–2348.
61 N. M. Shavaleev, S. V. Eliseeva, R. Scopelliti and J. C. G. Bünzli, *Inorg. Chem.*, 2015, **54**, 9166–9173.
62 W. D. Horrocks and D. R. Sudnick, *Acc. Chem. Res.*, 1981, **14**, 384–392.
63 G. Bao, S. Wen, G. Lin, J. Yuan, J. Lin, K. L. Wong, J. C. G. Bünzli and D. Jin, *Coord. Chem. Rev.*, 2021, **429**, 213642.
64 Y. Zha, Z. Bian and Z. Liu, *Polyhedron*, 2025, **272**, 117452.
65 Y. L. Li, H. L. Wang, Z. H. Zhu, Y. F. Wang, F. P. Liang and H. H. Zou, *Nat. Commun.*, 2024, **15**, 2896.
66 A. G. Bispo Jr, N. A. Oliveira, I. M. S. Diogenis and F. A. Sigoli, *Coord. Chem. Rev.*, 2025, **523**, 216279.
67 I. F. Costa, L. Blois, T. B. Paolini, I. P. Assunção, E. E. S. Teotonio, M. C. F. C. Felinto, R. T. Moura, R. L. Longo, W. M. Faustino, L. D. Carlos, O. L. Malta, A. N. Carneiro Neto and H. F. Brito, *Coord. Chem. Rev.*, 2024, **502**, 215590.
68 L. Llanos, P. Cancino, P. Mella, P. Fuentealba and D. Aravena, *Coord. Chem. Rev.*, 2024, **505**, 215675.
69 P. P. Ferreira da Rosa, Y. Kitagawa and Y. Hasegawa, *Coord. Chem. Rev.*, 2020, **406**, 213153.
70 O. G. Willis, F. Zinna and L. Di Bari, *Angew. Chem., Int. Ed.*, 2023, **62**, e202302358.
71 F. Pointillart, O. Cador, B. Le Guennic and L. Ouahab, *Coord. Chem. Rev.*, 2017, **346**, 150–175.
72 S. J. Bradberry, A. J. Savyasachi, M. Martinez-Calvo and T. Gunnlaugsson, *Coord. Chem. Rev.*, 2014, **273–274**, 226–241.
73 A. De Bettencourt-Dias, P. S. Barber and S. Viswanathan, *Coord. Chem. Rev.*, 2014, **273–274**, 165–200.
74 L. Su, X. Liu, Q. Niu and Z. Li, *J. Mater. Chem. C*, 2024, **12**, 10759–10774.
75 D. E. Barry, D. F. Caffrey and T. Gunnlaugsson, *Chem. Soc. Rev.*, 2016, **45**, 3244–3274.
76 F. Ahmed, M. Muzammal Hussain, W. Ullah Khan and H. Xiong, *Coord. Chem. Rev.*, 2024, **499**, 215486.
77 D. Yang, H. Li and H. Li, *Coord. Chem. Rev.*, 2024, **514**, 215875.
78 J. C. G. Bünzli, *Coord. Chem. Rev.*, 2015, **293–294**, 19–47.
79 A. Beeby, I. M. Clarkson, R. S. Dickins, S. Faulkner, D. Parker, L. Royle, A. S. de Sousa, J. A. Gareth Williams and M. Woods, *J. Chem. Soc., Perkin Trans. 2*, 1999, 493–503.
80 E. A. Suturina, K. Mason, M. Botta, F. Carniato, I. Kuprov, N. F. Chilton, E. J. L. McInnes, M. Vonci and D. Parker, *Dalton Trans.*, 2019, **48**, 8400–8409.
81 L. B. Jennings, S. Shuvaev, M. A. Fox, R. Pal and D. Parker, *Dalton Trans.*, 2018, **47**, 16145–16154.
82 A. C. Harnden, E. A. Suturina, A. S. Batsanov, P. K. Senanayake, M. A. Fox, K. Mason, M. Vonci, E. J. L. McInnes, N. F. Chilton and D. Parker, *Angew. Chem., Int. Ed.*, 2019, **131**, 10396–10400.
83 A. T. Frawley, H. V. Linford, M. Starck, R. Pal and D. Parker, *Chem. Sci.*, 2018, **9**, 1042–1049.
84 S. Shuvaev and D. Parker, *Dalton Trans.*, 2019, **48**, 4471–4473.

85 E. R. H. Walter, J. A. G. Williams and D. Parker, *Chem. Commun.*, 2017, **53**, 13344–13347.
86 S. Shuvaev, M. A. Fox and D. Parker, *Angew. Chem., Int. Ed.*, 2018, **57**, 7488–7492.
87 J. D. Fradgley, M. Starck, M. Laget, E. Bourrier, E. Dupuis, L. Lamarque, E. Trinquet, J. M. Zwier and D. Parker, *Chem. Commun.*, 2021, **57**, 5814–5817.
88 M. Starck, J. D. Fradgley, R. Pal, J. M. Zwier, L. Lamarque and D. Parker, *Chem. – Eur. J.*, 2021, **27**, 766–777.
89 Y. Zhang, X. Ma, H. F. Chau, W. Thor, L. Jiang, S. Zha, W. Y. Fok, H. N. Mak, J. Zhang, J. Cai, C. F. Ng, H. Li, D. Parker, L. Li, G. L. Law and K. L. Wong, *ACS Appl. Nano Mater.*, 2021, **4**, 271–278.
90 D. F. De Rosa, M. Starck, D. Parker and R. Pal, *Chem. – Eur. J.*, 2024, **30**, e202303227.
91 D. Parker, J. D. Fradgley and K. L. Wong, *Chem. Soc. Rev.*, 2021, **50**, 8193–8213.
92 K. Binnemans, *Coord. Chem. Rev.*, 2015, **295**, 1–45.
93 S. V. Eliseeva and J. C. G. Bünzli, *Chem. Soc. Rev.*, 2010, **39**, 189–227.
94 J.-C. G. Bünzli and S. V. Eliseeva, in *Lanthanide Luminescence: Photophysical, Analytical and Biological Aspects*, ed. P. Hanninen and H. Harma, Springer-Verlag, Berlin Heidelberg, 2010, pp. 1–45.
95 Y. Hasegawa, Y. Wada and S. Yanagida, *J. Photochem. Photobiol., C*, 2004, **5**, 183–202.
96 M. Hasegawa, H. Ohmagari, H. Tanaka and K. Machida, *J. Photochem. Photobiol., C*, 2022, **50**, 100484.
97 W. Thor, H. Y. Kai, Y. H. Yeung, Y. Wu, T. L. Cheung, L. K. B. Tam, Y. Zhang, L. J. Charbonnière, P. A. Tanner and K. L. Wong, *JACS Au*, 2024, **4**, 3813–3822.
98 A. K. R. Junker, L. R. Hill, A. L. Thompson, S. Faulkner and T. J. Sørensen, *Dalton Trans.*, 2018, **47**, 4794–4803.
99 W. Thor, Y. Zhang, K. L. Wong and P. A. Tanner, *Chem. Commun.*, 2021, **57**, 10727–10730.
100 E. Kasprzycka, A. N. Carneiro Neto, V. A. Trush, O. L. Malta, L. Jerzykiewicz, V. M. Amirkhanov, J. Legendziewicz and P. Gawryszewska, *Spectrochim. Acta, Part A*, 2022, **274**, 121072.
101 V. R. M. Nielsen, P. R. Nawrocki and T. J. Sørensen, *J. Phys. Chem. A*, 2023, **127**, 3577–3590.
102 V. R. M. Nielsen, M. Grasser, B. Le Guennic and T. J. Sørrensen, *Inorg. Chem.*, 2025, **64**, 3463–3475.
103 S. S. Mortensen, M. A. Marciniak Nielsen, P. Nawrocki and T. J. Sørensen, *J. Phys. Chem. A*, 2022, **126**, 8596–8605.
104 P. R. Nawrocki and T. J. Sørensen, *Phys. Chem. Chem. Phys.*, 2023, **25**, 19300–19336.
105 S. S. Mortensen, V. R. M. Nielsen and T. J. Sørensen, *Dalton Trans.*, 2024, **53**, 10079–10092.
106 N. Kofod, R. Arppe-Tabbara and T. J. Sørensen, *J. Phys. Chem. A*, 2019, **123**, 2734–2744.
107 M. Storm Thomsen, A. S. Anker, L. Kacenauskaite and T. J. Sørensen, *Dalton Trans.*, 2022, **51**, 8960–8963.
108 V. R. M. Nielsen, M. Grasser, S. S. Mortensen, B. Le Guennic and T. J. Sørensen, *Inorg. Chem.*, 2024, **63**, 18596–18607.
109 V. R. M. Nielsen, B. Le Guennic and T. J. Sørensen, *J. Phys. Chem. A*, 2024, **128**, 5740–5751.
110 N. Kofod and T. J. Sørensen, *Dalton Trans.*, 2024, **53**, 9741–9749.
111 Y. Zhang, W. Thor, K. L. Wong and P. A. Tanner, *J. Phys. Chem. C*, 2021, **125**, 7022–7033.
112 N. Kofod, P. Nawrocki and T. J. Sørensen, *J. Phys. Chem. Lett.*, 2022, **13**, 3096–3104.
113 N. Kofod and T. J. Sørensen, *J. Phys. Chem. Lett.*, 2022, **13**, 11968–11973.
114 A. Ćirić, Ł. Marciniak and M. D. Dramićanin, *Sci. Rep.*, 2022, **12**, 563.
115 V. D. Savchenko, K. P. Zhuravlev and V. I. Tsaryuk, *J. Lumin.*, 2024, **276**, 120839.
116 S. Bej, X. Wang, J. Zhang, X. Yang and P. Ren, *Coord. Chem. Rev.*, 2024, **513**, 215862.
117 N. Wu, C. Bo and S. Guo, *ACS Sens.*, 2024, **9**, 4402–4434.
118 T. Gorai, W. Schmitt and T. Gunnlaugsson, *Dalton Trans.*, 2021, **50**, 770–784.
119 A. F. Henwood, I. N. Hegarty, E. P. McCarney, J. I. Lovitt, S. Donohoe and T. Gunnlaugsson, *Coord. Chem. Rev.*, 2021, **449**, 214206.
120 B. Golesorkhi, I. Taarit, H. Bolvin, H. Nozary, J. R. Jiménez, C. Besnard, L. Guénée, A. Fürstenberg and C. Piguet, *Dalton Trans.*, 2021, **50**, 7955–7968.
121 S. S. Mortensen and T. J. Sørensen, *Eur. J. Inorg. Chem.*, 2023, e202300159.
122 L. Arrico, C. Benetti and L. Di Bari, *ChemPhotoChem*, 2021, **5**, 815–821.
123 J. P. Byrne, J. A. Kitchen and T. Gunnlaugsson, *Chem. Soc. Rev.*, 2014, **43**, 5302–5325.
124 M. A. Halcrow, *Coord. Chem. Rev.*, 2005, **249**, 2880–2908.
125 H. Hofmeier and U. S. Schubert, *Chem. Soc. Rev.*, 2004, **33**, 373–399.
126 K. Tokunaga, *Phys. Chem. Chem. Phys.*, 2009, **11**, 1463–1473.
127 R. Carr, N. H. Evans and D. Parker, *Chem. Soc. Rev.*, 2012, **41**, 7673–7686.
128 A. Aebischer, F. Gumy and J. C. G. Bünzli, *Phys. Chem. Chem. Phys.*, 2009, **11**, 1346–1353.
129 S. E. Plush, N. A. Clear, J. P. Leonard, A. M. Fanning and T. Gunnlaugsson, *Dalton Trans.*, 2010, **39**, 3644–3652.
130 R. Shi, L. Yu, Y. Tian, X. Wang, Z. Sun, B. Qi and F. Luo, *Mater. Chem. Phys.*, 2022, **280**, 125806.
131 C. M. Balogh, I. N'Dala-Louika, I. Suleimanov, A. Pons, M. Jouffrieau, C. Camp, F. Chaput, L. Veyre, C. Thieuleux, O. Maury and F. Riobé, *Adv. Opt. Mater.*, 2024, **12**, 2400091.
132 X. S. Lin, Y. Yu, L. P. Zhou, L. He, T. Chen and Q. F. Sun, *Dalton Trans.*, 2022, **51**, 4836–4842.
133 O. Kotova, S. Blasco, B. Twamley, J. O'Brien, R. D. Peacock, J. A. Kitchen, M. Martínez-Calvo and T. Gunnlaugsson, *Chem. Sci.*, 2015, **6**, 457–471.
134 A. Galanti, O. Kotova, S. Blasco, C. J. Johnson, R. D. Peacock, S. Mills, J. J. Boland, M. Albrecht and T. Gunnlaugsson, *Chem. – Eur. J.*, 2016, **22**, 9709–9723.
135 C. Lincheneau, C. Destribats, D. E. Barry, J. A. Kitchen, R. D. Peacock and T. Gunnlaugsson, *Dalton Trans.*, 2011, **40**, 12005–12016.

136 J. P. Leonard, P. Jensen, T. McCabe, J. E. O'Brien, R. D. Peacock, P. E. Kruger and T. Gunnlaugsson, *J. Am. Chem. Soc.*, 2007, **129**, 10986–10987.
137 O. Kotova, J. A. Kitchen, C. Lincheneau, R. D. Peacock and T. Gunnlaugsson, *Chem. – Eur. J.*, 2013, **19**, 16181–16186.
138 H. Y. Wong, W. S. Lo, K. H. Yim and G. L. Law, *Chem*, 2019, **5**, 3058–3095.
139 L. E. MacKenzie and R. Pal, *Nat. Rev. Chem.*, 2021, **5**, 109–124.
140 K. Staszak, K. Wieszczycka, V. Marturano and B. Tylkowski, *Coord. Chem. Rev.*, 2019, **397**, 76–90.
141 L. Llanos, P. Cancino, P. Mella, P. Fuentealba and D. Aravena, *Coord. Chem. Rev.*, 2024, **505**, 215675.
142 K. Taniguchi, M. Nishio, S. Kishiue, P. J. Huang, S. Kimura and H. Miyasaka, *Phys. Rev. Mater.*, 2019, **3**, 045202.
143 J. A. Kitchen, D. E. Barry, L. Mercs, M. Albrecht, R. D. Peacock and T. Gunnlaugsson, *Angew. Chem., Int. Ed.*, 2012, **51**, 704–708.
144 D. E. Barry, J. A. Kitchen, M. Albrecht, S. Faulkner and T. Gunnlaugsson, *Langmuir*, 2013, **29**, 11506–11515.
145 D. E. Barry, J. A. Kitchen, L. Mercs, R. D. Peacock, M. Albrecht and T. Gunnlaugsson, *Dalton Trans.*, 2019, **48**, 11317–11325.
146 A. T. O'Neil, J. A. Harrison and J. A. Kitchen, *Chem. Commun.*, 2021, **57**, 8067–8070.
147 A. T. O'Neil, A. Chalard, J. Malmström and J. A. Kitchen, *Dalton Trans.*, 2023, **52**, 2255–2261.
148 S. J. Bradberry, A. J. Savyasachi, R. D. Peacock and T. Gunnlaugsson, *Faraday Discuss.*, 2015, **185**, 413–431.
149 D. F. Caffrey, T. Gorai, B. Rawson, M. Martínez-Calvo, J. A. Kitchen, N. S. Murray, O. Kotova, S. Comby, R. D. Peacock, P. Stachelek, R. Pal and T. Gunnlaugsson, *Adv. Sci.*, 2024, **11**, 2307448.
150 S. Di Pietro, D. Iacopini, A. Moscardini, R. Bizzarri, M. Pineschi, V. Di Bussolo and G. Signore, *Molecules*, 2021, **26**, 1265.
151 M. Starck, L. E. Mackenzie, A. S. Batsanov, D. Parker and R. Pal, *Chem. Commun.*, 2019, **55**, 14115–14118.
152 K. R. Johnson and A. De Bettencourt-Dias, *Inorg. Chem.*, 2019, **58**, 13471–13480.
153 K. R. Johnson, S. B. Vittardi, M. A. Gracia-Nava, J. J. Rack and A. de Bettencourt-Dias, *Chem. – Eur. J.*, 2020, **26**, 7274–7280.
154 R. A. Tigaa, X. Aerken, A. Fuchs and A. de Bettencourt-Dias, *Eur. J. Inorg. Chem.*, 2017, 5310–5317.
155 C. V. Rodrigues, K. R. Johnson, V. C. Lombardi, M. O. Rodrigues, J. A. Sobrinho and A. De Bettencourt-Dias, *J. Med. Chem.*, 2021, **64**, 7724–7734.
156 J. H. S. K. Monteiro, D. Machado, L. M. De Hollanda, M. Lancellotti, F. A. Sigoli and A. De Bettencourt-Dias, *Chem. Commun.*, 2017, **53**, 11818–11821.
157 J. H. S. K. Monteiro, N. R. Fetto, M. J. Tucker and A. De Bettencourt-Dias, *Inorg. Chem.*, 2020, **59**, 3193–3199.
158 J. H. S. K. Monteiro, N. R. Fetto, M. J. Tucker, F. A. Sigoli and A. de Bettencourt-Dias, *J. Lumin.*, 2022, **245**, 118768.
159 K. Wojtczak, E. Zahorska, I. J. Murphy, F. Koppel, G. Cooke, A. Titz and J. P. Byrne, *Chem. Commun.*, 2023, **59**, 8384–8387.
160 M. T. Phi, H. Singer, F. Zäh, C. Haisch, S. Schneider, H. J. M. Op den Camp and L. J. Daumann, *ChemBioChem*, 2024, **25**, e202300811.
161 B. Jahn, A. Pol, H. Lumpe, T. R. M. Barends, A. Dietl, C. Hogendoorn, Huub J. M. Op Den Camp and L. J. Daumann, *ChemBioChem*, 2018, **19**, 1147–1153.
162 K. Matsumoto, K. Suzuki, T. Tsukuda and T. Tsubomura, *Inorg. Chem.*, 2010, **49**, 4717–4719.
163 B. D. Ward and L. H. Gade, *Chem. Commun.*, 2012, **48**, 10587–10599.
164 J. Yuasa, T. Ohno, K. Miyata, H. Tsumatori, Y. Hasegawa and T. Kawai, *J. Am. Chem. Soc.*, 2011, **133**, 9892–9902.
165 K. Binnemans, *Chem. Rev.*, 2009, **109**, 4283–4374.
166 C. Freund, W. Porzio, U. Giovanella, F. Vignali, M. Pasini, S. Destri, A. Mech, S. Di Pietro, L. Di Bari and P. Mineo, *Inorg. Chem.*, 2011, **50**, 5417–5429.
167 D. Singh, S. Bhagwan, A. Dalal, K. Nehra, R. K. Saini, K. Singh, A. P. Simantilleke, S. Kumar and I. Singh, *Rare Met.*, 2021, **40**, 2873–2881.
168 I. M. S. Diogenis, A. G. Bispo-Jr, R. V. Pirovani, L. F. Saraiva, F. C. Gozzo, C. R. D. Correia, I. O. Mazali, R. A. Nome and F. A. Sigoli, *J. Mater. Chem. C*, 2024, **12**, 5097–5107.
169 J. K. Clegg, F. Li and L. F. Lindoy, *Coord. Chem. Rev.*, 2022, **455**, 214355.
170 O. G. Willis, F. Petri, G. Pescitelli, A. Pucci, E. Cavalli, A. Mandoli, F. Zinna and L. Di Bari, *Angew. Chem., Int. Ed.*, 2022, **61**, e202208326.
171 M. Górecki, L. Carpita, L. Arrico, F. Zinna and L. Di Bari, *Dalton Trans.*, 2018, **47**, 7166–7177.
172 F. Zinna, L. Arrico and L. Di Bari, *Chem. Commun.*, 2019, **55**, 6607–6609.
173 Y. Okayasu, K. Wakabayashi and J. Yuasa, *Inorg. Chem.*, 2022, **61**, 15108–15115.
174 A. De Bettencourt-Dias, J. S. K. Rossini and J. A. Sobrinho, *Dalton Trans.*, 2020, **49**, 17699–17708.
175 J. Liu, W. Song, H. Niu, Y. Lu, H. Yang, W. Li, Y. Zhao and Z. Miao, *Inorg. Chem.*, 2024, **63**, 18429–18437.
176 J. Liu, Y. Zhang, R. Yao, H. Ren, W. Wang, H. Feng, W. Li and Z. Miao, *Molecules*, 2024, **29**, 5887.
177 C. L. Liu, R. L. Zhang, C. S. Lin, L. P. Zhou, L. X. Cai, J. T. Kong, S. Q. Yang, K. L. Han and Q. F. Sun, *J. Am. Chem. Soc.*, 2017, **139**, 12474–12479.
178 D. M. Lyubov, A. N. Carneiro Neto, A. Fayoumi, K. A. Lyssenko, V. M. Korshunov, I. V. Taydakov, F. Salles, Y. Guari, J. Larionova, L. D. Carlos, J. Long and A. A. Trifonov, *J. Mater. Chem. C*, 2022, **10**, 7176–7188.
179 A. Abhervé, M. Mastropasqua Talamo, N. Vanthuyne, F. Zinna, L. Di Bari, M. Grasser, B. Le Guennic and N. Avarvari, *Eur. J. Inorg. Chem.*, 2022, e202200010.
180 H. Bolvin, A. Fürstenberg, B. Golesorkhi, H. Nozary, I. Taarit and C. Piguet, *Acc. Chem. Res.*, 2022, **55**, 442–456.
181 B. Golesorkhi, S. Naseri, L. Guénée, I. Taarit, F. Alves, H. Nozary and C. Piguet, *J. Am. Chem. Soc.*, 2021, **143**, 15326–15334.
182 I. Taarit, F. Alves, A. Benchohra, L. Guénée, B. Golesorkhi, A. Rosspeintner, A. Fürstenberg and C. Piguet, *J. Am. Chem. Soc.*, 2023, **145**, 8621–8633.

183 B. Golesorkhi, I. Taarit, H. Bolvin, H. Nozary, J. R. Jiménez, C. Besnard, L. Guénée, A. Fürstenberg and C. Piguet, *Dalton Trans.*, 2021, **50**, 7955–7968.
184 S. Naseri, I. Taarit, H. Bolvin, J. C. Bünzli, A. Fürstenberg, L. Guénée, G. Le-Hoang, M. Mirzakhani, H. Nozary, A. Rosspeintner and C. Piguet, *Angew. Chem., Int. Ed.*, 2023, **62**, e202314503.
185 K. Baudet, V. Kale, M. Mirzakhani, L. Babel, S. Naseri, C. Besnard, H. Nozary and C. Piguet, *Inorg. Chem.*, 2020, **59**, 62–75.
186 G. Le-Hoang, L. Guénée, S. Naseri, C. Besnard and C. Piguet, *Helv. Chim. Acta*, 2023, **106**, e202200190.
187 S. Naseri, M. Mirzakhani, C. Besnard, L. Guénée, L. Briant, H. Nozary and C. Piguet, *Chem. – Eur. J.*, 2023, **29**, e202202727.
188 G. Le-Hoang, L. Guénée, Q. Sommer and C. Piguet, *Inorg. Chem.*, 2024, **63**, 3712–3723.
189 Y. Li, J. C. Huffman and A. H. Flood, *Chem. Commun.*, 2007, 2692–2694.
190 A. Indapurkar, B. Henriksen, J. Tolman and J. Fletcher, *J. Pharm. Sci.*, 2013, **102**, 2589–2598.
191 R. M. Meudtner, M. Ostermeier, R. Goddard, C. Limberg and S. Hecht, *Chem. – Eur. J.*, 2007, **13**, 9834–9840.
192 J. P. Byrne, M. Martínez-Calvo, R. D. Peacock and T. Gunnlaugsson, *Chem. – Eur. J.*, 2016, **22**, 486–490.
193 I. N. Hegarty, C. S. Hawes and T. Gunnlaugsson, *Org. Chem. Front.*, 2023, **10**, 1915–1926.
194 N. Shukla, V. Singhmar, J. Sayala and A. K. Patra, *Inorg. Chem.*, 2025, **64**, 1287–1301.
195 F. Han, Q. Teng, Y. Zhang, Y. Wang and Q. Shen, *Inorg. Chem.*, 2011, **50**, 2634–2643.
196 K. Q. Mo, X. F. Ma, H. L. Wang, Z. H. Zhu, Y. C. Liu, H. H. Zou and F. P. Liang, *Sci. Rep.*, 2019, **9**, 12231.
197 C. Camp, V. Guidal, B. Biswas, J. Pécaut, L. Dubois and M. Mazzanti, *Chem. Sci.*, 2012, **3**, 2433–2448.
198 F. Lucio-Martínez, Z. Garda, B. Váradi, F. K. Kálmán, D. Esteban-Gómez, É. Tóth, G. Tircsó and C. Platas-Iglesias, *Inorg. Chem.*, 2022, **61**, 5157–5171.
199 M. Poncet, C. Besnard, J. R. Jiménez and C. Piguet, *Inorg. Chem.*, 2024, **63**, 18345–18354.
200 K. M. Ayers, N. D. Schley and G. Ung, *Eur. J. Inorg. Chem.*, 2019, 3769–3775.
201 D. Schnable, K. Freedman, K. M. Ayers, N. D. Schley, M. Kol and G. Ung, *Inorg. Chem.*, 2020, **59**, 8498–8504.
202 K. M. Ayers, N. D. Schley and G. Ung, *Inorg. Chem.*, 2020, **59**, 7657–7665.
203 L. Arrico, C. De Rosa, L. Di Bari, A. Melchior and F. Piccinelli, *Inorg. Chem.*, 2020, **59**, 5050–5062.
204 M. Leonzio, A. Melchior, G. Faura, M. Tolazzi, F. Zinna, L. Di Bari and F. Piccinelli, *Inorg. Chem.*, 2017, **56**, 4413–4422.
205 M. Cui, A. L. Wang, C. L. Gao, L. Zhou, T. Wu, S. Fang, H. P. Xiao, F. C. Li and X. L. Li, *Dalton Trans.*, 2021, **50**, 1007–1018.
206 Y. Peng, T. Wang, C. Gao, F. Li and X. L. Li, *CrystEngComm*, 2024, **26**, 3867–3873.
207 A. B. Solea, L. Yang, A. Crochet, K. M. Fromm, C. Allemann and O. Mamula, *Chem*, 2022, **4**, 18–30.
208 O. Mamula, M. Lama, S. G. Telfer, A. Nakamura, R. Kuroda, H. Stoeckli-Evans and R. Scopelitti, *Angew. Chem., Int. Ed.*, 2005, **44**, 2527–2531.
209 A. Scrivanti, M. Bortoluzzi, A. Morandini, A. Dolmella, F. Enrichi, R. Mazzaro and A. Vomiero, *New J. Chem.*, 2018, **42**, 11064–11072.
210 K. R. Johnson, V. C. Lombardi and A. de Bettencourt-Dias, *Chem. – Eur. J.*, 2020, **26**, 12060–12066.
211 N. Souri, P. Tian, A. Lecointre, Z. Lemaire, S. Chafaa, J. M. Strub, S. Cianférani, M. Elhabiri, C. Platas-Iglesias and L. J. Charbonnière, *Inorg. Chem.*, 2016, **55**, 12962–12974.
212 N. Souri, P. Tian, C. Platas-Iglesias, K. L. Wong, A. Nonat and L. J. Charbonnière, *J. Am. Chem. Soc.*, 2017, **139**, 1456–1459.
213 R. C. Knighton, L. K. Soro, W. Thor, J. M. Strub, S. Cianférani, Y. Mély, M. Lenertz, K. L. Wong, C. Platas-Iglesias, F. Przybilla and L. J. Charbonnière, *J. Am. Chem. Soc.*, 2022, **144**, 13356–13365.
214 L. Petitpoisson, A. Mahamoud, V. Mazan, M. Sy, O. Jeannin, E. Tóth, L. J. Charbonnière, M. Elhabiri and A. M. Nonat, *Inorg. Chem.*, 2024, **63**, 22829–22844.
215 W. Chen, X. Tang, W. Dou, B. Wang, L. Guo, Z. Ju and W. Liu, *Chem. – Eur. J.*, 2017, **23**, 9804–9811.
216 Y. Yao, Y. Zhou, T. Zhu, T. Gao, H. Li and P. Yan, *ACS Appl. Mater. Interfaces*, 2020, **12**, 15338–15347.
217 J. J. Pang, Z. Q. Yao, K. Zhang, Q. W. Li, Z. X. Fu, R. Zheng, W. Li, J. Xu and X. H. Bu, *Angew. Chem., Int. Ed.*, 2023, **62**, e202217456.
218 R. Sanchez-Fernandez, I. Obregon-Gomez, A. Sarmiento, M. E. Vazquez and E. Pazos, *Chem. Commun.*, 2024, **60**, 12650.
219 O. Kotova, S. Comby, C. Lincheneau and T. Gunnlaugsson, *Chem. Sci.*, 2017, **8**, 3419–3426.
220 X. Q. Guo, L. P. Zhou, S. J. Hu, L. X. Cai, P. M. Cheng and Q. F. Sun, *J. Am. Chem. Soc.*, 2021, **143**, 6202–6210.
221 W. W. Qin, Y. L. Li, Z. H. Zhu, F. P. Liang, Q. Hu and H. H. Zou, *Inorg. Chem. Front.*, 2023, **10**, 6269–6281.
222 Y. Zhang, B. Ali, J. Wu, M. Guo, Y. Yu, Z. Liu and J. Tang, *Inorg. Chem.*, 2019, **58**, 3167–3174.
223 T.-T. Wang, H. Wang and W.-B. Sun, *Inorg. Chem. Front.*, 2025, **12**, 1918.
224 X. L. Li, L. Zhao, J. Wu, W. Shi, N. Struch, A. Lützen, A. K. Powell, P. Cheng and J. Tang, *Chem. Sci.*, 2022, **13**, 10048–10056.
225 J. X. Liu, K. Chen and C. Redshaw, *Chem. Soc. Rev.*, 2023, **52**, 1428–1455.
226 Y. L. Li, H. L. Wang, Z. H. Zhu, F. P. Liang and H. H. Zou, *Coord. Chem. Rev.*, 2023, **493**, 215322.
227 K. H. Yim, C. T. Yeung, H. Y. Wong and G. L. Law, *Inorg. Chem. Front.*, 2021, **8**, 2952.
228 L. Hu, Y. Yang, Y. Gao, Y. Wei, J. Zhu and W. Wu, *Chem. Eng. J.*, 2024, **488**, 150965.
229 J. M. Lehn, A. Rigault, J. Siegel, J. Harrowfield, B. Chevrier and D. Moras, *Proc. Natl. Acad. Sci. U. S. A.*, 1987, **84**, 2565–2569.

230 C. Piguet, G. Bernardinelli and G. Hopfgartner, *Chem. Rev.*, 1997, **97**, 2005–2062.
231 O. Kotova, S. Comby, K. Pandurangan, F. Stomeo, J. E. O'Brien, M. Feeney, R. D. Peacock, C. P. McCoy and T. Gunnlaugsson, *Dalton Trans.*, 2018, **47**, 12308–12317.
232 C. L. Liu, L. P. Zhou, D. Tripathy and Q. F. Sun, *Chem. Commun.*, 2017, **53**, 2459–2462.
233 M. Albrecht and S. Kotila, *Angew. Chem., Int. Ed. Engl.*, 1995, **34**, 4–7.
234 K. H. Yim, C. T. Yeung, M. R. Probert, W. T. K. Chan, L. E. Mackenzie, R. Pal, W. T. Wong and G. L. Law, *Commun. Chem.*, 2021, **4**, 116.
235 S. Comby, F. Stomeo, C. P. Mccoy and T. Gunnlaugsson, *Helv. Chim. Acta*, 2009, **92**, 2461–2473.
236 F. Stomeo, C. Lincheneau, J. P. Leonard, J. E. O. Brien, R. D. Peacock, C. P. Mccoy and T. Gunnlaugsson, *J. Am. Chem. Soc.*, 2009, **131**, 9636–9637.
237 C. Lincheneau, R. D. Peacock and T. Gunnlaugsson, *Chem. – Asian J.*, 2010, **5**, 500–504.
238 D. E. Barry, J. A. Kitchen, K. Pandurangan, A. J. Savyasachi, R. D. Peacock and T. Gunnlaugsson, *Inorg. Chem.*, 2020, **59**, 2646–2650.
239 I. N. Hegarty, D. E. Barry, J. P. Byrne, O. Kotova and T. Gunnlaugsson, *Chem. Commun.*, 2023, **59**, 6044–6047.
240 D. E. Barry, O. Kotova, N. A. O'Shea, S. R. Donohoe, A. J. Savyasachi and T. Gunnlaugsson, *Mater. Chem. Front.*, 2025, **9**(2), 258–270.
241 J. Zhang, Y. Zhou, Y. Yao, Z. Cheng, T. Gao, H. Li and P. Yan, *J. Mater. Chem. C*, 2020, **8**, 6788–6796.
242 L. X. Cai, L. L. Yan, S. C. Li, L. P. Zhou and Q. F. Sun, *Dalton Trans.*, 2018, **47**, 14204–14210.
243 R. Chen, Q. Q. Yan, S. J. Hu, X. Q. Guo, L. X. Cai, D. N. Yan, L. P. Zhou and Q. F. Sun, *Org. Chem. Front.*, 2021, **8**, 2576–2582.
244 R. Chen, Q. Q. Yan, S. J. Hu, X. Q. Guo, L. P. Zhou and Q. F. Sun, *Dalton Trans.*, 2022, **52**, 37–43.
245 X. Guo, X. Zhang, S. Hu, L. Zhou and Q. Sun, *Chem. Res. Chin. Univ.*, 2024, **40**, 842–848.
246 B. Golesorkhi, L. Guénée, H. Nozary, A. Fürstenberg, Y. Suffren, S. V. Eliseeva, S. Petoud, A. Hauser and C. Piguet, *Chem. – Eur. J.*, 2018, **24**, 13158–13169.
247 C. Egger, L. Guénée, N. Deorukhkar and C. Piguet, *Dalton Trans.*, 2024, **53**, 6050–6062.
248 D. Zare, Y. Suffren, H. Nozary, A. Hauser and C. Piguet, *Angew. Chem., Int. Ed.*, 2017, **56**, 14612–14617.
249 N. Deorukhkar, C. Egger, L. Guénée, C. Besnard and C. Piguet, *J. Am. Chem. Soc.*, 2024, **146**, 308–318.
250 T. Lathion, A. Fürstenberg, C. Besnard, A. Hauser, A. Bousseksou and C. Piguet, *Inorg. Chem.*, 2020, **59**, 1091–1103.
251 T. Lathion, N. Deorukhkar, C. Egger, H. Nozary and C. Piguet, *Dalton Trans.*, 2024, **53**, 17731–18056.
252 D. J. Bell, T. Zhang, N. Geue, C. J. Rogers, P. E. Barran, A. M. Bowen, L. S. Natrajan and I. A. Riddell, *Chem. – Eur. J.*, 2023, **29**, e202302497.
253 D. J. Bell, L. S. Natrajan and I. A. Riddell, *Coord. Chem. Rev.*, 2022, **472**, 214786.
254 E. G. Percástegui, *Eur. J. Inorg. Chem.*, 2021, 4425–4438.
255 F. Guo, D. F. Li, F. Gao, K. Xu, J. Zhang, X. G. Yi, D. P. Li and Y. X. Li, *Inorg. Chem.*, 2022, **61**, 17089–17100.
256 J. Li, M. Kou, S. Zhou, F. Dong, X. Huang, X. Tang, Y. Tang and W. Liu, *Nat. Commun.*, 2025, **16**, 2169.
257 S. M. Jansze, G. Cecot, M. D. Wise, K. O. Zhurov, T. K. Ronson, A. M. Castilla, A. Finelli, P. Pattison, E. Solari, R. Scopelliti, G. E. Zelinskii, A. V. Vologzhanina, Y. Z. Voloshin, J. R. Nitschke and K. Severin, *J. Am. Chem. Soc.*, 2016, **138**, 2046–2054.
258 J. Su, F. Yin, X. F. Duan, J. Y. Zhou, L. P. Zhou, C. Bin Tian and Q. F. Sun, *Inorg. Chem. Front.*, 2025, **12**, 3073–3082.
259 X. Q. Guo, P. Yu, L. P. Zhou, S. J. Hu, X. F. Duan, L. X. Cai, L. Bao, X. Lu and Q. F. Sun, *Nat. Synth.*, 2025, **4**, 359–369.
260 X. Z. Li, L. P. Zhou, L. L. Yan, D. Q. Yuan, C. S. Lin and Q. F. Sun, *J. Am. Chem. Soc.*, 2017, **139**, 8237–8244.
261 Z. Wang, L. He, B. Liu, L. P. Zhou, L. X. Cai, S. J. Hu, X. Z. Li, Z. Li, T. Chen, X. Li and Q. F. Sun, *J. Am. Chem. Soc.*, 2020, **142**, 16409–16419.
262 Q. Y. Zhu, L. P. Zhou, L. X. Cai, S. J. Hu, X. Z. Li and Q. F. Sun, *Inorg. Chem.*, 2022, **61**, 16814–16821.
263 X. Q. Guo, L. P. Zhou, S. J. Hu and Q. F. Sun, *Dalton Trans.*, 2024, **53**, 4772–4780.
264 X.-F. Duan, H. Ji, L.-P. Zhou, S.-J. Hu, J. Fu, P. Duan, X.-Q. Guo and Q.-F. Sun, *CCS Chem.*, 2025, 1–9.
265 C. T. Yeung, K. H. Yim, H. Y. Wong, R. Pal, W. S. Lo, S. C. Yan, M. Yee-Man Wong, D. Yufit, D. E. Smiles, L. J. McCormick, S. J. Teat, D. K. Shuh, W. T. Wong and G. L. Law, *Nat. Commun.*, 2017, **8**, 1128.
266 C. T. Yeung, W. T. K. Chan, S. C. Yan, K. L. Yu, K. H. Yim, W. T. Wong and G. L. Law, *Chem. Commun.*, 2015, **51**, 592–595.
267 K.-H. Yim, C.-T. Yeung, M. Y.-M. Wong, M. R. Probert and G.-L. Law, *Chem. – Eur. J.*, 2022, **28**, e202201655.
268 C. L. Liu, R. L. Zhang, C. S. Lin, L. P. Zhou, L. X. Cai, J. T. Kong, S. Q. Yang, K. L. Han and Q. F. Sun, *J. Am. Chem. Soc.*, 2017, **139**, 12474–12479.
269 X. Q. Guo, L. P. Zhou, L. X. Cai and Q. F. Sun, *Chem. – Eur. J.*, 2018, **24**, 6936–6940.
270 S. J. Hu, X. Q. Guo, L. P. Zhou, L. X. Cai and Q. F. Sun, *Chin. J. Chem.*, 2019, **37**, 657–662.
271 S. Y. Wu, X. Q. Guo, L. P. Zhou and Q. F. Sun, *Inorg. Chem.*, 2019, **58**, 7091–7098.
272 S. J. Hu, X. Q. Guo, L. P. Zhou, L. X. Cai, C. Bin Tian and Q. F. Sun, *Chin. J. Chem.*, 2023, **41**, 797–804.
273 Z. Zhu, S. Hu, Z. Liu, L. Zhou, C. Tian and Q. Sun, *Chin. Chem. Lett.*, 2024, **36**, 109641.
274 Y. Zhou, F. Yin, S. J. Hu, L. P. Zhou, J. Yang and Q. F. Sun, *Inorg. Chem.*, 2025, **64**, 6927–6934.
275 N. Klangwart, C. Ruijs, C. S. Hawes, T. Gunnlaugsson and O. Kotova, *Supramol. Chem.*, 2022, **34**, 10–19.
276 L. P. Zhou, X. S. Feng, S. J. Hu and Q. F. Sun, *J. Am. Chem. Soc.*, 2023, **145**, 17845–17855.
277 T. Zhao, Y. F. Zhang, G. H. Wang, X. X. Wang, P. F. Feng and S. Q. Zang, *Angew. Chem., Int. Ed.*, 2025, e202421426.
278 J. F. Stoddart,*Mechanically Interlocked Molecules (MIMs) – Molecular Shuttles, Switches, and Machines*, Weinheim, Germany, 1998.

279 C. J. Bruns and J. Fraser Stoddart, *The Nature of the Mechanical Bond: From Molecules to Machines*, John Wiley & Sons, 1st edn, 2017, pp. 4–54.
280 N. H. Evans, *ChemPlusChem*, 2020, **85**, 783–792.
281 A. Savoini, P. R. Gallagher, A. Saady and S. M. Goldup, *J. Am. Chem. Soc.*, 2024, **146**, 8472–8479.
282 S. M. Goldup, *Acc. Chem. Res.*, 2024, **57**, 1696–1708.
283 J. E. M. Lewis, P. D. Beer, S. J. Loeb and S. M. Goldup, *Chem. Soc. Rev.*, 2017, **46**, 2577–2591.
284 A. Saura-Sanmartin, A. Pastor, A. Martinez-Cuezva, G. Cutillas-Font, M. Alajarin and J. Berna, *Chem. Soc. Rev.*, 2022, **51**, 4949–4976.
285 T. G. Johnson and M. J. Langton, *J. Am. Chem. Soc.*, 2023, **145**, 27167–27184.
286 M. Nandi, S. Bej, T. Jana and P. Ghosh, *Chem. Commun.*, 2023, **59**, 14776–14790.
287 S. Mena-Hernando and E. M. Pérez, *Chem. Soc. Rev.*, 2019, **48**, 5016–5032.
288 C. Lincheneau, B. Jean-Denis and T. Gunnlaugsson, *Chem. Commun.*, 2014, **50**, 2857–2860.
289 M. Nandi, S. Bej, T. K. Ghosh and P. Ghosh, *Chem. Commun.*, 2019, **55**, 3085–3088.
290 Y. A. Mondjinou, B. P. Loren, C. J. Collins, S. H. Hyun, A. Demoret, J. Skulsky, C. Chaplain, V. Badwaik and D. H. Thompson, *Bioconjugate Chem.*, 2018, **29**, 3550–3560.
291 D. A. Leigh, L. Pirvu, F. Schaufelberger, D. J. Tetlow and L. Zhang, *Angew. Chem., Int. Ed.*, 2018, **57**, 10484–10488.
292 A. Ramström, D. R. S. Pooler, H. Abasov, M. Tomar, S. Crespi and F. Schaufelberger, *Angew. Chem., Int. Ed.*, 2025, **64**, e202505666.
293 Q. Zhou, X. Dong, G. Chi, X. Y. Cao, N. Zhang, S. Wu, Y. Ma, Z. H. Zhang and L. Zhang, *J. Am. Chem. Soc.*, 2024, **146**, 22405–22412.
294 L. Zhang, A. J. Stephens, A. L. Nussbaumer, J. F. Lemonnier, P. Jurček, I. J. Vitorica-Yrezabal and D. A. Leigh, *Nat. Chem.*, 2018, **10**, 1083–1088.
295 D. A. Leigh, J. J. Danon, S. D. P. Fielden, J. F. Lemonnier, G. F. S. Whitehead and S. L. Woltering, *Nat. Chem.*, 2021, **13**, 117–122.
296 J. J. Danon, A. Krüger, D. A. Leigh, J.-F. Lemonnier, A. J. Stephens, I. J. Vitorica-Yrezabal and S. L. Woltering, *Science*, 2017, **355**, 159–162.
297 M. Calvaresi, A. S. Duwez, D. A. Leigh, D. Sluysmans, Y. Song, F. Zerbetto and L. Zhang, *Chem*, 2023, **9**, 65–75.
298 D. A. Leigh, L. Pirvu and F. Schaufelberger, *J. Am. Chem. Soc.*, 2019, **141**, 6054–6059.
299 N. Katsonis, F. Lancia, D. A. Leigh, L. Pirvu, A. Ryabchun and F. Schaufelberger, *Nat. Chem.*, 2020, **12**, 939–944.
300 Z. Ashbridge, E. Kreidt, L. Pirvu, F. Schaufelberger, J. H. Stenlid, F. Abild-Pedersen and D. A. Leigh, *Science*, 2022, **375**, 1035–1044.
301 Z. Ashbridge, O. M. Knapp, E. Kreidt, D. A. Leigh, L. Pirvu and F. Schaufelberger, *J. Am. Chem. Soc.*, 2022, **144**, 17232–17240.
302 O. Kotova, S. J. Bradberry, A. J. Savyasachi and T. Gunnlaugsson, *Dalton Trans.*, 2018, **47**, 16377–16387.
303 R. Laishram, S. Sarkar, U. Maitra and S. J. George, *J. Mater. Chem. C*, 2024, **12**, 15418–15422.
304 R. A. Tigaa, X. Aerken, A. Fuchs and A. de Bettencourt-Dias, *Eur. J. Inorg. Chem.*, 2017, 5310–5317.
305 S. Lim, Y. Cho, J. H. Kang, M. Hwang, Y. Park, S. K. Kwak, S. H. Jung and J. H. Jung, *J. Am. Chem. Soc.*, 2024, **146**, 18484–18497.
306 Y. Liang, P. Zhao, Z. Yan, Q. Zhang, Y. Liu and R. Zhang, *Macromolecules*, 2025, **58**, 149–157.
307 G. Le-Hoang, L. Guénée, M. Bertrand-Avebe, L. Babel, A. Rosspeintner and C. Piguet, *Inorg. Chem.*, 2025, **64**, 3941–3958.
308 I. N. Hegarty, S. J. Bradberry, J. I. Lovitt, J. M. Delente, N. Willis-Fox, R. Daly and T. Gunnlaugsson, *Mater. Chem. Front.*, 2023, **7**, 906–916.
309 I. N. Hegarty, A. F. Henwood, S. J. Bradberry and T. Gunnlaugsson, *Org. Biomol. Chem.*, 2023, **21**, 1549–1557.
310 S. J. Bradberry, G. Dee, O. Kotova, C. P. McCoy and T. Gunnlaugsson, *Chem. Commun.*, 2019, **55**, 1754–1757.
311 O. Kotova, C. O'Reilly, S. T. Barwich, L. E. Mackenzie, A. D. Lynes, A. J. Savyasachi, M. Ruether, R. Pal, M. E. Möbius and T. Gunnlaugsson, *Chem*, 2022, **8**, 1395–1414.
312 A. J. Savyasachi, O. Kotova, E. T. Luis, A. D. Lynes, S. Mills, S. A. Bright, G. J. McManus, M. E. Möbius, D. C. Williams, R. Pal, J. J. Boland and T. Gunnlaugsson, *Chem*, 2024, **11**, 102321.
313 T. A. Gudmundsson, O. Kotova, S. Barwich, M. E. Möbius and T. Gunnlaugsson, *Chem. – Eur. J.*, 2025, **31**, e202403919.
314 J. M. Delente, O. Kotova, N. Willis-Fox, J. E. O'Brien, B. Twamley, R. Daly and T. Gunnlaugsson, *Adv. Opt. Mater.*, 2025, **13**, 2402714.
315 S. Liao, Z. Li, L. Ren, T. Lin, C. Lin, C. Zhao, M. Gao and X. Wu, *ACS Appl. Polym. Mater.*, 2025, **7**, 700–709.
316 N. C. Martinez-Gomez, H. N. Vu and E. Skovran, *Inorg. Chem.*, 2016, **55**, 10083–10089.
317 A. M. Zytnick, S. M. Gutenthaler-Tietze, A. T. Aron, Z. L. Reitz, M. T. Phi, N. M. Good, D. Petras, L. J. Daumann and N. C. Martinez-Gomez, *Proc. Natl. Acad. Sci. U. S. A.*, 2024, **121**, e2322096121.
318 B. Yu, Z. H. Zhu, W. W. Qin, H. L. Wang, Y. L. Li, F. P. Liang and H. H. Zou, *ACS Mater. Lett.*, 2024, **6**, 3312–3326.
319 R. M. Pallares, Y. Li and R. J. Abergel, *TrAC, Trends Anal. Chem.*, 2023, **167**, 117251.
320 R. M. Pallares, D. D. An, P. Tewari, E. T. Wang and R. J. Abergel, *ACS Sens.*, 2020, **5**, 1281–1286.
321 R. M. Pallares and R. J. Abergel, *Toxicology*, 2024, **509**, 153967.
322 R. M. Pallares, S. Hébert, M. Sturzbecher-Hoehne and R. J. Abergel, *New J. Chem.*, 2021, **45**, 14364–14368.
323 E. J. Werner and S. M. Biros, *Org. Chem. Front.*, 2019, **6**, 2067–2094.
324 M. Gut, T. Wilhelm, O. Beniston, S. Ogundipe, C. C. Kuo, K. Nguyen and A. Furst, *Adv. Mater.*, 2025, **37**, 2412607.
325 R. M. Pallares, M. Charrier, S. Tejedor-Sanz, D. Li, P. D. Ashby, C. M. Ajo-Franklin, C. Y. Ralston and R. J. Abergel, *J. Am. Chem. Soc.*, 2022, **144**, 854–861.

326 X. Z. Li, L. P. Zhou, L. L. Yan, Y. M. Dong, Z. L. Bai, X. Q. Sun, J. Diwu, S. Wang, J. C. Bünzli and Q. F. Sun, *Nat. Commun.*, 2018, **9**, 547.
327 H. Lumpe, A. Menke, C. Haisch, P. Mayer, A. Kabelitz, K. V. Yusenko, A. Guilherme Buzanich, T. Block, R. Pöttgen, F. Emmerling and L. J. Daumann, *Chem. – Eur. J.*, 2020, **26**, 10133–10139.
328 M. V. Evsiunina, E. K. Khult, P. I. Matveev, P. Kalle, P. S. Lemport, V. S. Petrov, S. A. Aksenova, Y. V. Nelyubina, D. S. Koshelev, V. V. Utochnikova, V. G. Petrov, Y. A. Ustynyuk and V. G. Nenajdenko, *Sep. Purif. Technol.*, 2024, **339**, 126621.
329 S. Pramanik, S. Kaur, I. Popovs, A. S. Ivanov and S. Jansone-Popova, *Eur. J. Inorg. Chem.*, 2024, e202400064.
330 T. Liu, K. R. Johnson, S. Jansone-Popova and D. E. Jiang, *JACS Au*, 2022, **2**, 1428–1434.
331 K. R. Johnson, D. M. Driscoll, J. T. Damron, A. S. Ivanov and S. Jansone-Popova, *JACS Au*, 2023, **3**, 584–591.
332 S. Pramanik, B. Li, D. M. Driscoll, K. R. Johnson, B. R. Evans, J. T. Damron, A. S. Ivanov, D. E. Jiang, J. Einkauf, I. Popovs and S. Jansone-Popova, *J. Am. Chem. Soc.*, 2024, **146**, 25669–25679.